



Functional microRNA screen uncovers O-linked N-acetylglucosamine transferase as a host factor modulating hepatitis C virus morphogenesis and infectivity

Katharina Herzog, Simonetta Bandiera, Sophie Pernot, Catherine Fauvelle, Frank Jühling, Amélie Weiss, Anne Bull, Sarah C. Durand, Béatrice Chane-Woon-Ming, Sébastien Pfeffer, et al.

► To cite this version:

Katharina Herzog, Simonetta Bandiera, Sophie Pernot, Catherine Fauvelle, Frank Jühling, et al.. Functional microRNA screen uncovers O-linked N-acetylglucosamine transferase as a host factor modulating hepatitis C virus morphogenesis and infectivity. *Gut*, 2020, 69 (2), pp.380-392. <10.1136/gutjnl-2018-317423>. <hal-02171225>

HAL Id: hal-02171225

<https://hal.science/hal-02171225v1>

Submitted on 28 Nov 2019

HAL is a multi-disciplinary open access archive for the deposit and dissemination of scientific research documents, whether they are published or not. The documents may come from teaching and research institutions in France or abroad, or from public or private research centers.

L'archive ouverte pluridisciplinaire **HAL**, est destinée au dépôt et à la diffusion de documents scientifiques de niveau recherche, publiés ou non, émanant des établissements d'enseignement et de recherche français ou étrangers, des laboratoires publics ou privés.



HAL Authorization



A functional microRNA screen uncovers O-linked N-acetylglucosamine transferase as a host factor modulating hepatitis C virus morphogenesis and infectivity

Journal:	<i>Gut</i>
Manuscript ID	gutjnl-2018-317423.R1
Article Type:	Original Article
Date Submitted by the Author:	n/a
Complete List of Authors:	<p>Herzog, Katharina; INSERM, U1110 Institute of Viral and Liver Diseases; University of Strasbourg</p> <p>Bandiera, Simonetta; INSERM, U1110 Institute of Viral and Liver Diseases; University of Strasbourg</p> <p>Pernot, Sophie; INSERM, U1110 Institute of Viral and Liver Diseases; University of Strasbourg</p> <p>Fauvelle, Catherine; INSERM, U1110 Institute of Viral and Liver Diseases; University of Strasbourg</p> <p>Jühling, Frank; INSERM, U1110 Institute of Viral and Liver Diseases; University of Strasbourg</p> <p>Weiss, Amélie; Institut de Genetique et de Biologie Moleculaire et Cellulaire</p> <p>Bull, Anne; INSERM, U1259</p> <p>Durand, Sarah; INSERM, U1110 Institute of Viral and Liver Diseases; University of Strasbourg</p> <p>Chane-Woon-Ming, Béatrice; CNRS, Architecture et Réactivité de l'ARN – UPR 9002, Institut de Biologie Moléculaire et Cellulaire du CNRS</p> <p>Pfeffer, Sébastien; CNRS, Architecture et Réactivité de l'ARN – UPR 9002, Institut de Biologie Moléculaire et Cellulaire du CNRS; University of Strasbourg</p> <p>Mercey, Marion; INSERM, U1209 Institute for Applied Biosciences</p> <p>Lerat, Hervé; INSERM, U1209 Institute for Applied Biosciences</p> <p>Meunier, Jean-Christophe; INSERM, U1259</p> <p>Raffelsberger, Wolfgang; Institut de Genetique et de Biologie Moleculaire et Cellulaire</p> <p>Brino, Laurent ; Institut de Genetique et de Biologie Moleculaire et Cellulaire</p> <p>Baumert, Thomas; INSERM, U1110</p> <p>Zeisel, Mirjam; INSERM, U1110 Institute of Viral and Liver Diseases; INSERM, U1052 Cancer Research Center of Lyon</p>
Keywords:	HEPATITIS C, HCV, HEPATOCYTE, MOLECULAR MECHANISMS

1
2
3
4
5
6
7
8
9
10
11
12
13
14
15
16
17
18
19
20
21
22
23
24
25
26
27
28
29
30
31
32
33
34
35
36
37
38
39
40
41
42
43
44
45
46
47
48
49
50
51
52
53
54
55
56
57
58
59
60



A functional microRNA screen uncovers O-linked N-acetylglucosamine transferase as a host factor modulating hepatitis C virus morphogenesis and infectivity

Katharina Herzog^{1,2*}, Simonetta Bandiera^{1,2*}, Sophie Pernot^{1,2}, Catherine Fauvelle^{1,2}, Frank Jühling^{1,2}, Amélie Weiss^{2,3,4,5}, Anne Bull⁶, Sarah C. Durand^{1,2}, Béatrice Chane-Woon-Ming^{2,7}, Sébastien Pfeffer^{2,7}, Marion Mercey⁸, Hervé Lerat⁸, Jean-Christophe Meunier⁶, Wolfgang Raffelsberger^{2,3,4,5}, Laurent Brino^{2,3,4,5}, Thomas F. Baumert^{1,2,9,#}, Mirjam B. Zeisel^{1,2,10,#}

¹Inserm, U1110, Institut de Recherche sur les Maladies Virales et Hépatiques, Strasbourg, France; ²Université de Strasbourg, Strasbourg, France; ³Institut de Génétique et de Biologie Moléculaire et Cellulaire, Illkirch, France ; ⁴CNRS, UMR7104, Illkirch, France ; ⁵Inserm, U1258, Illkirch, France ; ⁶Inserm U1259, Faculté de Médecine, Université François Rabelais and CHRU de Tours, Tours, France ; ⁷Architecture et Réactivité de l'ARN – UPR 9002, Institut de Biologie Moléculaire et Cellulaire du CNRS, Strasbourg, France; ⁸Institute for Applied Biosciences, Centre de Recherche UGA - Inserm U1209 - CNRS 5309, Grenoble, France ⁹Institut Hospitalo-Universitaire, Pôle Hépato-digestif, Hôpitaux Universitaires de Strasbourg, Strasbourg, France; ¹⁰Inserm, U1052, CNRS UMR 5286, Centre Léon Bérard (CLB), Cancer Research Center of Lyon (CRCL), Université de Lyon (UCBL), Lyon, France

*Authors contributed equally to this work

Word count. Abstract: 196 words; main manuscript: 3991 words; 55 references; 7 figures; 1 table; Supplementary information (including 1 Supplementary Table and 1 Supplementary Figure)

#Corresponding authors. Dr. Mirjam B. Zeisel, Inserm U1052 – CRCL, 151 cours Albert Thomas, 69424 Lyon Cedex 03, France, Phone: +33472681970, Fax: +33472681971, E-mail: mirjam.zeisel@inserm.fr and Prof. Thomas F. Baumert, Inserm U1110, Institut de

1
2
3
4
5
6
7
8
9
10
11
12
13
14
15
16
17
18
19
20
21
22
23
24
25
26
27
28
29
30
31
32
33
34
35
36
37
38
39
40
41
42
43
44
45
46
47
48
49
50
51
52
53
54
55
56
57
58
59
60

1 Recherche sur les Maladies Virales et Hépatiques, 3 rue Koeberlé, 67000 Strasbourg,
2 France, Phone: +33368853703, Fax: +33368853724, Email: thomas.baumert@unistra.fr

3
4 **Financial support.** This work was supported by the European Union (INTERREG-IV-Rhin
5 Supérieur-FEDER-Hepato-Regio-Net 2012 to T.F.B. and M.B.Z., ERC-AdG-2014-671231-
6 HEPCIR, EU H2020-667273-HEPCAR to T.F.B), ANRS (2012/239 to T.F.B., M.B.Z. and
7 L.B.), ARC, Paris and Institut Hospitalo-Universitaire, Strasbourg (TheraHCC IHUARC
8 IHU201301187 to T.F.B.), the Impulsion Program of the IDEXLYON (to M.B.Z.), Ligue contre
9 le cancer (to M.B.Z.), Inserm, and University of Strasbourg. This work has been published
10 under the framework of the LABEX ANR-10-LABX-0028_HepSYS, ANR-10-LABX-36
11 NetRNA and Inserm Plan Cancer 2019-2023 and benefits from funding from the state
12 managed by the French National Research Agency as part of the Investments for the future
13 program. S.P. and K.H. were supported by PhD fellowships from the French Ministry of
14 Research and the IdEx program of the University of Strasbourg, respectively.

15
16 **Author contribution.** M.B.Z. coordinated and supervised research. K.H., S.B., S.P., C.F.,
17 A.W., L.B., J-C.M. and M.B.Z. designed experiments. K.H., S.B., S.P, C. F., A.W., A.B.,
18 S.C.D., M.M., H.L. and J-C.M. performed experiments. K.H., S.B., S.P., C. F., F.J., A.W.,
19 A.B., B.C.W.M., S.P., J-C.M., W.R., L.B., T.F.B. and M.B.Z. analyzed data. K.H., S.B., and
20 M.B.Z. wrote the paper.

21
22 **Competing interests:** The authors do not have competing interest.

Abstract

Objective: Infection of human hepatocytes by the hepatitis C virus (HCV) is a multistep process involving both viral and host factors. microRNAs (miRNAs) are small non-coding RNAs that post-transcriptionally regulate gene expression. Given that miRNAs were indicated to regulate between 30% and 75% of all human genes, we aimed to investigate the functional and regulatory role of miRNAs for the HCV life cycle.

Design: To systematically reveal human miRNAs affecting the HCV life cycle, we performed a two-step functional high-throughput miRNA mimic screen in Huh7.5.1 cells infected with recombinant cell culture-derived HCV. miRNA targeting was then assessed using a combination of computational and functional approaches.

Results: We uncovered miR-501-3p and miR-619-3p as novel modulators of HCV assembly/release. We discovered that these miRNAs regulate O-linked N-acetylglucosamine (O-GlcNAc) transferase (OGT) protein expression and identified OGT and O-GlcNAcylation as regulators of HCV morphogenesis and infectivity. Furthermore, increased OGT expression in patient-derived liver tissue was associated with HCV-induced liver disease and cancer.

Conclusion: miR-501-3p and miR-619-3p and their target OGT are previously undiscovered regulatory host factors for HCV assembly and infectivity. In addition to its effect on HCV morphogenesis, OGT may play a role in HCV-induced liver disease and hepatocarcinogenesis.

1
2
3
4
5
6
7
8
9
10
11
12
13
14
15
16
17
18
19
20
21
22
23
24
25
26
27
28
29
30
31
32
33
34
35
36
37
38
39
40
41
42
43
44
45
46
47
48
49
50
51
52
53
54
55
56
57
58
59
60

Significance of this study	
1	<p>What is already known about this subject?</p> <ul style="list-style-type: none">♦ To establish chronic infection, the hepatitis C virus (HCV) hijacks cellular factors including microRNAs (miRNAs), known to post-transcriptionally regulate gene expression.♦ miRNAs may positively or negatively modulate HCV infection either by directly targeting the viral genome or indirectly by regulating virus-associated cellular pathways[1, 2]. <p>What are the new findings?</p> <ul style="list-style-type: none">♦ A functional miRNA mimic screen uncovered miR-501-3p and miR-619-3p to enhance late steps of HCV infection.♦ miR-501-3p regulates the expression of O-linked N-acetylglucosamine transferase (OGT) at the protein level.♦ Silencing of OGT expression or inhibition of O-linked N-acetylglucosaminylation (O-GlcNAcylation) leads to an increase in the infectivity and size of HCV particles.♦ OGT expression increases in patient-derived liver tissue during liver disease progression and cancer. <p>How might it impact on clinical practice in the foreseeable future?</p> <ul style="list-style-type: none">♦ As upregulation of OGT and increased O-GlcNAcylation of proteins have been associated with various forms of cancer, OGT may play a dual role in HCV morphogenesis as well as pathogenesis of HCV-induced liver disease and carcinogenesis.

2
3

1 Introduction

Chronic hepatitis C is a major cause of chronic liver disease and hepatocellular carcinoma (HCC). Since the approval of pan-genotypic direct-acting antivirals (DAAs), it is considered a curable disease in more than 90% of treated patients. Nonetheless, an estimated 71 million individuals are still infected by the hepatitis C virus (HCV) and several challenges remain; viral cure reduces but does not eliminate the HCC risk in patients with advanced fibrosis[3], the majority of infected patients has limited access to therapy and DAA failure/viral resistance has been reported in a subset of patients[4, 5]. To overcome these limitations, approaches to target host factors involved in HCV infection and pathogenesis are developed[6, 7]. Interestingly, defined host factors that contribute to the establishment of chronic HCV infection and represent potential antiviral targets, e.g. epidermal growth factor receptor[8], also play a role in liver disease pathogenesis and represent candidate targets for treatment of advanced liver disease and HCC prevention[9]. Thus, uncovering host factors usurped by HCV not only contributes to a better understanding of virus-host interactions underlying the HCV life cycle but also to the identification of potential targets for treatment of liver disease and prevention of HCC.

The establishment of various models to study HCV infection has shed light on the molecular mechanisms that govern the HCV life cycle, which can be subdivided into early steps, including viral entry, translation and replication as well as late steps, including assembly and release of new virions. Each step of the HCV replication cycle relies on specific virus-host interactions that involve host proteins and microRNAs (miRNAs)[7], small non-coding RNAs that regulate gene expression at the post-transcriptional level. One miRNA can target numerous messenger RNAs (mRNAs) by base-pairing with a complementary site that is typically located within the 3' untranslated region (3'UTR) of the mRNA. Accumulating evidence indicates that miRNAs participate to HCV replication by exerting pro- or antiviral effects. The breakthrough discovery of the direct targeting of HCV by miR-122, the most abundant miRNA in the liver, revealed the crucial role of this miRNA for HCV translation/replication that contributes to progression to chronic HCV infection[1, 10]. miR-

1
2
3 1 122 antisense oligonucleotides were subsequently developed as host-targeting antivirals[11,
4
5 2 12]. Other miRNAs can indirectly target HCV by regulating host factors that participate in
6
7 3 antiviral responses and immune surveillance[2, 13, 14]. Since up to 60% of all human
8
9 4 protein-coding genes were reported to be under miRNA-mediated regulation and miRNAs
10
11 5 are involved in basically every biological process, we hypothesized that miRNAs provide a
12
13 6 tool for loss-of-function approaches to uncover novel HCV host factors. We performed
14
15 7 genome-wide high-throughput modulation of the human miRNome and analyzed their impact
16
17 8 on HCV infection by combining computational and functional approaches.
18
19
20 9

21
22 10 **Material and methods**

23
24 11 **Cells, cell culture conditions, viruses, virus purification, infectivity assays, miRNAs,**
25
26 12 **antagomiRs, siRNAs, antibodies, immunoblot, immunocapture, electron microscopy**
27
28 13 **analysis of viral particles and gene expression analysis in liver tissue** are described in
29
30 14 the Supplementary information.
31
32
33 15

34
35 16 **Functional miRNA/siRNA screens.** Huh7.5.1 cells were transfected with the miRIDIAN
36
37 17 human miRNA mimic library (miRBase 19) comprising more than 2000 mature miRNAs or 28
38
39 18 ON-TARGETplus smart pool siRNAs (20 nM, Dharmacon) using Interferin HTS (Polyplus) in
40
41 19 a 96-well format[8]. After 48h, a viability test (Presto Blue, Thermo Scientific) was performed
42
43 20 prior to a two-step infection assay[15, 16, 17]. During part 1 of the protocol, 50 µL of HCV cell
44
45 21 culture-derived particles (HCVcc, JcR2a) were incubated with cells during 4h. The inoculum
46
47 22 was removed and cells were incubated with 150 µl of medium for 48h. In part 2, supernatants
48
49 23 from part 1 cells were transferred onto naïve Huh7.5.1 cells and part 1 cells were lysed to
50
51 24 determine luciferase activity[17, 18]. After 72h, part 2 cells were lysed to determine luciferase
52
53 25 activity[17]. siCD81 (20 nM), antagomiR-122 (100 nM) and siApoE (20 nM) were used as
54
55 26 positive controls[17]. A non-targeting siRNA with no sequence complementarity to any
56
57 27 human gene or homology to any human miRNA was used as negative control.
58
59
60 28

Inhibitor treatment. Four hours following HCV RNA electroporation[8], Huh7.5.1 cells were incubated with vehicle or inhibitors of OGT (peracetylated 5-thio-N-acetylglucosamine (Ac₄5S-GlcNAc)[19]) or OGA (Thiamet G (Sigma))[20]. After 96h, supernatants were transferred onto naïve Huh7.5.1 cells for 72h prior to determination of luciferase activity while electroporated cells were lysed to determine luciferase activity.

Gene expression analyses. Total RNA was purified[17] and transcribed into cDNA using Maxima reverse transcriptase (Thermo Scientific). *GAPDH* and *OGT* mRNA was detected by real time qPCR using iTaq™ Universal Probes Supermix (Bio-Rad) and TaqMan Gene Expression Assay (Thermo Scientific). Relative *OGT/GAPDH* gene expression was calculated by the $\Delta\Delta C_t$ method[21].

Dual luciferase reporter gene assay. The human *OGT* 3'UTR sequence was retrieved from NCBI (NM_181672.2) and Ensembl genome browser (ENST00000373719.3). A fragment of the *OGT* 3'UTR (positions 3380-3837, NM_181672.2) (Thermo Fisher Scientific GENEART) was cloned between the *NotI* and *XhoI* sites downstream of a *Renilla* luciferase cassette in a psiCHECK2 plasmid (Promega). A mutated version of this construct (9-bp substitution in the predicted miR-501-3p target site) was generated as described[22]. The functionality of the *OGT* 3'UTR was assessed as described[23]. The miRIDIAN mimic negative control 1 was used as control. *Renilla* and *firefly* luciferase activity was assessed 48h after transfection into HeLa cells using Dual-Luciferase Reporter assay (Promega).

Bioinformatic and statistical analysis. Data analysis and statistical treatment for the miRNA mimic screen were performed in R (www.r-project.org). Cell measurement data used in further analysis were cell viability and luciferase activity. In total 26 sets of plates (performed in triplicate) were tested. The presence of multiple wells with negative and positive controls on each plate allowed stepwise normalization intra- and inter-plate. First, intra-plate zonal bias was examined and a model of median effects across the entire screen

1
2
3 1 determined using the median-polish algorithm[24] and all plates corrected accordingly. Then
4
5 2 the dataset was examined for outlier plates, i.e. plates where all individual measurements
6
7 3 correlate very poorly with the other remaining replicates. Three and 9 plates were excluded
8
9 4 for part 1 and part 2 of the screen, respectively, based on poor median correlation ($r < 0.7$)
10
11 5 so that the remaining plates correlation improved substantially ($> 40\%$). Next, the plates were
12
13 6 normalized inter replicates using the particularly robust quantile-quantile approach[25].
14
15 7 Finally, the data were tested using a moderated t-test (empirical Bayes shrinkage, R-
16
17 8 package limma[26]) for the null-hypothesis of no change of a given miRNA compared to the
18
19 9 negative control. The resulting p -values for independent testing of each miRNA where
20
21 10 corrected for the multiple testing situation and expressed as local false discovery rate (lfdr,
22
23 11 R-package fdrtool[27]). The testing was performed independently for part 1 and 2 of the
24
25 12 screen and candidate miRNAs selected for each part. For data from part 1, a lfdr threshold of
26
27 13 0.00027 was used. Data from part 2 were subject to increase inherent stochastic noise and
28
29 14 for this reason the minimum acceptable relative risk of false positives was increased to
30
31 15 0.1226 (i.e. maximum 15% risk for each of the retained hits).

32
33
34 16 Other datasets were analyzed using the two-tailed Mann-Whitney test, Wilcoxon test,
35
36 17 Spearman correlation or the two-tailed unpaired t-test for data with normal distribution as
37
38 18 assessed by D'Agostino and Pearson omnibus and Shapiro-Wilk normality tests (GraphPad
39
40 19 Prism v.6 package).

41
42
43
44
45
46
47 22 **Results**

48
49 23 **Genome-wide identification of human miRNAs affecting the HCV life cycle.** We
50
51 24 performed a genome-wide screen in human hepatoma Huh7.5.1 cells using a genomic
52
53 25 miRNA mimics library and a two-step infection assay[17] with a luciferase reporter virus
54
55 26 (JcR2a), which allowed us to functionally assess the role of miRNAs during the early steps
56
57 27 (part 1 - viral entry/translation/replication) and the late steps (part 2 - viral
58
59 28 assembly/release/infectivity) of the HCV life cycle (Fig. 1A). Silencing of *CD81* and *ApoE*,

two essential host factors required for HCV entry or assembly, respectively, was performed in parallel using small interfering RNA (siRNA) as controls. Silencing of *CD81* resulted in a reduction of HCV infection in part 1 and consequently in part 2 of the screen since reduced viral entry in the first part of the assay leads to a reduced production of viral particles (Fig. 1B)[17]. Silencing of *ApoE* resulted in a marked inhibition of HCV infection only in part 2 of the assay, consistent with the role of ApoE in HCV assembly (Fig. 1B)[17]. The screen identified 427 miRNAs (corresponding to about 16% of the library) that significantly modulated HCV infection (Ifdr < threshold, Supplementary Table 1 and Fig. 1C): 186 miRNAs affected HCV infection in part 1, 309 miRNAs affected HCV infection in part 2, including 68 hits in part 1 and part 2. The limited number of part 1 and 2 hits may be due to the fact that a single miRNA may modulate the expression of several proteins, which may have different roles in the viral life cycle. Most hits were observed to dampen HCV infection independently of any significant alteration of cell viability (data not shown). The 186 miRNAs modulating the early steps of HCV infection all decreased viral infection. Among the 309 miRNAs that had an impact in part 2, 11 miRNAs increased HCV infection by at least 3-fold while 298 miRNAs inhibited HCV infection by at least 2.7-fold. Hits from the screen included the let-7 family[2, 28], miR-27a[29] and miR-29 family[30] that were already shown to inhibit HCV infection, as well as miR-21[31] and miR-146a-5p[17] that were shown to stimulate HCV infection thus supporting the relevance of our findings. Collectively, our screen identified a set of miRNAs whose overexpression overall impairs HCV infection by affecting viral entry/translation/replication and/or virion assembly/egress/infectivity.

miR-619-3p, miR-501-3p and OGT play a role in late steps of the HCV life cycle. We focused our analysis on miRNAs that modulate late steps of the HCV life cycle, as the molecular mechanisms of HCV assembly/release remain only partially understood. Our screen identified 241 miRNAs that modulated late steps without affecting early steps of infection: 11 miRNAs increased HCV infection while 230 miRNAs decreased HCV infection. Among the miRNAs that increased HCV infection, miR-140-3p, miR-501-3p, miR-619-3p and

1
2
3 1 miR-4778-5p have not yet been associated with HCV. Since they enhanced HCV infection in
4
5 2 part 2 without affecting part 1, these miRNAs may target host genes that control virus
6
7 3 assembly/egress/infectivity. We first confirmed the effect of these miRNAs in independent
8
9 4 experiments using the same protocol as for the screen. Overexpression of miR-619-3p or
10
11 5 miR-501-3p consistently led to an increase in the infection of progeny virions (Fig. 1D) while
12
13 6 infection was decreased with progeny virions from antagomiR-transfected cells
14
15 7 (Supplementary Figure S1A). miR-619-3p or miR-501-3p were thus selected for further
16
17 8 investigation. To study the molecular mechanisms by which these miRNAs affect HCV
18
19 9 infection, we generated a list of predicted miRNA targets using DIANA, TargetScan Human
20
21 10 v6.2 and miRDB databases, and selected candidate targets based on their expression in our
22
23 11 Huh7.5.1 cells as assessed by microarray (data not shown). Ingenuity Pathway Analysis
24
25 12 enabled us to refine the gene list by selecting 28 genes involved in the following functional
26
27 13 networks or pathways that contribute to the HCV life cycle[32, 33, 34]: lipid metabolism and
28
29 14 cholesterol biosynthesis, protein maturation and processing at the endoplasmic reticulum
30
31 15 (ER), components of the endosomal sorting complex, adipocyte biogenesis, cellular
32
33 16 morphology and cell inflammation (Table 1).

34
35
36
37 17 To assess whether knock-down of these 28 candidate targets affects virus
38
39 18 production, we performed a siRNA-based screen using siRNA pools exhibiting strong
40
41 19 silencing without cytotoxicity (Fig. 2). Silencing of *CD81* and antagomiR-122 served as
42
43 20 controls for part 1; knock-down of *ApoE* served as control for part 2 (Fig. 2). Hits were
44
45 21 defined as genes whose knock-down modulated HCV infection in at least one part of the
46
47 22 screen with high significance (Fig. 2, p -value < 0.0001, Mann-Whitney U-test). HCV
48
49 23 entry/translation/replication was significantly modulated by silencing of *PPP3CA*, *CEBPA*,
50
51 24 *MID1*, *WDFY3*, *DCX* and *SLC35D1*. HCV assembly/egress/infectivity was significantly
52
53 25 modulated by knock-down of *PPP3CA*, *CSDE1*, *GAN*, *USP37*, *CEBPA*, *MID1*, *WDFY3*, *DCX*,
54
55 26 *MAPK9*, *SLC35D1*, *DCC*, *RNF144A*, *PPP2R2C* and *OGT*. Strikingly, only the silencing of
56
57 27 *OGT* was associated with an enhancement of HCV assembly/release/infectivity (p -value =
58
59 28 0.0002), while that of the other hits was associated with reduced HCV infection (Fig. 2).

These results indicate that the down-regulation of *OGT* phenocopies the effect of miR-501-3p and miR-619-3p on HCV infection (Fig. 2) and suggest *OGT* as a novel player in the HCV life cycle.

miR-501-3p post-transcriptionally regulates *OGT* expression. To study whether miR-501-3p and miR-619-3p target *OGT*, we analyzed *OGT* RNA and protein levels in Huh7.5.1 cells following overexpression of miR-501-3p or miR-619-3p. While neither miRNA had an impact on *OGT* RNA levels (Fig. 3A), up-regulation of miR-501-3p significantly decreased *OGT* protein expression by ~65% (Fig. 3B, p -value < 0.05, t-test). miR-619-3p also decreased *OGT* expression but less robustly than miR-501-3p (Fig. 3B), prompting us to focus our investigation on miR-501-3p. To assess whether *OGT* is a functional target of miR-501-3p, we subcloned a fragment of the *OGT* mRNA 3'UTR that harbors the predicted miR-501-3p target site in the *Renilla* luciferase expression cassette (RLuc) of a dual luciferase reporter construct. Co-transfection of miR-501-3p mimic with the wild-type 3'UTR reporter (RLuc wt *OGT* 3'UTR) significantly decreased luciferase activity as compared to the empty vector (Fig. 3C, p -value < 0.05, t-test). In contrast, the repression of luciferase expression was lost when the reporter with mutated miR-501-3p binding site (RLuc mt *OGT* 3'UTR) was used (Fig. 3C). These data are consistent in indicating that miR-501-3p mediates post-transcriptional regulation of *OGT*.

O-GlcNAcylation modulates HCVcc infectivity. To investigate whether *OGT* modulates HCV assembly and/or infectivity, we determined infectious virus titer (TCID₅₀) and HCV RNA levels to calculate the specific infectivity of HCVcc particles generated in *OGT*-silenced Huh7.5.1 cells. Interestingly, *OGT*-silencing led to a significant increase in the TCID₅₀ and the specific infectivity of HCVcc (Fig. 4A, p -value < 0.05, Mann-Whitney test). Noteworthy, the effect of *OGT* on HCVcc infectivity was genotype-independent as demonstrated by increased infectivity of HCVcc bearing the envelope glycoproteins of genotypes 1a, 1b and 2a upon *OGT*-silencing (Fig. 4B). We next sought to investigate how *OGT* could modulate

1
2
3 1 HCVcc infectivity. OGT is the only enzyme that catalyzes the addition of N-
4
5 2 acetylglucosamine (O-GlcNAc) to serine and threonine residues of proteins. Moreover, OGT
6
7 3 has a scaffold function and promotes binding of proteins in multiprotein complexes[35]. To
8
9 4 assess whether the enzymatic activity of OGT modulates HCVcc infectivity, we used
10
11 5 pharmacological inhibitors of OGT (Ac₄5S-GlcNAc) or O-GlcNAcase (OGA) (Thiamet G), the
12
13 6 OGT counterpart that removes O-GlcNAc (Fig. 4C). Ac₄5S-GlcNAc led to a significant
14
15 7 enhancement of HCVcc infectivity in a dose-dependent manner, while the opposite effect
16
17 8 was observed with Thiamet G (Fig. 4D, *p*-value < 0.05, Mann-Whitney test). Collectively,
18
19 9 these results demonstrate that O-GlcNAcylation modulates HCVcc infectivity.
20
21
22
23

24 11 **OGT-silencing affects HCVcc biophysical properties and size distribution.** To further
25
26 12 assess how OGT may impact HCVcc morphogenesis, we analyzed the structural and
27
28 13 biophysical properties of HCVcc produced in siCtrl- and siOGT-transfected Huh7.5.1 cells
29
30 14 following iodixanol gradient ultracentrifugation. Silencing of OGT led to the production of
31
32 15 more infectious HCVcc with higher density (Fig. 5A-B) as well as higher ApoE concentrations
33
34 16 (Fig. 5C) suggesting that OGT/O-GlcNAcylation affects the biophysical properties of HCVcc.
35
36 17 No change in apoB concentrations were observed between HCVcc produced from siCtrl- or
37
38 18 siOGT-transfected cells (Fig. 5D), in line with the model that HCV lipovirions contain
39
40 19 several exchangeable ApoE molecules and one non-exchangeable apoB[36]. We also
41
42 20 visualized HCVcc by electron microscopy (EM) following anti-E2 antibody
43
44 21 immunocapture[36] to assess whether OGT-silencing had an impact on HCVcc size. Particle
45
46 22 size distribution was assessed from a series of randomly acquired electron micrographs. A
47
48 23 shift towards bigger sizes was observed for sucrose-cushion purified HCVcc generated in
49
50 24 OGT-silenced Huh7.5.1 cells as compared to control HCVcc (Fig. 6A-B). This shift was also
51
52 25 observed in different fractions of iodixanol gradient-separated HCVcc (Fig. 6C-F) in line with
53
54 26 the higher infectivity and ApoE concentrations of HCVcc generated in OGT-silenced
55
56 27 Huh7.5.1 cells (Fig. 5A-C). These data suggest that OGT-silencing affects the lipidation of
57
58 28 HCVcc.
59
60

OGT expression increases in liver disease. Since silencing of OGT promotes HCV infectivity, we assessed whether HCV infection in turn had an effect on miR-501-3p and OGT expression. In Huh7.5.1 cells, HCV infection lead to small but significant increase of miR-501-3p and decrease of OGT levels (Fig. 7A-B and Supplementary Fig. 1B; p -value < 0.05 , Mann-Whitney test), which may promote viral infection given the pro- and antiviral roles of miR-501-3p and O-GlcNAcylation, respectively (Fig. 1C-D and 4D). In contrast, no significant difference of OGT expression was observed between the livers of HCV transgenic and wild-type mice[37] (data not shown) suggesting that HCV proteins do not directly modulate OGT expression. In liver tissue from HCV-infected patients, HCV RNA levels were not correlated with OGT expression (Fig. 7C, Spearman correlation: 0.06004019, p -value = 0.7661) suggesting that in patients there is likely no direct effect of HCV on OGT expression.

O-GlcNAcylation has been associated with a variety of cancers, including HCC recurrence linked to increased O-GlcNAcylation after liver transplantation[38]. We therefore investigated OGT expression in chronic liver disease and HCC. While there was a trend for increased OGT expression in liver tissue from HCV-infected patients with fibrosis and inflammation (Fig. 7D-E), OGT levels were markedly and significantly elevated in the tumor liver tissue of patients chronically infected with HCV or hepatitis B virus and patients with alcoholic liver disease or non-alcoholic fatty liver disease as compared to non-tumor tissue (Fig. 7F, p -value < 0.05 , Wilcoxon test). These data suggest that OGT expression increases in HCC in an etiology-independent manner. Collectively, these results suggest that OGT expression is likely increased in HCV-induced liver disease and cancer through inflammation and fibrosis rather than by HCV itself.

Discussion

By focusing on miRNAs affecting late steps of the viral life cycle, we uncovered that i) miR-501-3p regulates the expression of OGT; ii) silencing of OGT expression or inhibition of its enzymatic activity increases the infectivity of HCV particles; and iii) OGT knock-down leads

1 to the release of bigger HCV particles. Our data suggest that O-GlcNAcylation affects HCV
2 morphogenesis and infectivity.

3 While we were characterizing the role of OGT/O-GlcNAcylation for HCV
4 morphogenesis, Li and colleagues published their functional genomics study of HCV-miRNA
5 interactions[2]. By conducting genome wide miRNA mimic and hairpin inhibitor screens, they
6 identified a set of miRNAs exhibiting a pro- or antiviral effect on HCV. Characterization of the
7 underlying molecular processes showed that miR-25, let-7 and miR-130 families restrict viral
8 infection by decreasing the expression of cellular HCV co-factors[2]. Despite similarities in
9 the cell type and HCV infection models used here and by Li and colleagues, our screen only
10 displays a small overlap with their study (9% common miRNA hits). This is not surprising
11 given the small overlap between previous siRNA screens to uncover HCV host factors[8, 15]
12 and is likely due i) to the different sizes of miRNA mimic libraries as the library used here was
13 more than 2-times larger than the one used by Li and co-workers, and ii) to the markedly
14 distinct pipelines for hit selection that were used in the two studies. Nonetheless, both
15 screens were consistent in confirming the proviral role of miR-146a-5p in promoting HCV
16 assembly/egress that we previously reported[17] and the global multistep inhibitory effects of
17 the let-7 family on HCV infection[28], further corroborating the involvement of these miRNAs
18 in fine-tuning the HCV life cycle. Both studies also consistently indicated that miR-518a-5p,
19 miR-517-3p, miR-185 and members of the miR-302 family inhibit early steps of HCV
20 infection, while miR-586, miR-620 and members of the miR-200 family inhibit late steps of
21 viral infection. Since none of these miRNAs except miR-185 has been previously associated
22 with HCV infection[39], it might be interesting to further characterize the involvement of these
23 miRNAs in HCV-host interactions. Interestingly, an overall proviral effect of miR-501-3p was
24 also observed by Li and colleagues[2], however the mechanism of action was not studied. By
25 characterizing the role of miR-501-3p in the HCV life cycle, we uncovered OGT as a miR-
26 501-3p target in liver-derived cells and showed for the first time a link between O-
27 GlcNAcylation and HCV infection. These results indicate that genome-wide miRNA functional

1 screens represent a powerful strategy to dissect the role of miRNAs in pathogen-host
2 interactions.

3 While N-glycosylation of HCV envelope glycoproteins plays an important role for
4 escape from virus-neutralizing antibodies[40], so far no functional association between HCV
5 and O-glycosylation has been reported. In contrast to N-linked glycosylation that consists of
6 the attachment of a glycan to a nitrogen of an asparagine residue of proteins in the ER/Golgi
7 prior to their trafficking to the plasma membrane and/or their secretion, the glycosylation of
8 serine and threonine residues with O-GlcNAc is a post-translational modification (PTM) of
9 intracellular proteins that are localized in the nucleus, cytoplasm or mitochondria. The O-
10 glycosylation/deglycosylation of proteins is catalyzed by a single pair of nucleo-cytoplasmic
11 enzymes, OGT/OGA. O-GlcNAcylation is complementary to protein
12 phosphorylation/dephosphorylation, another more broadly known abundant protein PTM that
13 involves numerous kinases/phosphatases. OGT/OGA are often found in protein complexes
14 that also include kinases/phosphatases and a protein can be either O-GlcNAcylated or
15 phosphorylated on a same residue to fine-tune cellular signaling[41]. O-GlcNAcylation and
16 phosphorylation on the same or neighboring serine or threonine residue is known as yin yang
17 site[42].

18 O-GlcNAcylation plays a major role in the regulation of metabolic pathways in the
19 liver, including insulin signaling, bile acid metabolism and lipogenesis[35]. The large number
20 of OGT/OGA substrates and cellular pathways regulated by O-GlcNAcylation hampers a
21 detailed characterization of the role of these proteins in HCV infection. Since i) HCV
22 assembly takes place at ER-derived membranes, ii) OGT/OGA are not known to localize in
23 the ER lumen, and iii) O-GlcNAcylation of extracellular proteins containing EGF-like domains
24 is catalyzed by EGF domain-specific OGT (EOGT) in the ER lumen in an OGT-independent
25 manner[43]), OGT/OGA most likely modulate HCV infection by post-translationally modifying
26 one or several cellular factors required for HCV morphogenesis rather than by affecting viral
27 proteins, although HCV glycoproteins contain putative O-GlcNAcylation sites as determined
28 using OGlcNAcScan, OGTsite and YingOYang1.2 bioinformatics tools (data not shown).

Regarding HCV host factors that may be regulated by OGT/OGA, O-GlcNAcylation sites have been predicted in human CLDN1[44] and OCLN at serine sites that can also be phosphorylated and this has been suggested to potentially play a role for HCV entry[45]. However, in our experimental setting we did not observe a significant effect of OGT-silencing on the early steps of HCV infection, suggesting that O-GlcNAcylation of CLDN1 and/or OCLN likely does not play a major role in HCV infection. Other host factors important for the HCV life cycle are well-known O-GlcNAcylated proteins, as for example various nuclear pore complex proteins (Nups) including Nup98, Nup153 and Nup155 that are involved in HCV replication and assembly and/or may be associated with viral particles[46, 47, 48]. However, since depletion of Nups was reported to alter HCV replication and/or assembly but to have no impact on the specific infectivity of HCV particles[46] in contrast to the depletion of OGT as shown here, it is unlikely that a modulation of Nup O-GlcNAcylation accounts for the effects of OGT-silencing and/or OGT/OGA inhibitors on HCVcc infectivity observed in our study. This is in line with our observation that OGT knock-down had no effect on Dengue virus (DENV) replication and infectivity (unpublished observations KH, MZ and Evelyne Schaffer, IBMC, Strasbourg), although Nup98 had been suggested to potentially play a role for DENV infection[46]. These data suggest that OGT does not broadly modulate the infectivity of viruses of the *Flaviviridae* family.

However, OGT and/or O-GlcNAcylation have been reported to play a role in the infection with other viruses[49, 50, 51]. Interestingly, while OGT expression modulates the levels of human papillomavirus 16 (HPV16) oncoproteins E6 and E7[52], E6 in turn can up-regulate OGT to increase O-GlcNAcylation and the oncogene activities of HPV[53], suggesting that OGT/O-GlcNAcylation could play a role in virus-induced cancer. In cell culture, HCV infection appeared to be associated with a minor decrease in OGT expression in line with an antiviral role of O-GlcNAcylation. In contrast, an increased OGT expression was observed in HCC tissues of HCV-infected patients. Since OGT has been suggested to activate oncogenic signaling pathways in non-alcoholic steatohepatitis-related HCC[54] and O-GlcNAcylation has been associated with HCC recurrence linked to increased O-

1 GlcNAcylation after liver transplantation[38], these data suggest that in addition to their effect
2 on the HCV life cycle, OGT/O-GlcNAcylation may also play a role in HCV-induced
3 hepatocarcinogenesis.

Acknowledgments

We wish to thank Gerald W. Hart and Stéphan Hardivillé, the CardioPEG CoreC4 (NHLBI P01 HL107153) for providing AL24 and for useful technical discussions. We are grateful to David Vocadlo (Simon Fraser University, Burnaby, Canada) for the gift of Ac₄5S-GlcNAc. We also thank Ralf Bartenschlager (University of Heidelberg, Germany) for providing the plasmids for production of HCVcc and Frank Chisari (The Scripps Research Institute, La Jolla, CA) for the gift of Huh7.5.1 cells. We acknowledge Evelyne Schaeffer (CNRS UPR3572, IBMC, Strasbourg) for the DENV experiment, Charlotte Bach and Christine Thumann (Inserm, U1110, Strasbourg) for excellent technical work during the functional miRNA mimic screen, as well as Armando A. Roca-Suarez (Inserm, U1110, Strasbourg), Hussein El Saghire (Inserm, U1110, Strasbourg), Arnaud Kopp (IGBMC, Department of Functional Genomics and Cancer) and Erika Girardi (UPR 9002, IBMC, Strasbourg) for helpful discussions. We thank the INGESTEM infrastructure for access to the IGBMC high-throughput screening workstation.

References

- 1 Jopling CL, Yi M, Lancaster AM, *et al.* Modulation of hepatitis C virus RNA abundance by a liver-specific MicroRNA. *Science* 2005;**309**:1577-81.
- 2 Li Q, Lowey B, Sodroski C, *et al.* Cellular microRNA networks regulate host dependency of hepatitis C virus infection. *Nat Commun* 2017;**8**:1789.
- 3 Baumert TF, Juhling F, Ono A, *et al.* Hepatitis C-related hepatocellular carcinoma in the era of new generation antivirals. *BMC Med* 2017;**15**:52.

- 1
2
3 1 4 Pawlotsky JM. Hepatitis C Virus Resistance to Direct-Acting Antiviral Drugs in
4 2 Interferon-Free Regimens. *Gastroenterology* 2016;**151**:70-86.
5
6
7 3 5 Dietz J, Susser S, Vermehren J, *et al.* Patterns of Resistance-Associated
8 4 Substitutions in Patients With Chronic HCV Infection Following Treatment With Direct-Acting
9 5 Antivirals. *Gastroenterology* 2018;**154**:976-88 e4.
10
11
12 6 6 Zeisel MB, Baumert TF. Clinical development of hepatitis C virus host-targeting
13 7 agents. *Lancet* 2017;**389**:674-5.
14
15
16 8 7 Zeisel MB, Crouchet E, Baumert TF, *et al.* Host-Targeting Agents to Prevent and
17 9 Cure Hepatitis C Virus Infection. *Viruses* 2015;**7**:5659-85.
18
19
20 10 8 Lupberger J, Zeisel MB, Xiao F, *et al.* EGFR and EphA2 are host factors for hepatitis
21 11 C virus entry and possible targets for antiviral therapy. *Nature Medicine* 2011;**17**:589-95.
22
23
24 12 9 Fuchs BC, Hoshida Y, Fujii T, *et al.* Epidermal growth factor receptor inhibition
25 13 attenuates liver fibrosis and development of hepatocellular carcinoma. *Hepatology*
26 14 2014;**59**:1577-90.
27
28
29 15 10 Masaki T, Arend KC, Li Y, *et al.* miR-122 stimulates hepatitis C virus RNA synthesis
30 16 by altering the balance of viral RNAs engaged in replication versus translation. *Cell Host*
31 17 *Microbe* 2015;**17**:217-28.
32
33
34 18 11 Janssen HL, Reesink HW, Lawitz EJ, *et al.* Treatment of HCV infection by targeting
35 19 microRNA. *N Engl J Med* 2013;**368**:1685-94.
36
37
38 20 12 van der Ree MH, de Vree JM, Stelma F, *et al.* Safety, tolerability, and antiviral effect
39 21 of RG-101 in patients with chronic hepatitis C: a phase 1B, double-blind, randomised
40 22 controlled trial. *Lancet* 2017;**389**:709-17.
41
42
43 23 13 Bandiera S, Pfeffer S, Baumert TF, *et al.* miR-122--a key factor and therapeutic target
44 24 in liver disease. *J Hepatol* 2015;**62**:448-57.
45
46
47 25 14 Li H, Jiang JD, Peng ZG. MicroRNA-mediated interactions between host and hepatitis
48 26 C virus. *World J Gastroenterol* 2016;**22**:1487-96.
49
50
51 27 15 Li Q, Brass AL, Ng A, *et al.* A genome-wide genetic screen for host factors required
52 28 for hepatitis C virus propagation. *Proc Natl Acad Sci U S A* 2009;**106**:16410-5.

- 1
2
3 16 Poenisch M, Metz P, Blankenburg H, *et al.* Identification of HNRNPK as regulator of
4 hepatitis C virus particle production. PLoS Pathog 2015;**11**:e1004573.
5
6
7 17 Bandiera S, Pernot S, El Saghire H, *et al.* Hepatitis C Virus-Induced Upregulation of
8 MicroRNA miR-146a-5p in Hepatocytes Promotes Viral Infection and Deregulates Metabolic
9 Pathways Associated with Liver Disease Pathogenesis. J Virol 2016;**90**:6387-400.
10
11
12 18 Da Costa D, Turek M, Felmlee DJ, *et al.* Reconstitution of the entire hepatitis C virus
13 life cycle in non-hepatic cells. J Virol 2012;**86**:11919-25.
14
15
16 19 Gloster TM, Zandberg WF, Heinonen JE, *et al.* Hijacking a biosynthetic pathway
17 yields a glycosyltransferase inhibitor within cells. Nat Chem Biol 2011;**7**:174-81.
18
19
20 20 Yuzwa SA, Macauley MS, Heinonen JE, *et al.* A potent mechanism-inspired O-
21 GlcNAcase inhibitor that blocks phosphorylation of tau in vivo. Nat Chem Biol 2008;**4**:483-90.
22
23
24 21 Schmittgen TD, Livak KJ. Analyzing real-time PCR data by the comparative C(T)
25 method. Nat Protoc 2008;**3**:1101-8.
26
27
28 22 Jin Y, Chen Z, Liu X, *et al.* Evaluating the microRNA targeting sites by luciferase
29 reporter gene assay. Methods Mol Biol 2013;**936**:117-27.
30
31
32 23 Van Renne N, Roca Suarez AA, Duong FHT, *et al.* miR-135a-5p-mediated
33 downregulation of protein tyrosine phosphatase receptor delta is a candidate driver of HCV-
34 associated hepatocarcinogenesis. Gut 2018;**67**:953-62.
35
36
37 24 Mosteller F, Tukey J. Data Analysis and Regression. Reading, MA: Addison-Wesley,
38 1977.
39
40
41 25 Amaratunga D, Cabrera J. Analysis of Data from Viral DNA Microchips. Journal of the
42 American Statistical Association 2001;**96**:1161.
43
44
45 26 Smyth GK. Linear models and empirical Bayes methods for assessing differential
46 expression in microarray experiments. Statistical Applications in Genetics and Molecular
47 Biology 2004;**3**:Article 3.
48
49
50 27 Strimmer K. fdrtool: a versatile R package for estimating local and tail area-based
51 false discovery rates. Bioinformatics 2008;**24**:1461-2.
52
53
54
55
56
57
58
59
60

- 1
2
3 1 28 Cheng M, Si Y, Niu Y, *et al.* High-throughput profiling of alpha interferon- and
4
5 2 interleukin-28B-regulated microRNAs and identification of let-7s with anti-hepatitis C virus
6
7 3 activity by targeting IGF2BP1. *J Virol* 2013;**87**:9707-18.
8
9 4 29 Shirasaki T, Honda M, Shimakami T, *et al.* MicroRNA-27a regulates lipid metabolism
10
11 5 and inhibits hepatitis C virus replication in human hepatoma cells. *J Virol* 2013;**87**:5270-86.
12
13 6 30 Bandyopadhyay S, Friedman RC, Marquez RT, *et al.* Hepatitis C virus infection and
14
15 7 hepatic stellate cell activation downregulate miR-29: miR-29 overexpression reduces
16
17 8 hepatitis C viral abundance in culture. *J Infect Dis* 2011;**203**:1753-62.
18
19 9 31 Chen Y, Chen J, Wang H, *et al.* HCV-induced miR-21 contributes to evasion of host
20
21 10 immune system by targeting MyD88 and IRAK1. *PLoS Pathog* 2013;**9**:e1003248.
22
23 11 32 Ariumi Y, Kuroki M, Maki M, *et al.* The ESCRT system is required for hepatitis C virus
24
25 12 production. *PLoS One* 2011;**6**:e14517.
26
27 13 33 Paul D, Madan V, Bartenschlager R. Hepatitis C virus RNA replication and assembly:
28
29 14 living on the fat of the land. *Cell Host Microbe* 2014;**16**:569-79.
30
31 15 34 Meyers NL, Fontaine KA, Kumar GR, *et al.* Entangled in a membranous web: ER and
32
33 16 lipid droplet reorganization during hepatitis C virus infection. *Curr Opin Cell Biol* 2016;**41**:117-
34
35 17 24.
36
37 18 35 Yang X, Qian K. Protein O-GlcNAcylation: emerging mechanisms and functions. *Nat*
38
39 19 *Rev Mol Cell Biol* 2017;**18**:452-65.
40
41 20 36 Piver E, Boyer A, Gaillard J, *et al.* Ultrastructural organisation of HCV from the
42
43 21 bloodstream of infected patients revealed by electron microscopy after specific
44
45 22 immunocapture. *Gut* 2017;**66**:1487-95.
46
47 23 37 Lerat H, Honda M, Beard MR, *et al.* Steatosis and liver cancer in transgenic mice
48
49 24 expressing the structural and nonstructural proteins of hepatitis C virus. *Gastroenterology*
50
51 25 2002;**122**:352-65.
52
53 26 38 de Queiroz RM, Carvalho E, Dias WB. O-GlcNAcylation: The Sweet Side of the
54
55 27 Cancer. *Front Oncol* 2014;**4**:132.
56
57
58
59
60

- 1
2
3 1 39 Singaravelu R, O'Hara S, Jones DM, *et al.* MicroRNAs regulate the immunometabolic
4 2 response to viral infection in the liver. *Nat Chem Biol* 2015;**11**:988-93.
5
6
7 3 40 Lavie M, Hanouille X, Dubuisson J. Glycan Shielding and Modulation of Hepatitis C
8 4 Virus Neutralizing Antibodies. *Front Immunol* 2018;**9**:910.
9
10
11 5 41 Hart GW, Slawson C, Ramirez-Correa G, *et al.* Cross talk between O-GlcNAcylation
12 6 and phosphorylation: roles in signaling, transcription, and chronic disease. *Annu Rev*
13 7 *Biochem* 2011;**80**:825-58.
14
15
16 8 42 Hart GW, Greis KD, Dong LY, *et al.* O-linked N-acetylglucosamine: the "yin-yang" of
17 9 Ser/Thr phosphorylation? Nuclear and cytoplasmic glycosylation. *Adv Exp Med Biol*
18 10 1995;**376**:115-23.
19
20
21 11 43 Sakaidani Y, Nomura T, Matsuura A, *et al.* O-linked-N-acetylglucosamine on
22 12 extracellular protein domains mediates epithelial cell-matrix interactions. *Nat Commun*
23 13 2011;**2**:583.
24
25
26 14 44 Butt AM, Khan IB, Hussain M, *et al.* Role of post translational modifications and novel
27 15 crosstalk between phosphorylation and O-beta-GlcNAc modifications in human claudin-1, -3
28 16 and -4. *Mol Biol Rep* 2012;**39**:1359-69.
29
30
31 17 45 Butt AM, Feng D, Nasrullah I, *et al.* Computational identification of interplay between
32 18 phosphorylation and O-beta-glycosylation of human occludin as potential mechanism to
33 19 impair hepatitis C virus entry. *Infect Genet Evol* 2012;**12**:1235-45.
34
35
36 20 46 Neufeldt CJ, Joyce MA, Levin A, *et al.* Hepatitis C virus-induced cytoplasmic
37 21 organelles use the nuclear transport machinery to establish an environment conducive to
38 22 virus replication. *PLoS Pathog* 2013;**9**:e1003744.
39
40
41 23 47 Lussignol M, Kopp M, Molloy K, *et al.* Proteomics of HCV virions reveals an essential
42 24 role for the nucleoporin Nup98 in virus morphogenesis. *Proc Natl Acad Sci U S A*
43 25 2016;**113**:2484-9.
44
45
46 26 48 Zhu Y, Liu TW, Madden Z, *et al.* Post-translational O-GlcNAcylation is essential for
47 27 nuclear pore integrity and maintenance of the pore selectivity filter. *J Mol Cell Biol* 2016;**8**:2-
48 28 16.
49
50
51
52
53
54
55
56
57
58
59
60

1
2
3 1 49 Jochmann R, Thureau M, Jung S, *et al.* O-linked N-acetylglucosaminylation of Sp1
4
5 2 inhibits the human immunodeficiency virus type 1 promoter. J Virol 2009;**83**:3704-18.
6
7 3 50 Groussaud D, Khair M, Tollenaere AI, *et al.* Hijacking of the O-GlcNAcZYME complex
8
9 4 by the HTLV-1 Tax oncoprotein facilitates viral transcription. PLoS Pathog
10
11 5 2017;**13**:e1006518.
12
13 6 51 Angelova M, Ortiz-Meoz RF, Walker S, *et al.* Inhibition of O-Linked N-
14
15 7 Acetylglucosamine Transferase Reduces Replication of Herpes Simplex Virus and Human
16
17 8 Cytomegalovirus. J Virol 2015;**89**:8474-83.
18
19 9 52 Kim M, Kim YS, Kim H, *et al.* O-linked N-acetylglucosamine transferase promotes
20
21 10 cervical cancer tumorigenesis through human papillomaviruses E6 and E7 oncogenes.
22
23 11 Oncotarget 2016;**7**:44596-607.
24
25 12 53 Zeng Q, Zhao RX, Chen J, *et al.* O-linked GlcNAcylation elevated by HPV E6
26
27 13 mediates viral oncogenesis. Proc Natl Acad Sci U S A 2016;**113**:9333-8.
28
29 14 54 Xu W, Zhang X, Wu JL, *et al.* O-GlcNAc transferase promotes fatty liver-associated
30
31 15 liver cancer through inducing palmitic acid and activating endoplasmic reticulum stress. J
32
33 16 Hepatol 2017;**67**:310-20.
34
35 17 55 Boldanova T, Suslov A, Heim MH, *et al.* Transcriptional response to hepatitis C virus
36
37 18 infection and interferon-alpha treatment in the human liver. EMBO Mol Med 2017;**9**:816-34.
38
39
40
41
42
43
44
45
46
47
48
49
50
51
52
53
54
55
56
57
58
59
60

Figure legends

Figure 1. High-throughput screen identifies human miRNAs that regulate the HCV life

cycle. (A) Schematic outline of the miRNA mimic screen strategy. Huh7.5.1 cells were transfected with miRNA mimics or controls prior to infection with *Renilla* luciferase HCVcc (JcR2a) two days later (part 1). Cell supernatants of part 1 were used to inoculate naïve Huh7.5.1 cells (part 2). Cells from part 1 and part 2 were lysed at the end of each infection step (2 and 3 days post infection, respectively) to determine luciferase activity. (B) Modulation of HCV entry and replication (part 1) and/or assembly and infectivity (part 2) upon transfection of control non-targeting siRNA (siCtrl, negative control), siCD81 (inhibiting viral entry) or siApoE (inhibiting viral assembly). By inhibiting HCV entry, siCD81 impacts part 1 as well as part 2. In contrast, by specifically impairing late steps of HCV replication cycle, siApoE inhibits HCV infection only in part 2. The box plots show the sample lower quartile (25th percentile; bottom of the box), the median (50th percentile; horizontal line in box) and the upper quartile (75th percentile; top of the box) of relative light units (RLU) in each lysate. The whiskers indicate s.d. Data are from three independent experiments. (C) Effects of miRNA overexpression on each part of the HCV life cycle. Data were tested using a moderated t-test (empirical Bayes shrinkage, R-package limma[26]) for the null-hypothesis of no change of a given miRNA compared to the negative control. The resulting p-values for independent testing of each miRNA were corrected for the multiple testing situation and expressed as local false discovery rate (lfdr, R-package fdrtool[27]). miRNAs having a significant effect on either part 1 or 2 of the screen are below the thresholds indicated by dashed lines (lfdr < 0.00027 or 0.1226, respectively). miRNAs that were previously reported to impact on HCV infection as well as miR-140-3p, miR-501-3p, miR-619-3p and miR-4778-5p are highlighted in blue (Log2(FC) < 0) or red (Log2(FC) > 0). Data are from three independent experiments. (D) Effect of miR-140-3p, miR-501-3p, miR-619-3p and miR-4778-5p on the HCV life cycle. Huh7.5.1 cells were transfected with siCtrl (Ctrl), miR-140-3p, miR-501-3p, miR-619-3p or miR-4778-5p and infection experiments were carried out as described in A. HCV infection was determined as luciferase activity. Results represent mean

1
2
3 1 percentage \pm s.d. from three independent experiments in triplicate. The dashed line indicates
4
5 2 values from control-transfected cells set at 100%. Statistics: *, p -value < 0.05, Mann-Whitney
6
7 3 test.
8
9
10 4

11 **Figure 2. OGT is a novel host cell factor involved in the late steps of the HCV life cycle.**

12
13
14 6 Huh7.5.1 cells were transfected with a set of siRNAs against 28 predicted targets of miR-
15
16 7 501-3p and/or miR-619-3p, and infected with HCVcc JcR2A according to the two-step
17
18 8 protocol depicted in Fig. 1A. siCD81, antagomiR-122 and siApoE were used as loss-of-
19
20 9 function controls to perturb HCV entry, translation/replication and assembly, respectively.
21
22 10 miR-501-3p and miR-619-3p, which were ineffective in part 1 of the screen but enhanced
23
24 11 HCV infection in part 2, were transfected in parallel. HCV infection was quantified as fold
25
26 12 change of luciferase activity with respect to negative control (siCtrl). Results for different
27
28 13 replicates are shown as individual points. For each gene, median fold change of luciferase
29
30 14 activity \pm s.d. is shown as black horizontal lines. The dashed line indicates a fold change of
31
32 15 1. Data are from three independent experiments in triplicate. Results for miR-501-3p, miR-
33
34 16 619-3p and siOGT that increase HCV infection in part 2 are depicted in red. Results for
35
36 17 siRNA targeting *PPP3CA*, *CEBPA*, *MID1*, *WDFY3*, *DCX*, *SLC35D1*, *CSDE1*, *GAN*, *USP37*,
37
38 18 *MAPK9*, *DCC*, *RNF144A*, or *PPP2R2C* that significantly modulated HCV infection in part 1
39
40 19 and/or part 2 but did not phenocopy the effect of miR-501-3p and miR-619-3p are depicted in
41
42 20 blue.
43
44
45 21

46
47 **Figure 3. miR-501-3p mediates post-transcriptional regulation of OGT by decreasing**

48
49 23 **its expression at the protein level.** Huh7.5.1 cells were transfected with siCtrl (Ctrl), a pool
50
51 24 of siRNA against *OGT*, miR-501-3p or miR-619-3p. After 96h, RNA and proteins were
52
53 25 purified, and OGT expression analyzed by RT-qPCR and Western blot. (A) Percentage of
54
55 26 *OGT* mRNA expression in miRNA-transfected cells as compared to negative control. Results
56
57 27 are presented as mean \pm s.d. and are from three independent experiments in triplicate. The
58
59 28 dashed line indicates values from control-transfected cells set at 100%. Statistics: *, p -value

1 < 0.05, t-test (B) OGT protein expression. Left: percentage of OGT protein expression in
 2 siRNA- or miRNA-transfected cells as assessed by quantification of Western blots. OGT
 3 levels were normalized to actin levels using ImageLab™ 5.2.1 software (BioRad). Results
 4 are presented as mean \pm s.d. and are from three independent experiments. The dashed line
 5 indicates values from control-transfected cells set at 100%. Statistics: *, p -value < 0.05, t-
 6 test. Right: representative Western blot analysis. (C) Analysis of miRNA targeting of *OGT*
 7 expression by dual luciferase reporter assay. Left: HeLa cells were co-transfected with a
 8 miR-501-3p mimic and a dual luciferase reporter plasmid containing either wild type miR-
 9 501-3p (RLuc wt *OGT* 3'UTR) or mutated miR-501-3p binding site (RLuc mt *OGT* 3'UTR) to
 10 modulate RLuc expression. Co-transfection of the miR-501-3p mimic and empty RLuc vector
 11 was used as control. Data are expressed as mean percentage of *Renilla* luciferase activity \pm
 12 s.d. normalized to *firefly* luciferase, and relative to co-transfection of the vectors with non-
 13 targeting miRNA (miR-Ctrl). Results are from three independent experiments in triplicate.
 14 The dashed line indicates values from control-transfected cells set at 100%. Statistics: *, p -
 15 value < 0.05, t-test. Right: Schematic representation of the used constructs.

17 **Figure 4. Silencing of *OGT* affects HCV morphogenesis and infectivity.** (A) Analysis of
 18 HCV infectivity. Huh7.5.1 cells were transfected with siCtrl, a pool of siRNA against *OGT* or
 19 ApoE as a loss-of-function control to perturb HCV assembly, prior to infection with HCVcc
 20 (Jc1) two days later (entry and replication). Mock-transfected cells were used as control
 21 (Ctrl). After another 48h, intra- and extracellular HCVcc particles were used to infect naïve
 22 Huh7.5.1 cells (assembly and infectivity). Virus supernatants of Huh7.5.1 cells were assayed
 23 by (left) endpoint dilution assay (TCID₅₀). Intra- and extracellular HCV RNA was purified and
 24 analyzed by RT-qPCR to calculate (right) the specific infectivity (TCID₅₀/RNA). Data are
 25 expressed as mean percentage as compared to control \pm s.d. Results are from four
 26 independent experiments in triplicate. The dashed line indicates values from control-
 27 transfected cells set at 100%. Statistics: *, p -value < 0.05, Mann-Whitney test. (B) Genotype-
 28 independent effect of *OGT* on HCV infection. Huh7.5.1 cells were transfected with siCtrl or

1 siOGT prior to infection with HCVcc JcR2a (genotype 2a), H77R2a (genotype 1a) or
 2 Con1R2a (genotype 1b). Experiments were carried out and analyzed as described in A. Data
 3 are expressed as mean percentage of Renilla luciferase activity as compared to control \pm s.d.
 4 Results are from three independent experiments in quadruplicate. The dashed line indicates
 5 values from control-transfected cells set at 100%. Statistics: *, p -value < 0.05, Mann-Whitney
 6 test. (C) Activity of OGT/OGA inhibitors on O-GlcNAcylation. The activity of Ac₄5S-GlcNAc
 7 (OGT inhibitor) or Thiamet G (OGA inhibitor) on O-GlcNAcylation of proteins in Huh7.5.1
 8 cells was demonstrated by Western blot as described in Supplementary Methods. (D) Effect
 9 of O-GlcNAcylation on HCV infectivity. Huh7.5.1 cells were electroporated with HCVcc
 10 (JcR2a), prior to treatment with increasing concentrations of Ac₄5S-GlcNAc (OGT inhibitor,
 11 left) or Thiamet G (OGA inhibitor, right) 4h later. After 96h, supernatants were transferred
 12 onto naïve Huh7.5.1 cells and electroporated cells were lysed to determine luciferase
 13 activity. Luciferase activity in infected Huh7.5.1 cells was assessed 72h later. Data are
 14 expressed as mean percentage as compared to control \pm s.d. Results are from three
 15 independent experiments in quadruplicate. The dashed line indicates values from vehicle-
 16 treated cells set at 100%. Statistics: *, p -value < 0.05, Mann-Whitney test.

Figure 5. Silencing of OGT modulates HCVcc biophysical properties. (A) Separation of
 HCVcc by iodixanol density gradient ultracentrifugation. HCVcc were produced in non-
 targeting siRNA control- or siOGT-transfected Huh7.5.1 cells. After overlaying HCVcc
 (JcR2A) on a 4%-40% iodixanol step gradient and ultracentrifugation for 16h, fractions of
 HCV particles were used to infect naïve Huh7.5.1 cells in order to determine TCID₅₀. HCV
 RNA of each fraction was purified and analyzed by RT-qPCR. Data are expressed as mean \pm
 s.d. from three independent experiments. (B) Specific infectivity (TCID₅₀/RNA) was
 calculated and the density was determined by weighting each fraction. Specific infectivity of
 each fraction is expressed as fold change as compared to the total infectivity of the control.
 Data are expressed as mean \pm s.d. from three independent experiments. (C-D) ApoE and
 ApoB concentrations in the individual fractions were determined by ELISA. The dashed lines

indicate limits of quantification of the assays. Data are expressed as mean \pm s.d. from three independent experiments.

Figure 6. Silencing of *OGT* increases the size of HCVcc. (A) Representative pictures of HCV particles generated in Huh7.5.1 cells transfected with non-targeting siRNA (siCtrl) or siOGT. (B-F) Comparative analysis of particle size distribution for immunocapture (IC) from HCV particles produced in Huh7.5.1 cells transfected with siCtrl or siOGT prior to infection with HCVcc (JcR2a) following sucrose-cushion purification (B) or iodixanol gradient fractionation (C-F) of HCVcc. HCVcc were transferred via anti-E2 antibody AR3A on electron microscopy (EM) grids through IC. Particle size distribution was assessed from a series of randomly acquired electron micrographs with Image-J software (NIH). Results from one of three (A-B) or two (C-F) independent experiments are shown. Black lines: size distribution of immunocaptured HCVcc produced in siCtrl-transfected cells. Grey lines: size distribution of immunocaptured HCVcc produced in siOGT-transfected cells.

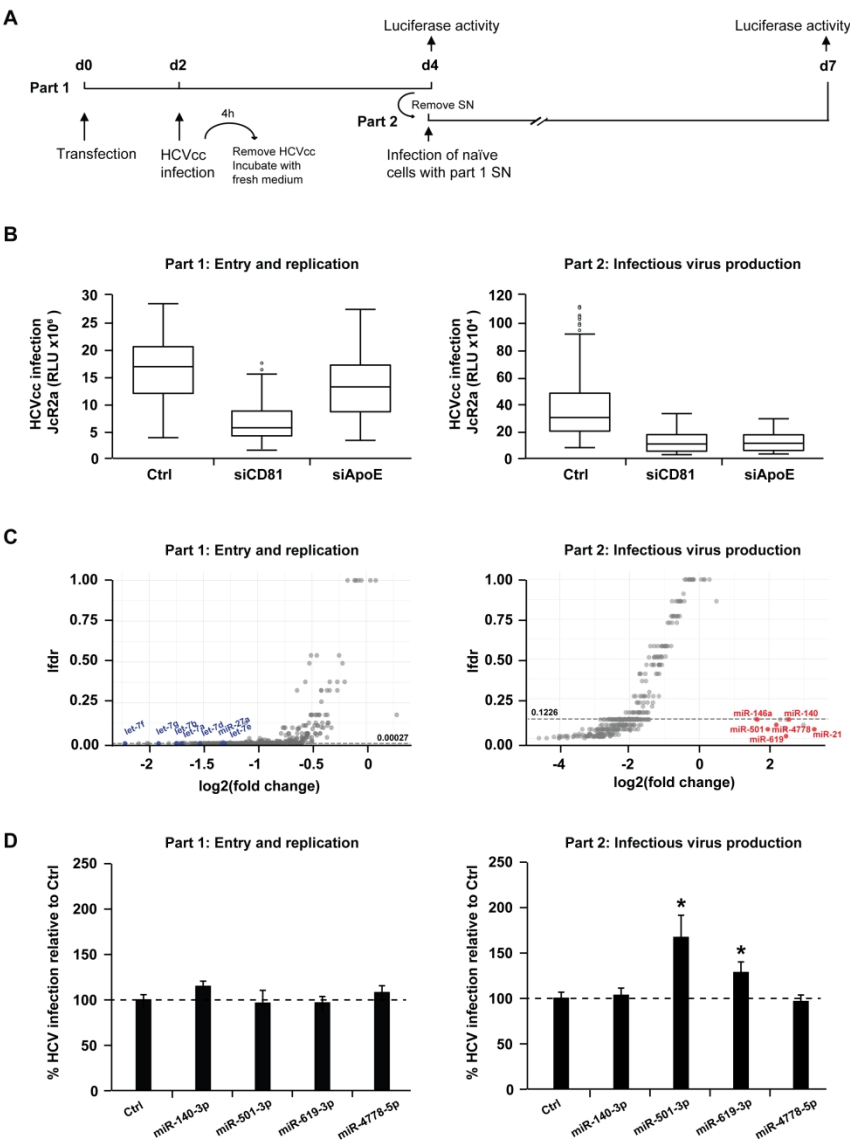
Figure 7. *OGT* expression increases in HCC. (A-B) Huh7.5.1 cells were infected with HCV (JcR2a). After 72h, RNA and proteins were purified, and *OGT* expression analyzed by RT-qPCR and Western blot. (A) Percentage of *OGT* mRNA expression relative to uninfected Huh7.5.1 cells (Ctrl). Results are presented as mean \pm s.d. from three independent experiments in duplicate. The dashed line indicates values from uninfected Huh7.5.1 cells set at 100%. Statistics: *, p -value < 0.05, Mann-Whitney test. (B) *OGT* protein expression. Left: percentage of *OGT* protein expression relative to uninfected Huh7.5.1 cells (Ctrl) following quantification of Western blots as described in Supplementary Methods. Results are presented as mean \pm s.d. from three independent experiments. The dashed line indicates values from uninfected Huh7.5.1 cells set at 100%. Statistics: *, p -value < 0.05, Mann-Whitney test. Right: representative Western blot analysis of *OGT* and actin. (C) *OGT* expression and viral load in liver tissue from 22 HCV-infected patients and 6 patients not infected with HCV described in[55]. Spearman correlation: ρ = 0.06004019, p -value = 0.77.

1
2
3
4
5
6
7
8
9
10
11
12
13
14
15
16
17
18
19
20
21
22
23
24
25
26
27
28
29
30
31
32
33
34
35
36
37
38
39
40
41
42
43
44
45
46
47
48
49
50
51
52
53
54
55
56
57
58
59
60

(D-E) OGT expression in liver tissue from 22 HCV-infected patients and 6 patients not infected with HCV according to fibrosis (D) or activity (E) scores described in[55]. Wilcoxon test: F1 vs F0 p-value = 0,38; F2 vs F0 p-value = 0,18; F3 vs F0 p-value = 0,43; F4 vs F0 p-value = 0,17; A1 vs A0 p-value = 0,28; A2 vs A0 p-value = 0,23; A3 vs A0 p-value = 0,09. (F) OGT expression in tumor (HCC) and non-tumor (Ctrl) liver tissue from 39 HCV-infected patients, 83 HBV-infected, 80 patients with alcoholic liver disease (ALD) and 13 patients with non-alcoholic liver disease (NAFLD) as described in Supplementary Methods. *, *p*-value < 0.05, Wilcoxon test.

Table 1. Computational analysis of miR-501-3p and miR-619-3p targets and pathway enrichment.

miRNA ID	Target gene symbol	Pathway or network
miR-501-3p	<i>MEF2A; PPP3CA; PPP3CC</i>	<i>Calcium signaling</i>
	<i>HMGCS1</i>	<i>Cholesterol biosynthesis</i>
	<i>AFF4; CHMP1B; CUX1; DCLK1;</i>	Inflammatory response, dermatological
	<i>LMX1A; PTBP2; RBMS1; RC3H1;</i>	diseases and conditions, inflammatory
	<i>SCN2A; SEC63; ZFH4</i>	disease
	<i>CDK6; CSDE1; GLI2; HOXD10;</i>	Cellular development, nervous system
	<i>LSM5; MEF2A; MYCN; OGT;</i>	development and function; organ
	<i>PPP2R2C; PPP2R5E; SEMA3C;</i>	morphology
	<i>TFDP2</i>	
	<i>CIT; COL10A1; FBNP1L; GAN;</i>	Cell death and survival; cellular
miR-619-3p	<i>HERC1; KPNA4; NONO; SHPRH;</i>	compromise; free radical scavenging
	<i>STRN; TARDBP; UBE2H; USP37</i>	
	<i>ATXN1; CBLL1; CEBPA; DCC;</i>	Cell morphology, cellular assembly and
	<i>PEX5L; RCC2; RNF144A; ZC3H12C</i>	organization; cellular function and
		maintenance
	<i>RUNX1T1; SMAD3</i>	<i>Adipocyte biogenesis</i>
	<i>FOXG1; GPBP1; MID1; MKL2; MSI1;</i>	Cell cycle; organismal injury and
	<i>PCBP2; WDFY3</i>	abnormalities; cancer
	<i>ACVR2B; DCX; ESRRG; MAPK9;</i>	Carbohydrate metabolism, energy
	<i>OGT; PCBP1; PDE3B; SMAD3;</i>	production; small molecule biochemistry
miR-619-3p	<i>SMARCC1; TGFB3; PAPOLA</i>	
	<i>RUNX1T1; SHANK2; SLC35D1</i>	Gene expression, lipid metabolism, small molecule biochemistry



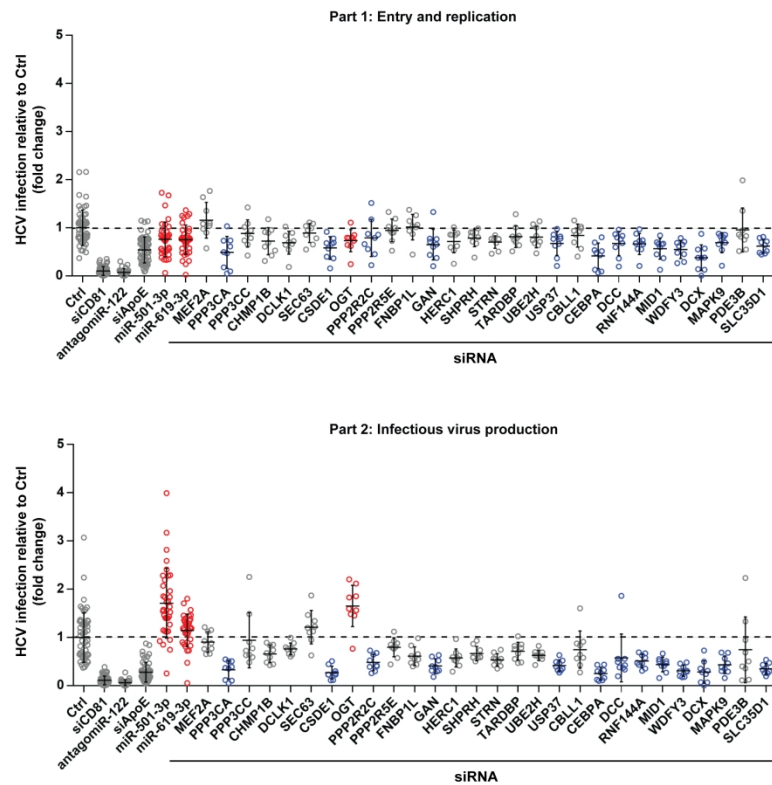


Figure 2

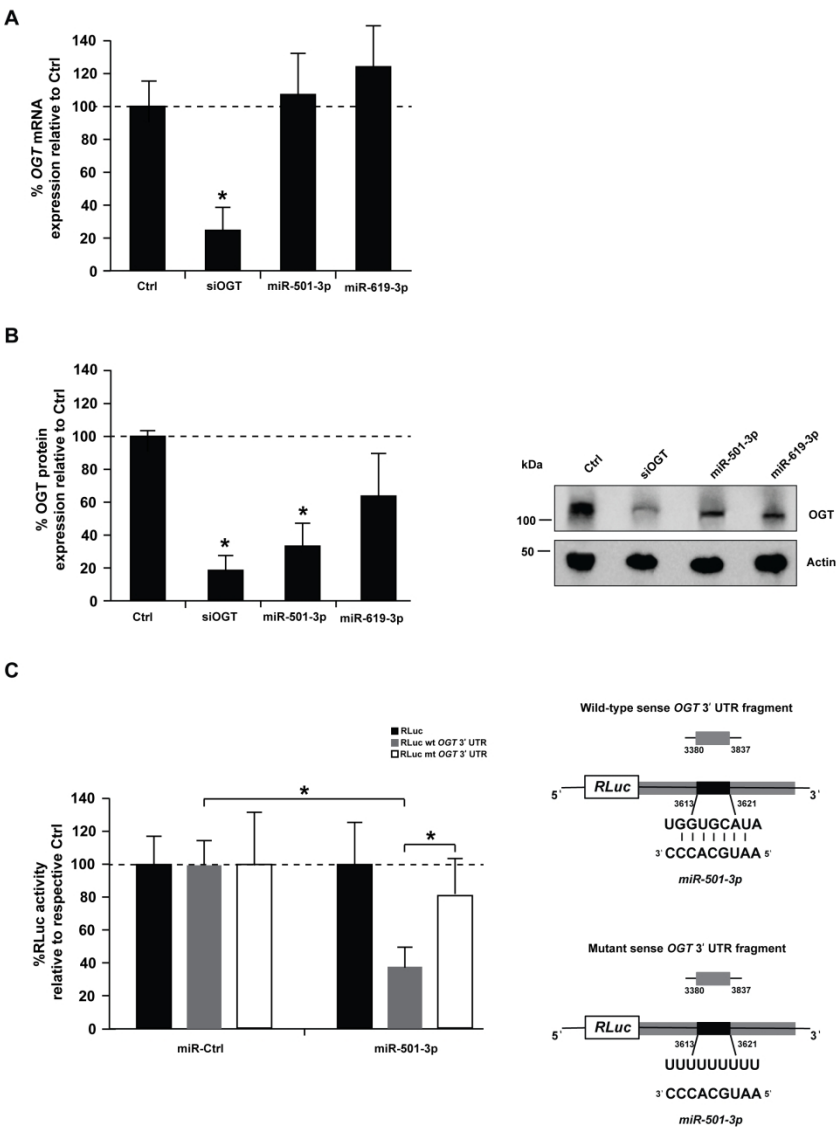


Figure 3

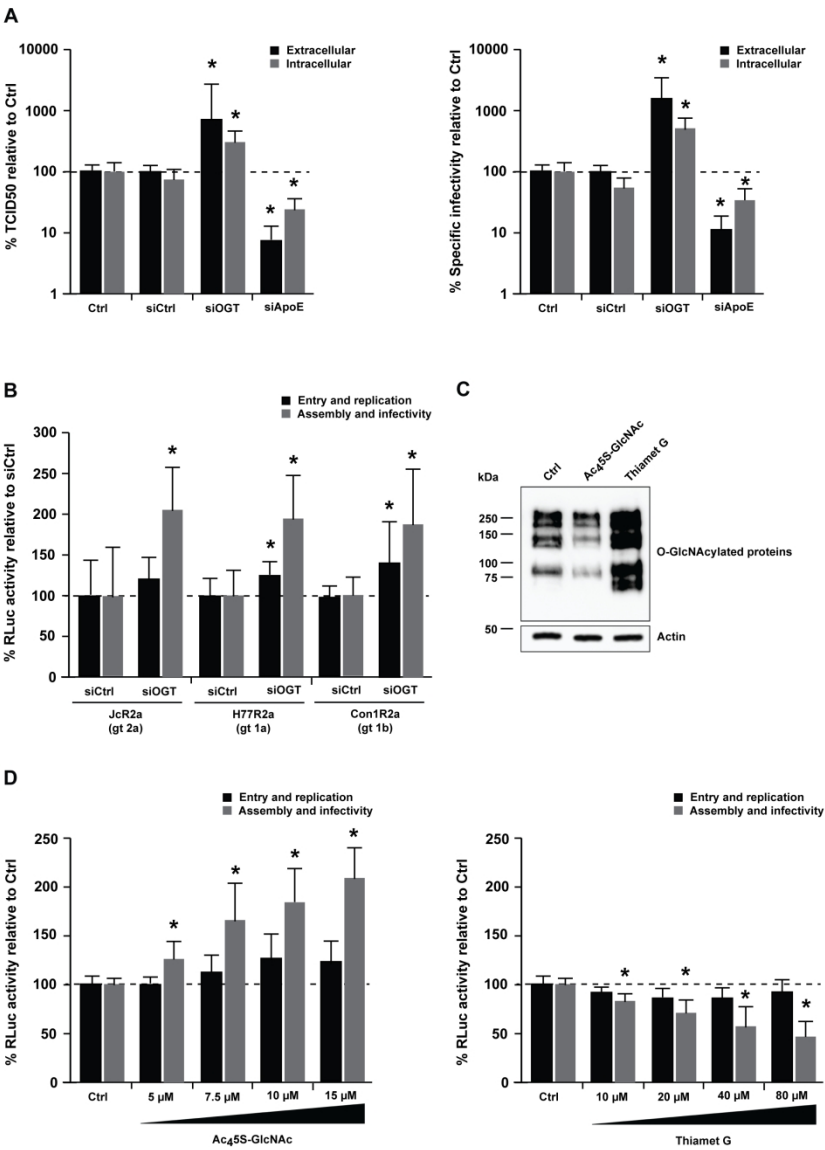


Figure 4

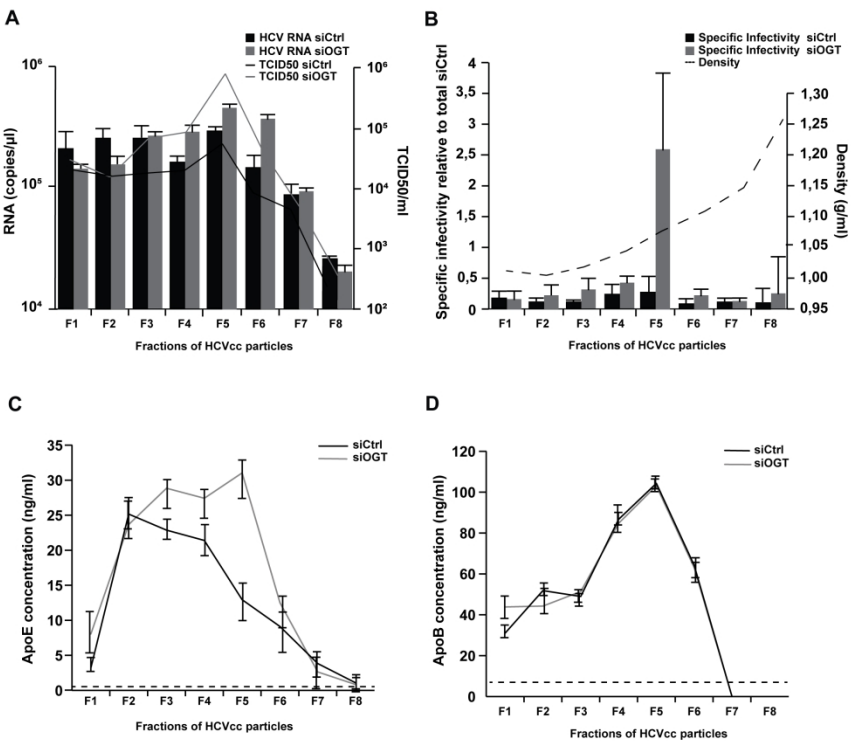


Figure 5

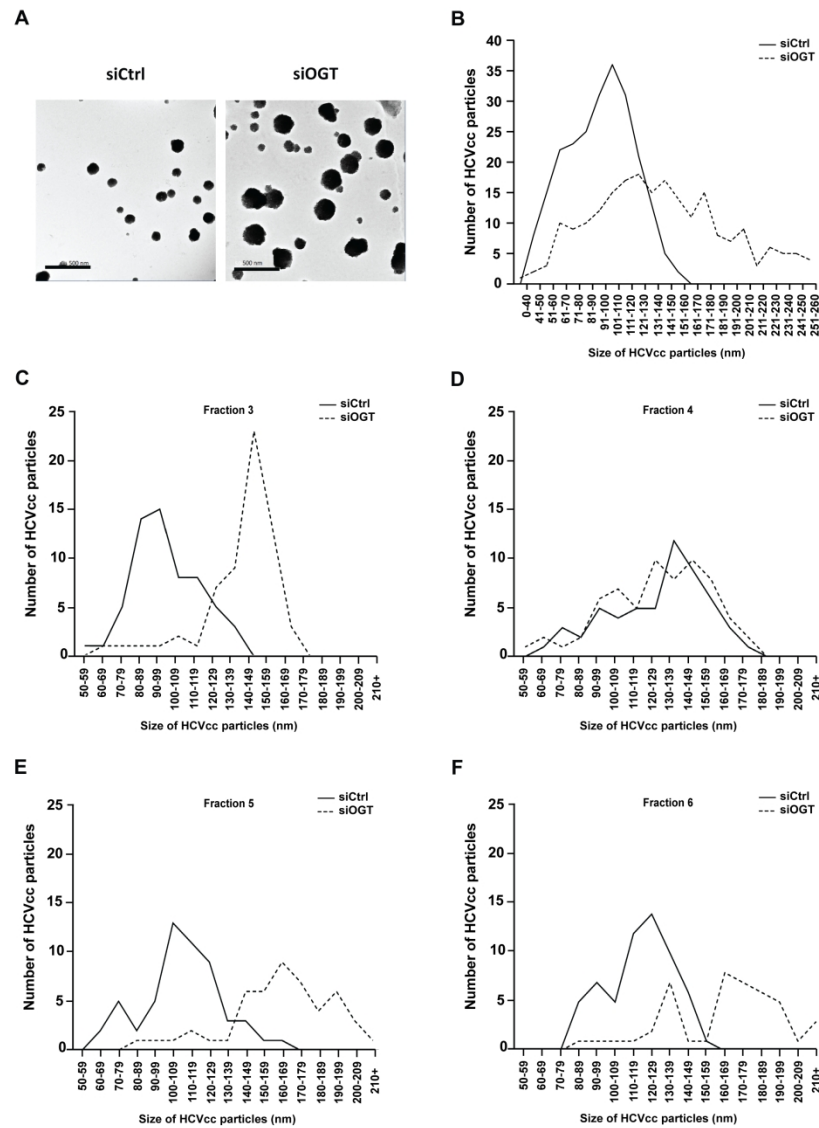


Figure 6

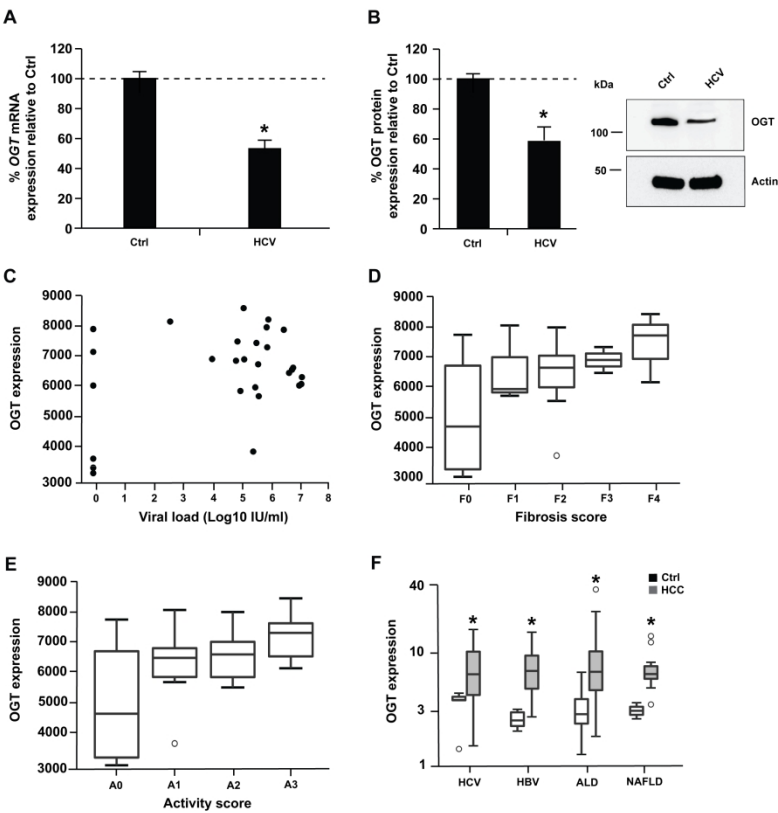


Figure 7

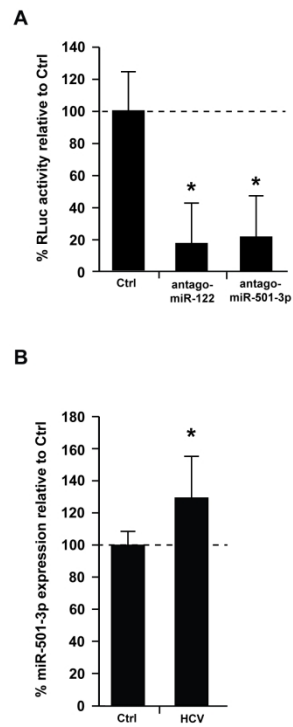


Figure S1

Supplementary Information

A functional microRNA screen uncovers O-linked N-acetylglucosamine transferase as a host factor modulating hepatitis C virus morphogenesis

Katharina Herzog^{1,2*}, Simonetta Bandiera^{1,2*}, Sophie Pernot^{1,2}, Catherine Fauvelle^{1,2}, Frank Jühling^{1,2}, Amélie Weiss^{2,3,4,5}, Anne Bull⁶, Sarah C. Durand^{1,2}, Béatrice Chane-Woon-Ming^{2,7}, Sébastien Pfeffer^{2,7}, Marion Mercey⁸, Hervé Lerat⁸, Jean-Christophe Meunier⁶, Wolfgang Raffelsberger^{2,3,4,5}, Laurent Brino^{2,3,4,5}, Thomas F. Baumert^{1,2,9,#}, Mirjam B. Zeisel^{1,2,10,#}

¹Inserm, U1110, Institut de Recherche sur les Maladies Virales et Hépatiques, Strasbourg, France; ²Université de Strasbourg, Strasbourg, France; ³Institut de Génétique et de Biologie Moléculaire et Cellulaire, Illkirch, France ; ⁴CNRS, UMR7104, Illkirch, France ; ⁵Inserm, U1258, Illkirch, France ; ⁶Inserm U1259, Faculté de Médecine, Université François Rabelais and CHRU de Tours, Tours, France ; ⁷Architecture et Réactivité de l'ARN – UPR 9002, Institut de Biologie Moléculaire et Cellulaire du CNRS, Strasbourg, France; ⁸Institute for Advanced Biosciences, Centre de Recherche UGA - Inserm U1209 - CNRS UMR 5309, Grenoble, France, ⁹Institut Hospitalo-Universitaire, Pôle Hépato-digestif, Hôpitaux Universitaires de Strasbourg, Strasbourg, France; ¹⁰Inserm, U1052, CNRS UMR 5286, Centre Léon Bérard (CLB), Cancer Research Center of Lyon (CRCL), Université de Lyon (UCBL), Lyon, France

*Authors contributed equally to this work

Supplementary Material and methods

Cells and cell culture conditions. The source and culture conditions of Huh7.5.1 cells have been described[1]. HeLa cells were purchased from ATCC and cultured in Dulbecco's modified Eagle medium (Gibco® DMEM GlutaMAX™, ThermoFisher Scientific) containing 1% sodium pyruvate as described for Huh7.5.1 cells[1].

Viruses and infectivity assays. Cell culture-derived recombinant cell culture-derived hepatitis C virus (HCVcc) Jc1 (genotype 2a/2a chimera), H77R2a (genotype 1a/2a chimera engineered for *Renilla* luciferase expression), Con1R2a (genotype 1b/2b chimera engineered for *Renilla* luciferase expression), and JcR2a (genotype 2a/2a chimera engineered for *Renilla* luciferase expression) were generated in Huh7.5.1 cells as described[1, 2, 3, 4]. HCVcc infectivity was determined by calculating the 50% tissue culture infectious dose (TCID₅₀) using anti-NS5A antibody as described[5, 6] or by assessing luciferase activity. HCVcc were used at 10⁵-10⁶ TCID₅₀/mL throughout the study. HCV RNA was purified using a QIAmp viral RNA minikit (Qiagen) and analyzed by one-step RT-qPCR using a Sensi Fast NO ROX kit (Bioline) according to the manufacturer's instructions. Standard curves were performed using 10-fold dilution series of HCV RNA.

Purification of HCVcc particles using sucrose cushion or iodixanol density gradient.

HCVcc (JcR2a) were concentrated 10-fold using a Vivaspin column (GE Healthcare). For sucrose cushion purification, HCVcc were purified by overlaying 3.5 mL of culture media on 1.5 mL of 20% sucrose, and by ultracentrifuging samples for 4h at 40,000 rpm on a SW-55 rotor (Beckman Coulter). Purified HCVcc were resuspended in 30 µL of PBS for analysis via immunocapture and electron microscopy. Density distributions of infectious HCVcc were determined by overlaying 0.5 mL culture media on a 5 mL, 4%-40% iodixanol step gradient, and ultracentrifuging samples for 16h at 40,000 rpm on a SW-55 rotor (Beckman Coulter): 625 µL fractions were carefully harvested from the top of each tube, and density was determined by weighing. Infectivity of each fraction was quantified by TCID₅₀ using anti-NS5A antibody as described[5, 6], while HCV RNA of fractions was purified and analyzed as described above. ApoB and ApoE concentrations of fractions were determined by enzyme-linked immunosorbent assay (Human Apolipoprotein B or E ELISA^{PRO} kit, Mabtech) undiluted or in a 1:50 dilution, respectively, according to the manufacturer's instructions (Mabtech).

1
2
3
4
5
6
7
8
9
10
11
12
13
14
15
16
17
18
19
20
21
22
23
24
25
26
27
28
29
30
31
32
33
34
35
36
37
38
39
40
41
42
43
44
45
46
47
48
49
50
51
52
53
54
55
56
57
58
59
60

miRNA mimics and siRNAs. Non-targeting control miRNA, miR-501-3p mimic, miR-619-3p mimic, antagomiR-122, antagomiR-501-3p, non-targeting control antagomiR, non-targeting control siRNA, siRNAs targeting *OGT*, *CD81* or *apolipoprotein E (ApoE)* and a library of 28 custom ON-TARGETplus smart pool siRNAs were purchased from Dharmacon (GE Healthcare).

miRNA expression analysis. Total RNA (100 ng) was purified from control or HCV-infected Huh7.5.1 cells using Tri reagent® (Thermo Scientific) and Direct-zol™ RNA purification kit (Zymo Research). Total RNA was first polyadenylated and reverse transcribed using a miScript II RT system (Qiagen) according to the manufacturer's instructions. The obtained cDNA was subjected to RT-qPCR using miScript SYBR Green kit (Qiagen). Primers were the mature miRNA sequence for the forward primer (Thermo Scientific) and the universal miScript primer (Qiagen) for the reverse primer. Data were analyzed by the $\Delta\Delta C_t$ method using small nucleolar RNA, C/D box 61 (SNORD61) as an endogenous reference and the non-infected samples as a calibrator[7].

Antibodies. Rabbit anti-OGT antibodies DM-17 and AL24 were purchased from Sigma or kindly provided by Dr. G. W. Hart and Dr. S. Hardivillé (Johns Hopkins University School of Medicine, Baltimore, MD)[8], respectively. Mouse anti- β -actin antibody was purchased from Abcam and mouse, rabbit or sheep HRP-conjugated secondary antibodies (A9044, A0545 and A3415, respectively) were purchased from Sigma. Sheep anti-NS5A serum for determination of TCID50 was a kind gift from M. Harris[9]. Human anti-E2 (AR3A) antibody[10] for electron microscopy analysis was kindly provided by Mansun Law (SCRIPPS, California, USA).

Western blotting. OGT and actin protein expression in human cells was assessed by Western blot as described[8] with some modifications. Briefly, cells were lysed in lysis buffer no. 6 (R&D Systems) according to the manufacturer's instructions. Equal amounts of protein

(40 µg) were size-separated through a Mini PROTEAN® TGX Stain-Free™ gel electrophoresis (Bio-Rad) and transferred to PVDF membranes (Bio-Rad). Immunoblots were performed using rabbit anti-OGT (1:2000) and mouse anti-β-actin (1:1000) antibodies[8, 11]. Antigen-antibody complexes were detected by incubating the membrane with the appropriate HRP-conjugated secondary antibodies (1:5000; 1:10,000) and imaged by enhanced chemiluminescence with a ChemiDoc MP imager (Bio-Rad). Quantification of protein expression was performed using ImageLab™ 5.2.1 software (BioRad). For analysis of OGT and GAPDH expression in liver tissue from HCV transgenic (FL-N/35) or wild-type mice[12], crude protein extracts were prepared by homogenization of frozen mouse livers (50–100 µg) in tissue lysis buffer from the Ambion PARIS RNA (Thermo Scientific) and protein isolation kit, supplemented with protease inhibitors (cOmplete™ EDTA-free protease inhibitor mixture, Sigma-Aldrich) and phosphatase inhibitors (PhosSTOP™, Sigma-Aldrich), using a tissue homogenizer (MP Fast Prep24, MP Biomedicals, Santa Ana, CA) and MP Lysing Matrix A tubes. Proteins were quantified using the BCA assay (Thermo Fisher Scientific). Western blotting was performed as described above.

Immunocapture and electron microscopy analysis of viral particles. Sucrose-cushion purified or iodixanol gradient fractionated HCVcc (JcR2a) produced in cells transfected with a non-targeting siRNA control or a pool of siRNA against OGT were transferred via anti-E2 antibody AR3A on electron microscopy (EM) grids through immunocapture (IC) as described[13]. Particles were stained with uranyl acetate dihydrate and observed in a JEOL 1230 electron microscope. Series of electron micrographs were acquired at random from IC EM grids. The images were then analyzed with Image-J software, to determine the particle size distribution.

Gene expression analysis in patient-derived liver tissue. For OGT expression analysis in patient's samples, raw data were retrieved from the Gene Expression Omnibus (GSE84346) and re-analyzed by quality-trimming (cutadapt) and mapping (HISAT2) to human genome

1
2
3 1 assembly hg19. Reads mapping to Gencode v.19 genes were counted using htseq-count and
4
5 2 normalized applying DESeq2. Activity and fibrosis scores as well as viral load were taken from
6
7 3 the supplemental data published in[14]. To analyze OGT expression in liver tissue of chronic
8
9 4 hepatitis B or C patients, FPKM values and clinical data were retrieved from The Cancer
10
11 5 Genome Atlas (TCGA, [https://www.cancer.gov/about-](https://www.cancer.gov/about-nci/organization/ccg/research/structural-genomics/tcga)
12
13 6 [https://www.cancer.gov/about-](https://www.cancer.gov/about-nci/organization/ccg/research/structural-genomics/tcga)
14
15 7 39 HCV-infected patients, 83 hepatitis B virus (HBV)-infected, 80 patients with alcoholic liver
16
17 8 disease (ALD) and 13 patients with non-alcoholic fatty liver disease (NAFLD).
18
19
20 9

21
22 10 **Supplementary References**

23
24 11 1 Zhong J, Gastaminza P, Cheng G, *et al.* Robust hepatitis C virus infection in vitro. Proc
25
26 12 Natl Acad Sci U S A 2005;**102**:9294-9.
27
28 13 2 Reiss S, Rebhan I, Backes P, *et al.* Recruitment and activation of a lipid kinase by
29
30 14 hepatitis C virus NS5A is essential for integrity of the membranous replication compartment.
31
32 15 Cell Host Microbe 2011;**9**:32-45.
33
34 16 3 Da Costa D, Turek M, Felmlee DJ, *et al.* Reconstitution of the entire hepatitis C virus
35
36 17 life cycle in non-hepatic cells. J Virol 2012;**86**:11919-25.
37
38 18 4 Fauvelle C, Felmlee DJ, Crouchet E, *et al.* Apolipoprotein E Mediates Evasion From
39
40 19 Hepatitis C Virus Neutralizing Antibodies. Gastroenterology 2016;**150**:206-17 e4.
41
42 20 5 Lindenbach BD, Evans MJ, Syder AJ, *et al.* Complete replication of hepatitis C virus in
43
44 21 cell culture. Science 2005;**309**:623-6.
45
46 22 6 Bandiera S, Pernot S, El Saghire H, *et al.* Hepatitis C Virus-Induced Upregulation of
47
48 23 MicroRNA miR-146a-5p in Hepatocytes Promotes Viral Infection and Deregulates Metabolic
49
50 24 Pathways Associated with Liver Disease Pathogenesis. J Virol 2016;**90**:6387-400.
51
52 25 7 Schmittgen TD, Livak KJ. Analyzing real-time PCR data by the comparative C(T)
53
54 26 method. Nat Protoc 2008;**3**:1101-8.
55
56 27 8 Iyer SP, Akimoto Y, Hart GW. Identification and cloning of a novel family of coiled-coil
57
58 28 domain proteins that interact with O-GlcNAc transferase. J Biol Chem 2003;**278**:5399-409.
59
60

Macdonald A, Crowder K, Street A, *et al.* The hepatitis C virus non-structural NS5A protein inhibits activating protein-1 function by perturbing ras-ERK pathway signaling. *J Biol Chem* 2003;**278**:17775-84.

Giang E, Dorner M, Prentoe JC, *et al.* Human broadly neutralizing antibodies to the envelope glycoprotein complex of hepatitis C virus. *Proc Natl Acad Sci U S A* 2012;**109**:6205-10.

Verrier ER, Colpitts CC, Bach C, *et al.* A targeted functional RNA interference screen uncovers glypican 5 as an entry factor for hepatitis B and D viruses. *Hepatology* 2016;**63**:35-48.

Lerat H, Honda M, Beard MR, *et al.* Steatosis and liver cancer in transgenic mice expressing the structural and nonstructural proteins of hepatitis C virus. *Gastroenterology* 2002;**122**:352-65.

Piver E, Boyer A, Gaillard J, *et al.* Ultrastructural organisation of HCV from the bloodstream of infected patients revealed by electron microscopy after specific immunocapture. *Gut* 2017;**66**:1487-95.

Boldanova T, Suslov A, Heim MH, *et al.* Transcriptional response to hepatitis C virus infection and interferon-alpha treatment in the human liver. *EMBO Mol Med* 2017;**9**:816-34.

Supplementary figure legends

Figure S1. (A) Effect of miR-501-3p inhibition on HCV infectivity. Huh7.5.1 cells were transfected with control antagomiR (Ctrl), antagomiR-122 as loss-of-function control to perturb HCV replication and antagomiR-501-3p, prior to infection with HCVcc (JcR2a) according to the two-step protocol depicted in Fig. 1A. After 48h, supernatants were transferred onto naive Huh7.5.1 cells. After 72h, Renilla Luciferase activity of infected Huh7.5.1 cells was determined. Data are expressed as mean percentage as compared to Ctrl \pm s.d. Results are from four independent experiments in quadruplicate. The dashed line indicates values from vehicle-treated cells set at 100%. Statistics: *, p -value < 0.05, Mann-Whitney test. (B) miR-501-3p expression upon HCV infection. Huh7.5.1 cells were infected with HCVcc (JcR2a).

1
2
3
4
5
6
7
8
9
10
11
12
13
14
15
16
17
18
19
20
21
22
23
24
25
26
27
28
29
30
31
32
33
34
35
36
37
38
39
40
41
42
43
44
45
46
47
48
49
50
51
52
53
54
55
56
57
58
59
60

1 After 72h, RNA was purified and miR-501-3p expression analyzed by RT-qPCR. Percentage
2 of miR-501-3p expression relative to uninfected Huh7.5.1 cells (Ctrl). Results are presented
3 as mean \pm s.d. from three independent experiments in duplicate. The dashed line indicates
4 values from uninfected Huh7.5.1 cells set at 100%. Statistics: *, p -value < 0.05, Mann-Whitney
5 test.

7 **Supplementary Table 1. A genome-wide miRNA mimic screen identifies cellular**
8 **miRNAs modulating HCV infection.** Log2(FC), lfdr and effect on HCV infection in part 1 and
9 part 2 of the screen are shown for the individual miRNAs of the miRNA mimic library. In red:
10 proviral effect, in blue: antiviral effect. FC: fold change, lfdr: local false discovery rate

miRNA ID	Mature Sanger ID	Library ID	Mature Sequence	Log2(FC)	Part 1	Part 2
					hfr	Effect on HCV
hsa-miR-7a	MIMAT0000062	C-300473-05	UGAGGUAGUAGGUAGUUAUAGU	-1.70171935969617	3.9917e-05	TRUE
hsa-miR-7b	MIMAT0000063	C-300476-05	UGAGGUAGUAGGUAGUUAUAGU	-1.74884091191792	8.3715e-05	TRUE
hsa-miR-7d	MIMAT0000065	C-300478-07	AGAGGUAGUAGGUAGUUAUAGU	-1.53075932976348	0.00023985	TRUE
hsa-miR-7e	MIMAT0000066	C-300479-05	UGUUGGAGUAGGUAGUUAUAGU	-1.302187596011	0.001457	FALSE
hsa-miR-7f	MIMAT0000067	C-300480-05	UGAGGUAGUAGGUAGUUAUAGU	-2.22178435619614	6.7884e-06	TRUE
hsa-miR-7g	MIMAT00000414	C-300583-05	UGAGGUAGUAGGUAGUUAUAGU	-1.91269526615093	6.7884e-06	TRUE
hsa-miR-101	MIMAT0000099	C-300518-07	UACAGUAGUAGGUAGUUAUAGU	-0.886376348041933	0.0030028	FALSE
hsa-miR-103-as	MIMAT0007402	C-301453-00	UAGAGCCUUGUAGGUAGUUAUAGU	-1.11208100417218	0.007487	FALSE
hsa-miR-106a*	MIMAT0004517	C-301159-01	CUGCAUUGUAGGUAGUUAUAGU	-1.32520110449511	3.9917e-05	TRUE
hsa-miR-1178	MIMAT0005823	C-301319-00	UUGUCUAGUAGGUAGUUAUAGU	-1.22556728667978	0.00061109	FALSE
hsa-miR-1178-5p	MIMAT0002940	C-301922-00	CAGGUAGUAGGUAGUUAUAGU	-1.16672245017752	0.00026644	TRUE
hsa-miR-1185	MIMAT0005798	C-301317-00	AGAGGUAGUAGGUAGUUAUAGU	-1.2315368528283	8.3715e-05	TRUE
hsa-miR-1200	MIMAT0005863	C-301326-00	CUCUAGUAGGUAGUUAUAGU	-1.24566404694154	0.00054279	FALSE
hsa-miR-1205	MIMAT0005869	C-301331-00	UUGUCUAGUAGGUAGUUAUAGU	-0.80151472738568	0.0033924	FALSE
hsa-miR-1207-3p	MIMAT0005872	C-301334-00	UAGGUAGUAGGUAGUUAUAGU	-1.10040811819255	0.0013963	FALSE
hsa-miR-122	MIMAT000421	C-300501-05	UGAGGUAGUAGGUAGUUAUAGU	-0.70369537171691	0.040577	FALSE
hsa-miR-122*	MIMAT0004590	C-301046-01	AACGCCUAGUAGGUAGUUAUAGU	-0.557131346052541	0.037103	FALSE
hsa-miR-1226	MIMAT0005577	C-301284-01	UACCCAGUAGGUAGUUAUAGU	-0.74174282716559	0.0099219	FALSE
hsa-miR-1228*	MIMAT0005582	C-301287-01	GUGGGGCGGAGGUAGUUAUAGU	-0.947568053691086	0.0049772	FALSE
hsa-miR-1237-5p	MIMAT0002946	C-302618-00	CGGGGGCGGAGGUAGUUAUAGU	-0.956259568604456	0.021994	FALSE
hsa-miR-1244	MIMAT0005896	C-301865-00	AAGUAGUAGGUAGUUAUAGU	-1.17945761818024	6.1693e-05	TRUE
hsa-miR-1245b-3p	MIMAT0019951	C-302405-00	UAGGUAGUAGGUAGUUAUAGU	-0.41484848981959	0.32544	FALSE
hsa-miR-125b-2-3p	MIMAT0005899	C-301882-00	AAGUAGUAGGUAGUUAUAGU	-0.42726873717492	0.061384	FALSE
hsa-miR-125b	MIMAT0005899	C-301884-00	AAGUAGUAGGUAGUUAUAGU	-1.57210875214914	1.5894e-05	TRUE
hsa-miR-125b-2*	MIMAT0004603	C-301061-01	UACAGUAGUAGGUAGUUAUAGU	-0.85902606837019	0.0052694	FALSE
hsa-miR-1260b	MIMAT0015041	C-301716-00	ACCCAGUAGGUAGUUAUAGU	-0.47631786253208	0.10991	FALSE
hsa-miR-1270	MIMAT0005924	C-301867-00	CUGGAGUAGGUAGUUAUAGU	-1.23553336541613	3.9917e-05	TRUE
hsa-miR-1277	MIMAT0005933	C-301411-00	UAGGUAGUAGGUAGUUAUAGU	-0.745198002045239	0.0074787	FALSE
hsa-miR-1278	MIMAT0005936	C-301417-00	UAGGUAGUAGGUAGUUAUAGU	-0.494528345361641	0.089234	FALSE
hsa-miR-128	MIMAT0005799	C-301315-00	UAGGUAGUAGGUAGUUAUAGU	-0.538161112092319	0.061384	FALSE
hsa-miR-1284	MIMAT0005941	C-301423-00	UAGGUAGUAGGUAGUUAUAGU	-0.41243673654273	0.099257	FALSE
hsa-miR-1287	MIMAT0005878	C-301341-00	UAGGUAGUAGGUAGUUAUAGU	-1.20683701032783	0.00023985	TRUE
hsa-miR-1288	MIMAT0005942	C-301424-00	UAGGUAGUAGGUAGUUAUAGU	-0.70489827053788	0.021078	FALSE
hsa-miR-129-3p	MIMAT0004605	C-301063-01	AAGUAGUAGGUAGUUAUAGU	-0.99962920325089	0.0021078	FALSE
hsa-miR-129	MIMAT0005881	C-301345-00	UGGGGAGUAGGUAGUUAUAGU	-1.212842026454	0.00061109	FALSE
hsa-miR-1293	MIMAT0005883	C-301347-00	UGGGGAGUAGGUAGUUAUAGU	-1.39687224389743	0.00026644	TRUE
hsa-miR-1294	MIMAT0005884	C-301348-00	UGGGGAGUAGGUAGUUAUAGU	-1.44051810095446	8.3715e-05	TRUE
hsa-miR-1295	MIMAT0005885	C-301349-00	UAGGGGAGUAGGUAGUUAUAGU	-1.2640855905457	0.00087976	FALSE
hsa-miR-1295b-5p	MIMAT0002293	C-302563-00	CAGGGGAGUAGGUAGUUAUAGU	-0.454374223389677	0.17522	FALSE
hsa-miR-1298	MIMAT0005800	C-301318-00	UAGGUAGUAGGUAGUUAUAGU	-0.26688291087125	0.32544	FALSE
hsa-miR-1302	MIMAT0005890	C-301869-00	UAGGGGAGUAGGUAGUUAUAGU	-1.35138412635794	3.6715e-05	TRUE
hsa-miR-1302	MIMAT0005890	C-301354-00	UAGGGGAGUAGGUAGUUAUAGU	-1.1168866347783	0.00013793	TRUE
hsa-miR-1307	MIMAT0005951	C-301434-00	UAGGUAGUAGGUAGUUAUAGU	-1.1204717697297	0.0004279	FALSE
hsa-miR-1307-5p	MIMAT0002727	C-301875-00	UAGGUAGUAGGUAGUUAUAGU	-0.8034810031417	0.0030028	FALSE
hsa-miR-1322	MIMAT0005953	C-301436-00	UAGGUAGUAGGUAGUUAUAGU	-1.23817643374983	6.1693e-05	TRUE
hsa-miR-1323	MIMAT0005795	C-301311-00	UAGGUAGUAGGUAGUUAUAGU	-0.756897047236657	0.096607	FALSE
hsa-miR-135b*	MIMAT0004698	C-301200-01	AAGUAGUAGGUAGUUAUAGU	-1.49530399618539	0.0018747	FALSE
hsa-miR-139-3p	MIMAT0004552	C-301036-03	UGAGGAGUAGGUAGUUAUAGU	-1.0205377094153	0.00079918	FALSE
hsa-miR-140-3p	MIMAT0004597	C-301055-01	UAGGGGAGUAGGUAGUUAUAGU	-0.17267560152275	1	FALSE
hsa-miR-142-3p	MIMAT0004034	C-300610-03	UAGGUAGUAGGUAGUUAUAGU	-1.00474764620935	0.00023985	TRUE
hsa-miR-146a	MIMAT0004449	C-300630-03	UAGGUAGUAGGUAGUUAUAGU	-0.279802119960867	0.17522	FALSE
hsa-miR-150*	MIMAT0004610	C-301067-01	UAGGUAGUAGGUAGUUAUAGU	-1.46501520999695	0.00023985	TRUE
hsa-miR-151b	MIMAT0010214	C-301973-00	UAGGUAGUAGGUAGUUAUAGU	-1.0368468961171	3.9917e-05	TRUE
hsa-miR-182	MIMAT0000259	C-300587-07	UAGGUAGUAGGUAGUUAUAGU	-0.581360116993454	0.03164	FALSE
hsa-miR-184	MIMAT0000454	C-300635-03	UGAGGAGUAGGUAGUUAUAGU	-1.3170077618768	3.9917e-05	TRUE
hsa-miR-185	MIMAT0000455	C-300636-07	UGAGGAGUAGGUAGUUAUAGU	-1.59673044023595	0.00013963	TRUE
hsa-miR-18b*	MIMAT0004751	C-301187-01	UGGGGAGUAGGUAGUUAUAGU	-0.825568919117559	0.0027607	FALSE
hsa-miR-1909	MIMAT0007883	C-301466-00	CGGGGAGUAGGUAGUUAUAGU	-0.511863313449074	0.17522	FALSE
hsa-miR-1915*	MIMAT0007891	C-301455-00	ACCUAGUAGGUAGUUAUAGU	-1.7193507114424	3.9917e-05	TRUE
hsa-miR-196b*	MIMAT0009201	C-301305-00	UAGGAGUAGGUAGUUAUAGU	-0.94390368412525	0.00054279	FALSE
hsa-miR-19b	MIMAT0000074	C-300489-03	UAGGUAGUAGGUAGUUAUAGU	-1.0416139258753	0.00013793	TRUE
hsa-miR-19b-1*	MIMAT0004481	C-301021-01	UAGGUAGUAGGUAGUUAUAGU	-1.88388148726454	0.0030028	FALSE
hsa-miR-19b-2*	MIMAT0004481	C-301022-01	UAGGUAGUAGGUAGUUAUAGU	-1.07103168148094	0.0030028	FALSE
hsa-miR-200b*	MIMAT0004571	C-301144-01	CAUUAUAGGUAGUUAUAGU	-1.05721574185849	0.0074787	FALSE
hsa-miR-203b-5p	MIMAT0019813	C-302277-00	UAGGUAGUAGGUAGUUAUAGU	-1.0335612225008	0.00016067	TRUE
hsa-miR-208a	MIMAT0000241	C-300537-03	AUAGGAGUAGGUAGUUAUAGU	-0.823665097293502	0.0030028	FALSE
hsa-miR-21	MIMAT0000076	C-300492-03	UAGGUAGUAGGUAGUUAUAGU	-0.76822663205262	0.096607	FALSE
hsa-miR-211-3p	MIMAT0022694	C-301905-00	CGAGGAGUAGGUAGUUAUAGU	-0.812107428438748	0.0027607	FALSE
hsa-miR-2114	MIMAT0011156	C-301489-00	UAGGUAGUAGGUAGUUAUAGU	-0.958796902783202	0.00016326	TRUE
hsa-miR-2114*	MIMAT0011157	C-301490-00	CGAGGAGUAGGUAGUUAUAGU	-1.02419077915881	0.00013793	TRUE
hsa-miR-2117	MIMAT0011162	C-301496-00	UAGGUAGUAGGUAGUUAUAGU	-0.80671734724896	0.00054279	FALSE
hsa-miR-216a-3p	MIMAT0022844	C-301886-00	UAGGUAGUAGGUAGUUAUAGU	-1.47806207174352	8.3715e-05	TRUE
hsa-miR-22	MIMAT000077	C-300493-03	UAGGUAGUAGGUAGUUAUAGU	-1.1626828808065	0.00054279	FALSE
hsa-miR-220b	MIMAT0005529	C-301218-01	CCAGGAGUAGGUAGUUAUAGU	-1.1086445415353	0.12653	FALSE
hsa-miR-221*	MIMAT0004568	C-301163-01	ACCUAGUAGGUAGUUAUAGU	-1.0647285020049	0.00016067	TRUE
hsa-miR-223*	MIMAT0004570	C-301197-01	CGUAGUAGGUAGUUAUAGU	-0.596047980424722	0.0074787	FALSE
hsa-miR-2276	MIMAT0011775	C-301481-00	UGGUAGUAGGUAGUUAUAGU	-1.23563628890583	3.9917e-05	TRUE
hsa-miR-2277-3p	MIMAT0011777	C-301482-00	UGGUAGUAGGUAGUUAUAGU	-1.22725149342576	3.9917e-05	TRUE
hsa-miR-23a*	MIMAT0004496	C-301025-01	GGGUAGUAGGUAGUUAUAGU	-0.773175976814457	0.0018747	FALSE
hsa-miR-25*	MIMAT0004498	C-301183-01	AGGGGAGUAGGUAGUUAUAGU	-1.14410824968417	0.0018747	FALSE
hsa-miR-2681-3p	MIMAT0013516	C-301978-00	UAGGUAGUAGGUAGUUAUAGU	-0.84154241088718	0.00023985	TRUE
hsa-miR-2682-3p	MIMAT0013518	C-301980-00	CGGUAGUAGGUAGUUAUAGU	-0.908772237884288	0.00013793	FALSE
hsa-miR-2682-5p	MIMAT0013517	C-301979-00	CAGGUAGUAGGUAGUUAUAGU	-1.24830345350196	1.5894e-05	TRUE
hsa-miR-26b	MIMAT0000083	C-300501-07	UAGGUAGUAGGUAGUUAUAGU	-0.405072630482104	0.12653	FALSE
hsa-miR-27a	MIMAT0000084	C-300502-03	UAGGUAGUAGGUAGUUAUAGU	-1.32790971191818	3.9917e-05	TRUE
hsa-miR-27a*	MIMAT0004501	C-301028-01	AGGGGAGUAGGUAGUUAUAGU	-0.887009503478049	0.0052694	FALSE
hsa-miR-27b*	MIMAT0004588	C-301154-01	AGAGGUAGUAGGUAGUUAUAGU	-1.00848877555625	0.0014577	FALSE
hsa-miR-28-5p	MIMAT0000085	C-300503-05	AGGGGAGUAGGUAGUUAUAGU	-0.35834466229635	0.17522	FALSE
hsa-miR-2861	MIMAT0013802	C-301642-00	GGGGGAGUAGGUAGUUAUAGU	-0.81548484708855	0.0046172	FALSE
hsa-miR-2964a-3p	MIMAT0019748	C-302218-00	AGGUAGUAGGUAGUUAUAGU	-1.13977373653624	6.1693e-05	TRUE
hsa-miR-298	MIMAT0004901	C-301692-00	UAGGUAGUAGGUAGUUAUAGU	-0.45612237350612	0.5468609121229	FALSE
hsa-miR-299	MIMAT0002880	C-300854-03	UGGUAGUAGGUAGUUAUAGU	-1.25864928851518	0.00023985	TRUE
hsa-miR-29a	MIMAT0004503	C-301178-01	ACGUAGUAGGUAGUUAUAGU	-1.35357089379882	0.0021076	FALSE
hsa-miR-29b-1*	MIMAT0004514	C-301150-01	CGGUAGUAGGUAGUUAUAGU	-0.970652939446982	0.015067	FALSE
hsa-miR-301b	MIMAT0004958	C-301252-01	CAGGUAGUAGGUAGUUAUAGU	-0.837318501823661	0.0014577	FALSE
hsa-miR-302b*	MIMAT0000714	C-300668-07	UAGGUAGUAGGUAGUUAUAGU	-0.550910910384927	0.037103	FALSE
hsa-miR-302f	MIMAT0005932	C-301410-00	UAGGUAGUAGGUAGUUAUAGU	-1.5960005623826	1.5894e-05	TRUE
hsa-miR-30b	MIMAT0000420	C-300590-03	UAGGUAGUAGGUAGUUAUAGU	-0.759206041294187	0.0018747	FALSE
hsa-miR-30c-1*	MIMAT0004674	C-301199-01	CUGGAGUAGGUAGUUAUAGU	-1.4378778685803	8.3715e-05	TRUE
hsa-miR-30c-2*	MIMAT0004550	C-301034-01	CUGGAGUAGGUAGUUAUAGU	-1.8694958597662	8.3715e-05	TRUE
hsa-miR-30d	MIMAT0000245	C-300543-03	UAGGUAGUAGGUAGUUAUAGU	-1.46973422958627	0.01326	FALSE
hsa-miR-3115	MIMAT0014977	C-301644-00	AUAGGUAGUAGGUAGUUAUAGU	-0.595634685518391	0.0052694	FALSE
hsa-miR-3116	MIMAT0014978	C-301645-00	UGGUAGUAGGUAGUUAUAGU	-1.81818516940984	6.7884e-06	TRUE
hsa-miR-3117	MIMAT0014979	C-301647-00	AUAGGUAGUAGGUAGUUAUAGU	-1.07944692693698	6.1693e-05	TRUE
hsa-miR-3119	MIMAT0014981	C-301651-00	UGGUAGUAGGUAGUUAUAGU	-0.77136494055742	0.00087976	FALSE
hsa-miR-3121	MIMAT0014983	C-301654-00	UAGGUAGUAGGUAGUUAUAGU	-0.550473953423974	0.0074787	FALSE
hsa-miR-3124	MIMAT0014986	C-301657-00	UGGGGAGUAGGUAGUUAUAGU	-1.13549064733399	3.9917e-05	TRUE
hsa-miR-3126-5p	MIMAT0014989	C-301661-00	UAGGGGAGUAGGUAGUUAUAGU	-1.43373948465677	1.5894e-05	TRUE
hsa-miR-3127	MIMAT0014990	C-301662-00	AUAGGGGAGUAGGUAGUUAUAGU	-0.992160086498039	0.00013793	TRUE
hsa-miR-3130-3p	MIMAT0014994	C-301665-00	CGGUAGUAGGUAGUUAUAGU	-0.845251817092445	0.0021076	FALSE
hsa-miR-3130-5p	MIMAT0014992	C-301663-00	UGGUAGUAGGUAGUUAUAGU	-1.15243166606231	6.1693e-05	TRUE
hsa-miR-3131	MIMAT0014996	C-301669				

<https://mc.manuscriptcentral.com/gut>

1	hsa-miR-4699-5p	MIMAT0019794	C-302259-00	AGAAAGUUGCAGAGUAGAUUCC	-0.32133335517737	0.096607	FALSE	-1.70896571432969	0.11887	TRUE
2	hsa-miR-4700-5p	MIMAT0019796	C-302262-00	UUGGGGAGGAGGAGGAGGAGGUGU	-0.63878129737828	0.0046172	FALSE	-2.49301512707352	0.023579	TRUE
3	hsa-miR-4701-5p	MIMAT0019798	C-302460-00	UUGGCCACACACACACACCCU	-1.25407592715591	0.00016326	TRUE	-2.10511844533172	0.1633	FALSE
4	hsa-miR-4706	MIMAT0019806	C-302269-00	AGGGGGGAGGAGGAGGAGGAGGUGU	-0.840574202002897	0.0030208	FALSE	-1.8037833355061	0.11887	TRUE
5	hsa-miR-4707-3p	MIMAT0019808	C-302270-00	AGCCGCGCCGAGGAGGAGGAGGUGU	-0.835246571498794	0.0007918	FALSE	-3.24071712891442	0.057617	TRUE
6	hsa-miR-4708-3p	MIMAT0019810	C-302273-00	AGCAAGCGGCGAGGAGGAGGAGGUGU	-0.96985371193823	0.00023985	TRUE	-0.525873276306624	0.86349	FALSE
7	hsa-miR-4708-5p	MIMAT0019809	C-302272-00	AGAGAUGGCCGUGGUGGUGU	-0.82268402582361	0.00079918	FALSE	-2.1022066879154	0.08542	TRUE
8	hsa-miR-4709-3p	MIMAT0019812	C-302275-00	UUGAAGAGGAGGUGGUGGUGGUGU	-0.66432740058703	0.0027607	FALSE	-1.68675985049984	0.11887	TRUE
9	hsa-miR-4709-5p	MIMAT0019811	C-302274-00	ACAACAGUAGGAGGAGGAGGAGGUGU	-1.0896980160567	9.6971e-05	TRUE	-0.80626334250579	0.5811	FALSE
10	hsa-miR-4711-5p	MIMAT0019816	C-302279-00	UGCAUCAGGCGGAGGAGGAGGAGGUGU	-0.502094584622719	0.015067	FALSE	-2.22495919207469	0.057617	TRUE
11	hsa-miR-4712-3p	MIMAT0019819	C-302282-00	AUAGAGGAGGAGGAGGAGGAGGUGU	-1.2600305636888	3.9917e-05	TRUE	-2.5282921027878	0.028781	TRUE
12	hsa-miR-4713-5p	MIMAT0019820	C-302283-00	UUCUCCACUACGAGGAGGAGGUGU	-1.410564942413791	3.6715e-05	TRUE	0.152837142024165	1	FALSE
13	hsa-miR-4714-5p	MIMAT0019822	C-302286-00	AACUCUGACCCUAGGUGGUGU	-0.971641326370144	0.00023985	TRUE	-1.9820676345786	0.08542	TRUE
14	hsa-miR-4715-3p	MIMAT0019825	C-302288-00	GUGCCACUUCUAGGAGGAGGAGGUGU	-0.837171497711227	0.0014577	FALSE	-1.6463933941666	0.11887	TRUE
15	hsa-miR-4720-3p	MIMAT0019834	C-302297-00	UGCUUAGUUGUAGGAGGAGGUGU	-0.267039311682	0.37761	FALSE	-2.41942301449004	0.057617	TRUE
16	hsa-miR-4726-3p	MIMAT0019846	C-302309-00	AGCCAGUUGCCUUGGUGGUGU	-1.05457826001572	0.0046172	FALSE	-1.96757030930303	0.11887	TRUE
17	hsa-miR-4726-5p	MIMAT0019845	C-302310-00	AGGCGGAGGAGGAGGAGGAGGUGU	-0.54873137329315	0.061384	FALSE	-2.20367296738285	0.11887	TRUE
18	hsa-miR-4730	MIMAT0019852	C-302314-00	CUGGCGGAGGAGGAGGAGGAGGUGU	-1.14323623137163	0.0021076	FALSE	-3.22072847594229	0.014453	TRUE
19	hsa-miR-4731-3p	MIMAT0019854	C-302316-00	CACACAAGUGGCCGCCACACU	-0.71528640890007	0.021994	FALSE	-2.11972721193743	0.11887	TRUE
20	hsa-miR-4733-5p	MIMAT0019857	C-302319-00	AUUCUCCAUUGGAGGAGGAGGUGU	-0.918486094585803	0.0074787	FALSE	-2.80327741332156	0.023579	TRUE
21	hsa-miR-4740-3p	MIMAT0019870	C-302329-00	GCCGAGAGGAGGAGGAGGAGGUGU	-0.824911201381423	0.015067	FALSE	-3.46216635615516	0.014453	TRUE
22	hsa-miR-4743-5p	MIMAT0019874	C-302462-00	UUGCCGAGGAGGAGGAGGAGGAGGUGU	-1.02760222969445	0.00061109	FALSE	-2.22597646616421	0.11887	TRUE
23	hsa-miR-4745-3p	MIMAT0019879	C-302464-00	UUGCCGCGGAGGAGGAGGAGGAGGUGU	-1.2374251488885	0.00016326	TRUE	-2.78131955234324	0.08542	TRUE
24	hsa-miR-4747-3p	MIMAT0019883	C-302339-00	AAAGCCCGGAGGAGGAGGAGGAGGUGU	-0.465231590374108	0.12653	FALSE	-2.30430878110898	0.023579	TRUE
25	hsa-miR-4747-5p	MIMAT0019882	C-302340-00	AGGAGGAGGAGGAGGAGGAGGAGGUGU	-0.431504671806173	0.1752	FALSE	-1.91877072137894	0.12226	TRUE
26	hsa-miR-4748	MIMAT0019884	C-302341-00	GAGGUGUUGGAGGAGGAGGAGGUGU	-0.55957276676544	0.061384	FALSE	-2.01827066334852	0.11887	TRUE
27	hsa-miR-4750-3p	MIMAT0022979	C-302491-00	CUAGACCCGAGGAGGAGGAGGAGGUGU	-0.71475404069532	0.0074787	FALSE	-2.39203721905178	0.11887	TRUE
28	hsa-miR-4755-5p	MIMAT0019895	C-302349-00	UUUCCUUCUACAGGAGGAGGAGGUGU	-0.539113669488979	0.061384	FALSE	-2.80807175968132	0.057617	TRUE
29	hsa-miR-4760-5p	MIMAT0019906	C-302359-00	UUUUAUUGAAGCAUGAAGGAGGUGU	-0.82374393447296	0.015067	FALSE	-2.78675399181231	0.028781	TRUE
30	hsa-miR-4768-5p	MIMAT0019920	C-302372-00	AUUCUUCUUGGAGGAGGAGGAGGUGU	-0.784576616178355	0.061384	FALSE	-2.06931455868509	0.11887	TRUE
31	hsa-miR-4774-3p	MIMAT0019930	C-302383-00	AUUGCCUACAUUGGAGGAGGAGGUGU	-0.980156502965659	0.03164	FALSE	-1.92072766628618	0.12226	TRUE
32	hsa-miR-4778-3p	MIMAT0019937	C-302393-00	UUUCUUCUUGGAGGAGGAGGAGGUGU	-0.468380465892249	0.17522	FALSE	-2.12161516444605	0.11887	TRUE
33	hsa-miR-4778-5p	MIMAT0019936	C-302392-00	AUUCUUGUAAAGGAGGAGGAGGAGGUGU	-0.108428651324849	1	FALSE	-2.20881648867654	0.08542	TRUE
34	hsa-miR-4782-3p	MIMAT0019945	C-302398-00	AUUCUUGUUCUACAUUGGAGGAGGUGU	-0.415227659309038	0.32544	FALSE	-1.91948198729733	0.11887	TRUE
35	hsa-miR-4792	MIMAT0019964	C-302418-00	CGGUGAGGCGGAGGAGGAGGUGU	-0.681007111878918	0.096607	FALSE	-2.3586952181417	0.057617	TRUE
36	hsa-miR-4799-5p	MIMAT0019976	C-302431-00	AUCUAAUUGCAGCAAGGAGGAGGUGU	-0.36222805879938	0.32544	FALSE	-1.8852338837028	0.11887	TRUE
37	hsa-miR-4800-5p	MIMAT0019978	C-302435-00	AGUGACCGGAGGAGGAGGAGGAGGUGU	-1.32275981315377	0.0074787	FALSE	-2.73500556024618	0.028781	TRUE
38	hsa-miR-4804-3p	MIMAT0019985	C-302441-00	UGCUUUAACUUGGCGGAGGAGGUGU	-0.336610566496397	0.37761	FALSE	-2.244385860605872	0.11887	TRUE
39	hsa-miR-486-3p	MIMAT0004762	C-301211-01	GUGGCGAGGAGGAGGAGGAGGUGU	-0.915928947716196	0.0027607	FALSE	-1.90219636227184	0.11887	TRUE
40	hsa-miR-487a	MIMAT0002178	C-300747-03	AUUAUACAGGAGGAGGAGGAGGUGU	-0.74716454562154	0.015067	FALSE	-2.42832566173827	0.040079	TRUE
41	hsa-miR-488	MIMAT0004763	C-301189-01	UUGAAGGCGUUAUUCUUGGAGGUGU	-0.908290356891222	0.01741	FALSE	-2.18110128296813	0.11887	TRUE
42	hsa-miR-491-3p	MIMAT0004765	C-301091-01	CUUUAUGCAGUUAUUCUUCUAC	-1.62232250510605	0.00023985	TRUE	-1.07582371390113	0.46329	FALSE
43	hsa-miR-492	MIMAT0002812	C-300757-05	AGGAGGCGGAGGAGGAGGAGGAGGUGU	-0.468584149980808	0.061384	FALSE	-2.7251166768836	0.014453	TRUE
44	hsa-miR-494	MIMAT0002816	C-300781-05	UGAACAAGGAGGAGGAGGAGGAGGUGU	-0.97021928477552	0.021076	FALSE	-3.24114885056762	0.014453	TRUE
45	hsa-miR-499b-3p	MIMAT0019898	C-302351-00	AACAUCAGGAGGAGGAGGAGGAGGUGU	-0.450448811865319	0.10991	FALSE	-1.9237723491978	0.11887	TRUE
46	hsa-miR-5001-3p	MIMAT0021022	C-302470-00	UUCUGCCUUGGAGGAGGAGGAGGUGU	-1.3342863345599	0.00013793	TRUE	-1.54637406738355	0.00677	FALSE
47	hsa-miR-5003-5p	MIMAT0021025	C-302474-00	UCACAACACUUGGAGGAGGAGGAGGUGU	-1.32073825957867	0.00013793	TRUE	-1.18738346839705	0.51579	FALSE
48	hsa-miR-5004-5p	MIMAT0021027	C-302477-00	UGAGGACAGGCGCAUUAUACGAGGUGU	-1.00354080968358	0.00079918	FALSE	-3.14572597959306	0.057617	TRUE
49	hsa-miR-5006-5p	MIMAT0021033	C-302479-00	UUGCCGAGGCGGAGGAGGAGGAGGUGU	-1.29090326952253	0.00013963	TRUE	-1.67173993218432	0.40677	FALSE
50	hsa-miR-501-3p	MIMAT0004774	C-301167-01	AUUGACCCGCGGAGGAGGAGGAGGUGU	-0.073177410080508	1	FALSE	-1.96439959148781	0.057617	TRUE
51	hsa-miR-5087	MIMAT0021079	C-301942-00	GGGUUUGUAGGAGGAGGAGGAGGUGU	-0.359393924285983	0.10991	FALSE	-1.7818859696044	0.11887	TRUE
52	hsa-miR-509-5p	MIMAT0004779	C-301166-01	UACUGCAGAGGAGGAGGAGGAGGUGU	-1.74945283535728	0.00013793	TRUE	-2.47315672999895	0.081661	TRUE
53	hsa-miR-5092	MIMAT0021084	C-302456-00	AUUCGACGCGUAGGAGGAGGAGGUGU	-1.18967239061038	0.00023985	TRUE	-1.517756387148	0.46329	FALSE
54	hsa-miR-513a-5p	MIMAT0020277	C-301084-07	UUCACAGGAGGAGGAGGAGGAGGUGU	-0.05970581093063	0.0074787	FALSE	-3.37670376481159	0.11887	TRUE
55	hsa-miR-513a-3p	MIMAT0022728	C-301908-00	UUAUUAUACUUGGAGGAGGAGGAGGUGU	-0.80302559359186	0.061472	FALSE	-2.73190794276724	0.014453	TRUE
56	hsa-miR-514	MIMAT0002883	C-300851-07	AUUGACACUUCUUGGAGGAGGAGGUGU	-0.348236527420602	0.12653	FALSE	-1.56224854603507	0.11887	TRUE
57	hsa-miR-516a-5p	MIMAT0004770	C-301104-01	UUCUCGAGGAGGAGGAGGAGGAGGUGU	-0.681407959396855	0.0046172	FALSE	-2.18673664105892	0.11887	TRUE
58	hsa-miR-517a	MIMAT0002852	C-300811-05	AUCGUGACACUUCUUGGAGGAGGUGU	-0.09820612826732	0.0018747	FALSE	-2.32535259864992	0.08542	TRUE
59	hsa-miR-517b-3p	MIMAT0002857	C-300817-06	AUCGUGACUUCUUGGAGGAGGAGGUGU	-1.68014710761636	3.9917e-05	TRUE	-1.4557777456063	0.26644	FALSE
60	hsa-miR-517c	MIMAT0002866	C-300832-03	AUCGUGACUUCUUGGAGGAGGAGGUGU	-1.39967029576568	0.00054279	FALSE	-3.92792989935189	0.009387	TRUE
61	hsa-miR-518a-5p	MIMAT0005457	C-301099-01	CUGCAAAAGGAGGAGGAGGAGGUGU	-1.69701165144962	0.00013963	TRUE	-3.84851299481868	0.014453	TRUE
62	hsa-miR-518b	MIMAT0002844	C-300798-03	CAAGGCGGCGGAGGAGGAGGAGGUGU	-1.13594844149699	0.00087976	FALSE	-2.22045683232246	0.08542	TRUE
63	hsa-miR-518c	MIMAT0002847	C-300804-03	AGGAGGCGGAGGAGGAGGAGGAGGUGU	-1.158703796257599	0.0014577	FALSE	-3.20841244998613	0.014453	TRUE
64	hsa-miR-519d-5p	MIMAT0002846	C-300803-03	AGGAGGCGGAGGAGGAGGAGGAGGUGU	-0.80849320930356	0.54078	FALSE	-3.42084790872384	0.081661	TRUE
65	hsa-miR-519f	MIMAT0021123	C-302496-00	AGGAGGAGGAGGAGGAGGAGGAGGUGU	-0.92371763588366	0.0014577	FALSE	-0.01918985190962	0.014453	TRUE
66	hsa-miR-519g-5p	MIMAT0021128	C-301981-00	AGGAGGAGGAGGAGGAGGAGGAGGUGU	-1.1676121443446	3.6715e-05	TRUE	-2.56840688714633	0.040079	TRUE
67	hsa-miR-520a-3p	MIMAT0002834	C-300788-03	AAAGUGCUUCCUUGGAGGAGGUGU	0.0374069999290813	1	FALSE	-2.98674734617433	0.08542	TRUE
68	hsa-miR-520c-3p	MIMAT0002846	C-300803-05	AAAGUGCUUCCUUGGAGGAGGUGU	-0.19938916868778	0.37761	FALSE	-1.76230191681356	0.11887	TRUE
69	hsa-miR-520h	MIMAT0002867	C-300833-03	CAAGGAGGAGGAGGAGGAGGAGGUGU	-0.694676795373559	0.015067	FALSE	-2.26960151079303	0.08542	TRUE
70	hsa-miR-532-5p	MIMAT0002888	C-300867-01	AUUGCCUUGGAGGAGGAGGAGGAGGUGU	-0.687783861572295	0.021994	FALSE	-3.38518185188287	0.014453	TRUE
71	hsa-miR-539-3p	MIMAT0002705	C-301909-00	AUUAUACAGGAGGAGGAGGAGGUGU	-0.712513192949551	0.0074787	FALSE	-1.777539713116	0.12226	TRUE
72	hsa-miR-544b	MIMAT0015004	C-301677-00	ACUGAGGAGGAGGAGGAGGAGGAGGUGU	-1.14820342901038	3.9917e-05	TRUE	-0.449549813604399	0.91039	FALSE
73	hsa-miR-548ab	MIMAT0018928	C-30190-00	AAAAGUAAUUGGAGGAGGAGGAGGUGU	-0.802579302030159	0.0021076	FALSE	-2.46432616915759	0.057617	TRUE
74	hsa-miR-548ac	MIMAT0018928	C-30190-00	AAAAGUAAUUGGAGGAGGAGGAGGUGU	-0.802579302030159	0.0021076	FALSE	-2.46432616915759	0.057617	TRUE
75	hsa-miR-548ae	MIMAT0018954	C-302019-00	CAAAAACUGGAGGAGGAGGAGGAGGUGU	-0.806375099488669	0.0030028	FALSE	-2.77725501988519	0.057617	TRUE
76	hsa-miR-548ah-3p	MIMAT0020957	C-302036-00	CAAAAACUGGAGGAGGAGGAGGAGGUGU	-0.668405768437197	0.0014577	FALSE	-2.22611084098903	0.081661	TRUE
77	hsa-miR-548at-5p	MIMAT0022277	C-302544-00	AAAAGUAAUUGGAGGAGGAGGAGGUGU	-0.0453519642557928	1	FALSE	-1.8924808826669	0.11887	TRUE
78	hsa-miR-548au-3p	MIMAT0022292	C							

hsa-miR-6504-3p	MIMAT0025465	C-302672-00	CAUUACAGCACAGCCAUUCU	-0.219268298279075	0.49143	FALSE	-2.3682663259571	0.08542	TRUE
hsa-miR-6505-3p	MIMAT0025467	C-302675-00	UGACUUCUACCCUUCUCAAAG	-1.41016990839787	0.00054279	FALSE	-2.92045878806631	0.040079	TRUE
hsa-miR-6507-5p	MIMAT0025470	C-302679-00	GAAGAAUAGGAGGACUUUGU	-0.637513482741369	0.03164	FALSE	-2.64696299700191	0.057617	TRUE
hsa-miR-6514-3p	MIMAT0025485	C-302693-00	CUGCCUGUUCUCCACUCCAG	-1.57253367763337	0.00023985	TRUE	-0.857463656453242	0.72813	FALSE
hsa-miR-652-5p	MIMAT0022709	C-301928-00	CAACCCUAGGAGAGGUGGCAUUA	-0.890578760958739	0.01741	FALSE	-2.04113601671063	0.11887	TRUE
hsa-miR-654-5p	MIMAT0003330	C-300988-01	UGGUGGGCCGAGAAAUUGUGC	-1.24102088307823	0.00054279	FALSE	-4.37321715649902	0.0018396	TRUE
hsa-miR-659	MIMAT0003337	C-300994-01	CUUGGUUCAGGGAGGGUCCCA	-0.865338332757254	0.0053924	FALSE	-2.2970254587848	0.12226	TRUE
hsa-miR-660-3p	MIMAT0022711	C-301897-00	ACCUCUGUGUGCAUGGAUUA	-0.914364872105563	0.0018747	FALSE	-2.7989676696545	0.028781	TRUE
hsa-miR-661	MIMAT0003324	C-300981-01	UGCCUGGGUCUCUGCCUGCGCGU	-0.966061272920722	0.0046172	FALSE	-2.04789510522588	0.11887	TRUE
hsa-miR-664b-3p	MIMAT0022272	C-302539-00	UUCAUUUGCCUCCAGCCUACA	-0.63588937093853	0.061384	FALSE	-2.38779084523873	0.057617	TRUE
hsa-miR-671-5p	MIMAT0003880	C-301000-03	AGGAAGCCUGGAGGGGUGGAG	-1.01268622344544	0.00023985	TRUE	-0.995050180707598	0.5811	FALSE
hsa-miR-6721-5p	MIMAT0025852	C-302707-00	UGGCGAGGGGCUUAUUGUAGGAG	-1.0522716562067	0.0021076	FALSE	-2.86092601806193	0.028781	TRUE
hsa-miR-7	MIMAT0000252	C-300546-07	UGGAAGACUAGUUAUUUGUUGU	-0.833080606802588	0.0014577	FALSE	-2.34382127982937	0.11887	TRUE
hsa-miR-718	MIMAT0012735	C-301486-00	CUUCCGCCCGCGGCGGUGG	-0.712476270533885	0.0014577	FALSE	-2.51688917044679	0.08542	TRUE
hsa-miR-744	MIMAT0004945	C-301242-01	UGCGGGGCUAGGGCUAACGCA	-1.31292964878657	0.0027607	FALSE	-2.17130853543699	0.057617	TRUE
hsa-miR-744*	MIMAT0004946	C-301241-01	CUGUUGCCACUAAACCUAACCU	-0.309425861300587	3.9917e-05	TRUE	-2.41920375944258	0.11887	TRUE
hsa-miR-764	MIMAT0010367	C-301640-00	GCAGGUGGUCACUUGUCCUCCU	-1.1596052122736	6.1693e-05	TRUE	-0.963991799367289	0.5811	FALSE
hsa-miR-767-3p	MIMAT0003883	C-301003-01	UCUGCUCAUACCCUAGGUUUUCU	-0.875815222995269	0.0021076	FALSE	-2.87852305265755	0.009387	TRUE
hsa-miR-801	MIMAT0005202	C-301014-01	GAUUGCUCUGCGUGCGGAUCGAC	-1.02838938735747	0.00023985	TRUE	0.128066636696993	1	FALSE
hsa-miR-873-3p	MIMAT0022717	C-301921-00	GGAGACUGAUGAUUCCCGGGA	-0.45500701580676	0.050037	FALSE	-2.17559760678154	0.08542	TRUE
hsa-miR-888*	MIMAT0004917	C-301227-01	GACUGACACCUUUGGUGUAA	-0.798719536763374	0.015067	FALSE	-1.83668949541677	0.11887	TRUE
hsa-miR-940	MIMAT0004983	C-301269-01	AAGGCAGGGCCCCCGUCCCC	-1.31504996360232	0.00054279	FALSE	-2.52010733193133	0.11887	TRUE
hsa-miR-96	MIMAT0000095	C-300514-07	UUUGGCACUAGCACAUUUUGCU	-0.788957233607577	0.0074787	FALSE	-2.19234338350236	0.11527	TRUE
hsa-miR-99a	MIMAT0000097	C-300516-03	AAACCGUAGAUCCGAUCUUGUG	-0.986802247020601	0.0030028	FALSE	-2.42723567464877	0.11887	TRUE

Legend
Antiviral effect
Proviral effect

Note: Hits were selected using the following Local False Discovery Rate (fdr) thresholds: 0.00027 in screen part 1 and 0.1226 in screen part 2. Positive log2 fold change values indicate a proviral effect of the miRNA on the HCV life cycle, while negative log2 fold change values indicate an antiviral effect.

A functional microRNA screen uncovers O-linked N-acetylglucosamine transferase as a host factor modulating hepatitis C virus morphogenesis and infectivity

Katharina Herzog^{1,2*}, Simonetta Bandiera^{1,2*}, Sophie Pernot^{1,2}, Catherine Fauvelle^{1,2}, Frank Jühling^{1,2}, Amélie Weiss^{2,3,4,5}, Anne Bull⁶, Sarah C. Durand^{1,2}, Béatrice Chane-Woon-Ming^{2,7}, Sébastien Pfeffer^{2,7}, Marion Mercey⁸, Hervé Lerat⁸, Jean-Christophe Meunier⁶, Wolfgang Raffelsberger^{2,3,4,5}, Laurent Brino^{2,3,4,5}, Thomas F. Baumert^{1,2,9,#}, Mirjam B. Zeisel^{1,2,10,#}

¹Inserm, U1110, Institut de Recherche sur les Maladies Virales et Hépatiques, Strasbourg, France; ²Université de Strasbourg, Strasbourg, France; ³Institut de Génétique et de Biologie Moléculaire et Cellulaire, Illkirch, France ; ⁴CNRS, UMR7104, Illkirch, France ; ⁵Inserm, U1258, Illkirch, France ; ⁶Inserm U1259, Faculté de Médecine, Université François Rabelais and CHRU de Tours, Tours, France ; ⁷Architecture et Réactivité de l'ARN – UPR 9002, Institut de Biologie Moléculaire et Cellulaire du CNRS, Strasbourg, France; ⁸Institute for Applied Biosciences, Centre de Recherche UGA - Inserm U1209 - CNRS 5309, Grenoble, France ⁹Institut Hospitalo-Universitaire, Pôle Hépato-digestif, Hôpitaux Universitaires de Strasbourg, Strasbourg, France; ¹⁰Inserm, U1052, CNRS UMR 5286, Centre Léon Bérard (CLB), Cancer Research Center of Lyon (CRCL), Université de Lyon (UCBL), Lyon, France

*Authors contributed equally to this work

Word count. Abstract: 196 words; main manuscript: 3991 words; 55 references; 7 figures; 1 table; Supplementary information (including 1 Supplementary Table and 1 Supplementary Figure)

#Corresponding authors. Dr. Mirjam B. Zeisel, Inserm U1052 – CRCL, 151 cours Albert Thomas, 69424 Lyon Cedex 03, France, Phone: +33472681970, Fax: +33472681971, E-mail: mirjam.zeisel@inserm.fr and Prof. Thomas F. Baumert, Inserm U1110, Institut de

1
2
3 1 Recherche sur les Maladies Virales et Hépatiques, 3 rue Koeberlé, 67000 Strasbourg,
4
5 2 France, Phone: +33368853703, Fax: +33368853724, Email: thomas.baumert@unistra.fr
6
7 3
8

9 4 **Financial support.** This work was supported by the European Union (INTERREG-IV-Rhin
10
11 5 Supérieur-FEDER-Hepato-Regio-Net 2012 to T.F.B. and M.B.Z., ERC-AdG-2014-671231-
12
13 6 HEPCIR, EU H2020-667273-HEPCAR to T.F.B.), ANRS (2012/239 to T.F.B., M.B.Z. and
14
15 7 L.B.), ARC, Paris and Institut Hospitalo-Universitaire, Strasbourg (TheraHCC IHUARC
16
17 8 IHU201301187 to T.F.B.), the Impulsion Program of the IDEXLYON (to M.B.Z.), Ligue contre
18
19 9 le cancer (to M.B.Z.), Inserm, and University of Strasbourg. This work has been published
20
21 10 under the framework of the LABEX ANR-10-LABX-0028_HepSYS, ANR-10-LABX-36
22
23 11 NetRNA and Inserm Plan Cancer 2019-2023 and benefits from funding from the state
24
25 12 managed by the French National Research Agency as part of the Investments for the future
26
27 13 program. S.P. and K.H. were supported by PhD fellowships from the French Ministry of
28
29 14 Research and the IdEx program of the University of Strasbourg, respectively.
30
31 15

32
33 16 **Author contribution.** M.B.Z. coordinated and supervised research. K.H., S.B., S.P., C.F.,
34
35 17 A.W., L.B., J-C.M. and M.B.Z. designed experiments. K.H., S.B., S.P, C. F., A.W., A.B.,
36
37 18 S.C.D., M.M., H.L. and J-C.M. performed experiments. K.H., S.B., S.P., C. F., F.J., A.W.,
38
39 19 A.B., B.C.W.M., S.P., J-C.M., W.R., L.B., T.F.B. and M.B.Z. analyzed data. K.H., S.B., and
40
41 20 M.B.Z. wrote the paper.
42
43 21

44
45 22 **Competing interests:** The authors do not have competing interest.
46
47 23
48
49
50
51
52
53
54
55
56
57
58
59
60

Abstract

Objective: Infection of human hepatocytes by the hepatitis C virus (HCV) is a multistep process involving both viral and host factors. microRNAs (miRNAs) are small non-coding RNAs that post-transcriptionally regulate gene expression. Given that miRNAs were indicated to regulate between 30% and 75% of all human genes, we aimed to investigate the functional and regulatory role of miRNAs for the HCV life cycle.

Design: To systematically reveal human miRNAs affecting the HCV life cycle, we performed a two-step functional high-throughput miRNA mimic screen in Huh7.5.1 cells infected with recombinant cell culture-derived HCV. miRNA targeting was then assessed using a combination of computational and functional approaches.

Results: We uncovered miR-501-3p and miR-619-3p as novel modulators of HCV assembly/release. We discovered that these miRNAs regulate O-linked N-acetylglucosamine (O-GlcNAc) transferase (OGT) protein expression and identified OGT and O-GlcNAcylation as regulators of HCV morphogenesis and infectivity. Furthermore, increased OGT expression in patient-derived liver tissue was associated with HCV-induced liver disease and cancer.

Conclusion: miR-501-3p and miR-619-3p and their target OGT are previously undiscovered regulatory host factors for HCV assembly and infectivity. In addition to its effect on HCV morphogenesis, OGT may play a role in HCV-induced liver disease and hepatocarcinogenesis.

Significance of this study

What is already known about this subject?

- ♦ To establish chronic infection, the hepatitis C virus (HCV) hijacks cellular factors including microRNAs (miRNAs), known to post-transcriptionally regulate gene expression.
- ♦ miRNAs may positively or negatively modulate HCV infection either by directly targeting the viral genome or indirectly by regulating virus-associated cellular pathways[1, 2].

What are the new findings?

- ♦ A functional miRNA mimic screen uncovered miR-501-3p and miR-619-3p to enhance late steps of HCV infection.
- ♦ miR-501-3p regulates the expression of O-linked N-acetylglucosamine transferase (OGT) at the protein level.
- ♦ Silencing of OGT expression or inhibition of O-linked N-acetylglucosaminylation (O-GlcNAcylation) leads to an increase in the infectivity and size of HCV particles.
- ♦ OGT expression increases in patient-derived liver tissue during liver disease progression and cancer.

How might it impact on clinical practice in the foreseeable future?

- ♦ As upregulation of OGT and increased O-GlcNAcylation of proteins have been associated with various forms of cancer, OGT may play a dual role in HCV morphogenesis as well as pathogenesis of HCV-induced liver disease and carcinogenesis.

1 Introduction

Chronic hepatitis C is a major cause of chronic liver disease and hepatocellular carcinoma (HCC). Since the approval of pan-genotypic direct-acting antivirals (DAAs), it is considered a curable disease in more than 90% of treated patients. Nonetheless, an estimated 71 million individuals are still infected by the hepatitis C virus (HCV) and several challenges remain; viral cure reduces but does not eliminate the HCC risk in patients with advanced fibrosis[3], the majority of infected patients has limited access to therapy and DAA failure/viral resistance has been reported in a subset of patients[4, 5]. To overcome these limitations, approaches to target host factors involved in HCV infection and pathogenesis are developed[6, 7]. Interestingly, defined host factors that contribute to the establishment of chronic HCV infection and represent potential antiviral targets, e.g. epidermal growth factor receptor[8], also play a role in liver disease pathogenesis and represent candidate targets for treatment of advanced liver disease and HCC prevention[9]. Thus, uncovering host factors usurped by HCV not only contributes to a better understanding of virus-host interactions underlying the HCV life cycle but also to the identification of potential targets for treatment of liver disease and prevention of HCC.

The establishment of various models to study HCV infection has shed light on the molecular mechanisms that govern the HCV life cycle, which can be subdivided into early steps, including viral entry, translation and replication as well as late steps, including assembly and release of new virions. Each step of the HCV replication cycle relies on specific virus-host interactions that involve host proteins and microRNAs (miRNAs)[7], small non-coding RNAs that regulate gene expression at the post-transcriptional level. One miRNA can target numerous messenger RNAs (mRNAs) by base-pairing with a complementary site that is typically located within the 3' untranslated region (3'UTR) of the mRNA. Accumulating evidence indicates that miRNAs participate to HCV replication by exerting pro- or antiviral effects. The breakthrough discovery of the direct targeting of HCV by miR-122, the most abundant miRNA in the liver, revealed the crucial role of this miRNA for HCV translation/replication that contributes to progression to chronic HCV infection[1, 10]. miR-

1
2
3 1 122 antisense oligonucleotides were subsequently developed as host-targeting antivirals[11,
4
5 2 12]. Other miRNAs can indirectly target HCV by regulating host factors that participate in
6
7 3 antiviral responses and immune surveillance[2, 13, 14]. Since up to 60% of all human
8
9 4 protein-coding genes were reported to be under miRNA-mediated regulation and miRNAs
10
11 5 are involved in basically every biological process, we hypothesized that miRNAs provide a
12
13 6 tool for loss-of-function approaches to uncover novel HCV host factors. We performed
14
15 7 genome-wide high-throughput modulation of the human miRNome and analyzed their impact
16
17 8 on HCV infection by combining computational and functional approaches.
18
19
20 9

21
22 10 **Material and methods**

23
24 11 **Cells, cell culture conditions, viruses, virus purification, infectivity assays, miRNAs,**
25
26 12 **antagomiRs, siRNAs, antibodies, immunoblot, immunocapture, electron microscopy**
27
28 13 **analysis of viral particles and gene expression analysis in liver tissue** are described in
29
30 14 the Supplementary information.
31
32
33 15

34
35 16 **Functional miRNA/siRNA screens.** Huh7.5.1 cells were transfected with the miRIDIAN
36
37 17 human miRNA mimic library (miRBase 19) comprising more than 2000 mature miRNAs or 28
38
39 18 ON-TARGETplus smart pool siRNAs (20 nM, Dharmacon) using Interferin HTS (Polyplus) in
40
41 19 a 96-well format[8]. After 48h, a viability test (Presto Blue, Thermo Scientific) was performed
42
43 20 prior to a two-step infection assay[15, 16, 17]. During part 1 of the protocol, 50 µL of HCV cell
44
45 21 culture-derived particles (HCVcc, JcR2a) were incubated with cells during 4h. The inoculum
46
47 22 was removed and cells were incubated with 150 µl of medium for 48h. In part 2, supernatants
48
49 23 from part 1 cells were transferred onto naïve Huh7.5.1 cells and part 1 cells were lysed to
50
51 24 determine luciferase activity[17, 18]. After 72h, part 2 cells were lysed to determine luciferase
52
53 25 activity[17]. siCD81 (20 nM), antagomiR-122 (100 nM) and siApoE (20 nM) were used as
54
55 26 positive controls[17]. A non-targeting siRNA with no sequence complementarity to any
56
57 27 human gene or homology to any human miRNA was used as negative control.
58
59
60 28

Inhibitor treatment. Four hours following HCV RNA electroporation[8], Huh7.5.1 cells were incubated with vehicle or inhibitors of OGT (peracetylated 5-thio-N-acetylglucosamine (Ac₄5S-GlcNAc)[19]) or OGA (Thiamet G (Sigma))[20]. After 96h, supernatants were transferred onto naïve Huh7.5.1 cells for 72h prior to determination of luciferase activity while electroporated cells were lysed to determine luciferase activity.

Gene expression analyses. Total RNA was purified[17] and transcribed into cDNA using Maxima reverse transcriptase (Thermo Scientific). *GAPDH* and *OGT* mRNA was detected by real time qPCR using iTaq™ Universal Probes Supermix (Bio-Rad) and TaqMan Gene Expression Assay (Thermo Scientific). Relative *OGT/GAPDH* gene expression was calculated by the $\Delta\Delta C_t$ method[21].

Dual luciferase reporter gene assay. The human *OGT* 3'UTR sequence was retrieved from NCBI (NM_181672.2) and Ensembl genome browser (ENST00000373719.3). A fragment of the *OGT* 3'UTR (positions 3380-3837, NM_181672.2) (Thermo Fisher Scientific GENEART) was cloned between the *NotI* and *XhoI* sites downstream of a *Renilla* luciferase cassette in a psiCHECK2 plasmid (Promega). A mutated version of this construct (9-bp substitution in the predicted miR-501-3p target site) was generated as described[22]. The functionality of the *OGT* 3'UTR was assessed as described[23]. The miRIDIAN mimic negative control 1 was used as control. *Renilla* and *firefly* luciferase activity was assessed 48h after transfection into HeLa cells using Dual-Luciferase Reporter assay (Promega).

Bioinformatic and statistical analysis. Data analysis and statistical treatment for the miRNA mimic screen were performed in R (www.r-project.org). Cell measurement data used in further analysis were cell viability and luciferase activity. In total 26 sets of plates (performed in triplicate) were tested. The presence of multiple wells with negative and positive controls on each plate allowed stepwise normalization intra- and inter-plate. First, intra-plate zonal bias was examined and a model of median effects across the entire screen

1
2
3 1 determined using the median-polish algorithm[24] and all plates corrected accordingly. Then
4
5 2 the dataset was examined for outlier plates, i.e. plates where all individual measurements
6
7 3 correlate very poorly with the other remaining replicates. Three and 9 plates were excluded
8
9 4 for part 1 and part 2 of the screen, respectively, based on poor median correlation ($r < 0.7$)
10
11 5 so that the remaining plates correlation improved substantially ($> 40\%$). Next, the plates were
12
13 6 normalized inter replicates using the particularly robust quantile-quantile approach[25].
14
15 7 Finally, the data were tested using a moderated t-test (empirical Bayes shrinkage, R-
16
17 8 package limma[26]) for the null-hypothesis of no change of a given miRNA compared to the
18
19 9 negative control. The resulting p -values for independent testing of each miRNA where
20
21 10 corrected for the multiple testing situation and expressed as local false discovery rate (lfdr,
22
23 11 R-package fdrtool[27]). The testing was performed independently for part 1 and 2 of the
24
25 12 screen and candidate miRNAs selected for each part. For data from part 1, a lfdr threshold of
26
27 13 0.00027 was used. Data from part 2 were subject to increase inherent stochastic noise and
28
29 14 for this reason the minimum acceptable relative risk of false positives was increased to
30
31 15 0.1226 (i.e. maximum 15% risk for each of the retained hits).
32
33

34
35 16 Other datasets were analyzed using the two-tailed Mann-Whitney test, Wilcoxon test,
36
37 17 Spearman correlation or the two-tailed unpaired t-test for data with normal distribution as
38
39 18 assessed by D'Agostino and Pearson omnibus and Shapiro-Wilk normality tests (GraphPad
40
41 19 Prism v.6 package).
42
43
44
45
46
47
48

49
50 22 **Results**
51
52 23 **Genome-wide identification of human miRNAs affecting the HCV life cycle.** We
53
54 24 performed a genome-wide screen in human hepatoma Huh7.5.1 cells using a genomic
55
56 25 miRNA mimics library and a two-step infection assay[17] with a luciferase reporter virus
57
58 26 (JcR2a), which allowed us to functionally assess the role of miRNAs during the early steps
59
60 27 (part 1 - viral entry/translation/replication) and the late steps (part 2 - viral
28 28 assembly/release/infectivity) of the HCV life cycle (Fig. 1A). Silencing of *CD81* and *ApoE*,

two essential host factors required for HCV entry or assembly, respectively, was performed in parallel using small interfering RNA (siRNA) as controls. Silencing of *CD81* resulted in a reduction of HCV infection in part 1 and consequently in part 2 of the screen since reduced viral entry in the first part of the assay leads to a reduced production of viral particles (Fig. 1B)[17]. Silencing of *ApoE* resulted in a marked inhibition of HCV infection only in part 2 of the assay, consistent with the role of ApoE in HCV assembly (Fig. 1B)[17]. The screen identified 427 miRNAs (corresponding to about 16% of the library) that significantly modulated HCV infection ($\text{Ifdr} < \text{threshold}$, Supplementary Table 1 and Fig. 1C): 186 miRNAs affected HCV infection in part 1, 309 miRNAs affected HCV infection in part 2, including 68 hits in part 1 and part 2. The limited number of part 1 and 2 hits may be due to the fact that a single miRNA may modulate the expression of several proteins, which may have different roles in the viral life cycle. Most hits were observed to dampen HCV infection independently of any significant alteration of cell viability (data not shown). The 186 miRNAs modulating the early steps of HCV infection all decreased viral infection. Among the 309 miRNAs that had an impact in part 2, 11 miRNAs increased HCV infection by at least 3-fold while 298 miRNAs inhibited HCV infection by at least 2.7-fold. Hits from the screen included the let-7 family[2, 28], miR-27a[29] and miR-29 family[30] that were already shown to inhibit HCV infection, as well as miR-21[31] and miR-146a-5p[17] that were shown to stimulate HCV infection thus supporting the relevance of our findings. Collectively, our screen identified a set of miRNAs whose overexpression overall impairs HCV infection by affecting viral entry/translation/replication and/or virion assembly/egress/infectivity.

miR-619-3p, miR-501-3p and OGT play a role in late steps of the HCV life cycle. We focused our analysis on miRNAs that modulate late steps of the HCV life cycle, as the molecular mechanisms of HCV assembly/release remain only partially understood. Our screen identified 241 miRNAs that modulated late steps without affecting early steps of infection: 11 miRNAs increased HCV infection while 230 miRNAs decreased HCV infection. Among the miRNAs that increased HCV infection, miR-140-3p, miR-501-3p, miR-619-3p and

1
2
3 1 miR-4778-5p have not yet been associated with HCV. Since they enhanced HCV infection in
4
5 2 part 2 without affecting part 1, these miRNAs may target host genes that control virus
6
7 3 assembly/egress/infectivity. We first confirmed the effect of these miRNAs in independent
8
9 4 experiments using the same protocol as for the screen. Overexpression of miR-619-3p or
10
11 5 miR-501-3p consistently led to an increase in the infection of progeny virions (Fig. 1D) while
12
13 6 infection was decreased with progeny virions from antagomiR-transfected cells
14
15 7 (Supplementary Figure S1A). miR-619-3p or miR-501-3p were thus selected for further
16
17 8 investigation. To study the molecular mechanisms by which these miRNAs affect HCV
18
19 9 infection, we generated a list of predicted miRNA targets using DIANA, TargetScan Human
20
21 10 v6.2 and miRDB databases, and selected candidate targets based on their expression in our
22
23 11 Huh7.5.1 cells as assessed by microarray (data not shown). Ingenuity Pathway Analysis
24
25 12 enabled us to refine the gene list by selecting 28 genes involved in the following functional
26
27 13 networks or pathways that contribute to the HCV life cycle[32, 33, 34]: lipid metabolism and
28
29 14 cholesterol biosynthesis, protein maturation and processing at the endoplasmic reticulum
30
31 15 (ER), components of the endosomal sorting complex, adipocyte biogenesis, cellular
32
33 16 morphology and cell inflammation (Table 1).
34
35
36
37 17 To assess whether knock-down of these 28 candidate targets affects virus
38
39 18 production, we performed a siRNA-based screen using siRNA pools exhibiting strong
40
41 19 silencing without cytotoxicity (Fig. 2). Silencing of *CD81* and antagomiR-122 served as
42
43 20 controls for part 1; knock-down of *ApoE* served as control for part 2 (Fig. 2). Hits were
44
45 21 defined as genes whose knock-down modulated HCV infection in at least one part of the
46
47 22 screen with high significance (Fig. 2, $p\text{-value} \leq 0.0001$, Mann-Whitney U-test). HCV
48
49 23 entry/translation/replication was significantly modulated by silencing of *PPP3CA*, *CEBPA*,
50
51 24 *MID1*, *WDFY3*, *DCX* and *SLC35D1*. HCV assembly/egress/infectivity was significantly
52
53 25 modulated by knock-down of *PPP3CA*, *CSDE1*, *GAN*, *USP37*, *CEBPA*, *MID1*, *WDFY3*, *DCX*,
54
55 26 *MAPK9*, *SLC35D1*, *DCC*, *RNF144A*, *PPP2R2C* and *OGT*. Strikingly, only the silencing of
56
57 27 *OGT* was associated with an enhancement of HCV assembly/release/infectivity ($p\text{-value} =$
58
59 28 0.0002), while that of the other hits was associated with reduced HCV infection (Fig. 2).
60

These results indicate that the down-regulation of *OGT* phenocopies the effect of miR-501-3p and miR-619-3p on HCV infection (Fig. 2) and suggest *OGT* as a novel player in the HCV life cycle.

miR-501-3p post-transcriptionally regulates *OGT* expression. To study whether miR-501-3p and miR-619-3p target *OGT*, we analyzed *OGT* RNA and protein levels in Huh7.5.1 cells following overexpression of miR-501-3p or miR-619-3p. While neither miRNA had an impact on *OGT* RNA levels (Fig. 3A), up-regulation of miR-501-3p significantly decreased *OGT* protein expression by ~65% (Fig. 3B, p -value ≤ 0.05 , t-test). miR-619-3p also decreased *OGT* expression but less robustly than miR-501-3p (Fig. 3B), prompting us to focus our investigation on miR-501-3p. To assess whether *OGT* is a functional target of miR-501-3p, we subcloned a fragment of the *OGT* mRNA 3'UTR that harbors the predicted miR-501-3p target site in the *Renilla* luciferase expression cassette (RLuc) of a dual luciferase reporter construct. Co-transfection of miR-501-3p mimic with the wild-type 3'UTR reporter (RLuc wt *OGT* 3'UTR) significantly decreased luciferase activity as compared to the empty vector (Fig. 3C, p -value < 0.05 , t-test). In contrast, the repression of luciferase expression was lost when the reporter with mutated miR-501-3p binding site (RLuc mt *OGT* 3'UTR) was used (Fig. 3C). These data are consistent in indicating that miR-501-3p mediates post-transcriptional regulation of *OGT*.

O-GlcNAcylation modulates HCVcc infectivity. To investigate whether *OGT* modulates HCV assembly and/or infectivity, we determined infectious virus titer (TCID₅₀) and HCV RNA levels to calculate the specific infectivity of HCVcc particles generated in *OGT*-silenced Huh7.5.1 cells. Interestingly, *OGT*-silencing led to a significant increase in the TCID₅₀ and the specific infectivity of HCVcc (Fig. 4A, p -value ≤ 0.05 , Mann-Whitney test). Noteworthy, the effect of *OGT* on HCVcc infectivity was genotype-independent as demonstrated by increased infectivity of HCVcc bearing the envelope glycoproteins of genotypes 1a, 1b and 2a upon *OGT*-silencing (Fig. 4B). We next sought to investigate how *OGT* could modulate

1 HCVcc infectivity. OGT is the only enzyme that catalyzes the addition of N-
2 acetylglucosamine (O-GlcNAc) to serine and threonine residues of proteins. Moreover, OGT
3 has a scaffold function and promotes binding of proteins in multiprotein complexes[35]. To
4 assess whether the enzymatic activity of OGT modulates HCVcc infectivity, we used
5 pharmacological inhibitors of OGT (Ac₄5S-GlcNAc) or O-GlcNAcase (OGA) (Thiamet G), the
6 OGT counterpart that removes O-GlcNAc (Fig. 4C). Ac₄5S-GlcNAc led to a significant
7 enhancement of HCVcc infectivity in a dose-dependent manner, while the opposite effect
8 was observed with Thiamet G (Fig. 4D, p -value ≤ 0.05 , Mann-Whitney test). Collectively,
9 these results demonstrate that O-GlcNAcylation modulates HCVcc infectivity.

10
11 **OGT-silencing affects HCVcc biophysical properties and size distribution.** To further
12 assess how OGT may impact HCVcc morphogenesis, we analyzed the structural and
13 biophysical properties of HCVcc produced in siCtrl- and siOGT-transfected Huh7.5.1 cells
14 following iodixanol gradient ultracentrifugation. Silencing of OGT led to the production of
15 more infectious HCVcc with higher density (Fig. 5A-B) as well as higher ApoE concentrations
16 (Fig. 5C) suggesting that OGT/O-GlcNAcylation affects the biophysical properties of HCVcc.
17 No change in apoB concentrations were observed between HCVcc produced from siCtrl- or
18 siOGT-transfected cells (Fig. 5D), in line with the model that HCV lipovirions contain
19 several exchangeable ApoE molecules and one non-exchangeable apoB[36]. We also
20 visualized HCVcc by electron microscopy (EM) following anti-E2 antibody
21 immunocapture[36] to assess whether OGT-silencing had an impact on HCVcc size. Particle
22 size distribution was assessed from a series of randomly acquired electron micrographs. A
23 shift towards bigger sizes was observed for sucrose-cushion purified HCVcc generated in
24 OGT-silenced Huh7.5.1 cells as compared to control HCVcc (Fig. 6A-B). This shift was also
25 observed in different fractions of iodixanol gradient-separated HCVcc (Fig. 6C-F) in line with
26 the higher infectivity and ApoE concentrations of HCVcc generated in OGT-silenced
27 Huh7.5.1 cells (Fig. 5A-C). These data suggest that OGT-silencing affects the lipidation of
28 HCVcc.

OGT expression increases in liver disease. Since silencing of OGT promotes HCV infectivity, we assessed whether HCV infection in turn had an effect on miR-501-3p and OGT expression. In Huh7.5.1 cells, HCV infection lead to small but significant increase of miR-501-3p and decrease of OGT levels (Fig. 7A-B and Supplementary Fig. 1B; p -value < 0.05, Mann-Whitney test), which may promote viral infection given the pro- and antiviral roles of miR-501-3p and O-GlcNAcylation, respectively (Fig. 1C-D and 4D). In contrast, no significant difference of OGT expression was observed between the livers of HCV transgenic and wild-type mice[37] (data not shown) suggesting that HCV proteins do not directly modulate OGT expression. In liver tissue from HCV-infected patients, HCV RNA levels were not correlated with OGT expression (Fig. 7C, Spearman correlation: 0.06004019, p -value = 0.7661) suggesting that in patients there is likely no direct effect of HCV on OGT expression.

O-GlcNAcylation has been associated with a variety of cancers, including HCC recurrence linked to increased O-GlcNAcylation after liver transplantation[38]. We therefore investigated OGT expression in chronic liver disease and HCC. While there was a trend for increased OGT expression in liver tissue from HCV-infected patients with fibrosis and inflammation (Fig. 7D-E), OGT levels were markedly and significantly elevated in the tumor liver tissue of patients chronically infected with HCV or hepatitis B virus and patients with alcoholic liver disease or non-alcoholic fatty liver disease as compared to non-tumor tissue (Fig. 7F, p -value < 0.05, Wilcoxon test). These data suggest that OGT expression increases in HCC in an etiology-independent manner. Collectively, these results suggest that OGT expression is likely increased in HCV-induced liver disease and cancer through inflammation and fibrosis rather than by HCV itself.

Discussion

By focusing on miRNAs affecting late steps of the viral life cycle, we uncovered that i) miR-501-3p regulates the expression of OGT; ii) silencing of OGT expression or inhibition of its enzymatic activity increases the infectivity of HCV particles; and iii) OGT knock-down leads

1 to the release of bigger HCV particles. Our data suggest that O-GlcNAcylation affects HCV
2 morphogenesis and infectivity.

3 While we were characterizing the role of OGT/O-GlcNAcylation for HCV
4 morphogenesis, Li and colleagues published their functional genomics study of HCV-miRNA
5 interactions[2]. By conducting genome wide miRNA mimic and hairpin inhibitor screens, they
6 identified a set of miRNAs exhibiting a pro- or antiviral effect on HCV. Characterization of the
7 underlying molecular processes showed that miR-25, let-7 and miR-130 families restrict viral
8 infection by decreasing the expression of cellular HCV co-factors[2]. Despite similarities in
9 the cell type and HCV infection models used here and by Li and colleagues, our screen only
10 displays a small overlap with their study (9% common miRNA hits). This is not surprising
11 given the small overlap between previous siRNA screens to uncover HCV host factors[8, 15]
12 and is likely due i) to the different sizes of miRNA mimic libraries as the library used here was
13 more than 2-times larger than the one used by Li and co-workers, and ii) to the markedly
14 distinct pipelines for hit selection that were used in the two studies. Nonetheless, both
15 screens were consistent in confirming the proviral role of miR-146a-5p in promoting HCV
16 assembly/egress that we previously reported[17] and the global multistep inhibitory effects of
17 the let-7 family on HCV infection[28], further corroborating the involvement of these miRNAs
18 in fine-tuning the HCV life cycle. Both studies also consistently indicated that miR-518a-5p,
19 miR-517-3p, miR-185 and members of the miR-302 family inhibit early steps of HCV
20 infection, while miR-586, miR-620 and members of the miR-200 family inhibit late steps of
21 viral infection. Since none of these miRNAs except miR-185 has been previously associated
22 with HCV infection[39], it might be interesting to further characterize the involvement of these
23 miRNAs in HCV-host interactions. Interestingly, an overall proviral effect of miR-501-3p was
24 also observed by Li and colleagues[2], however the mechanism of action was not studied. By
25 characterizing the role of miR-501-3p in the HCV life cycle, we uncovered OGT as a miR-
26 501-3p target in liver-derived cells and showed for the first time a link between O-
27 GlcNAcylation and HCV infection. These results indicate that genome-wide miRNA functional

1 screens represent a powerful strategy to dissect the role of miRNAs in pathogen-host
2 interactions.

3 While N-glycosylation of HCV envelope glycoproteins plays an important role for
4 escape from virus-neutralizing antibodies[40], so far no functional association between HCV
5 and O-glycosylation has been reported. In contrast to N-linked glycosylation that consists of
6 the attachment of a glycan to a nitrogen of an asparagine residue of proteins in the ER/Golgi
7 prior to their trafficking to the plasma membrane and/or their secretion, the glycosylation of
8 serine and threonine residues with O-GlcNAc is a post-translational modification (PTM) of
9 intracellular proteins that are localized in the nucleus, cytoplasm or mitochondria. The O-
10 glycosylation/deglycosylation of proteins is catalyzed by a single pair of nucleo-cytoplasmic
11 enzymes, OGT/OGA. O-GlcNAcylation is complementary to protein
12 phosphorylation/dephosphorylation, another more broadly known abundant protein PTM that
13 involves numerous kinases/phosphatases. OGT/OGA are often found in protein complexes
14 that also include kinases/phosphatases and a protein can be either O-GlcNAcylated or
15 phosphorylated on a same residue to fine-tune cellular signaling[41]. O-GlcNAcylation and
16 phosphorylation on the same or neighboring serine or threonine residue is known as yin yang
17 site[42].

18 O-GlcNAcylation plays a major role in the regulation of metabolic pathways in the
19 liver, including insulin signaling, bile acid metabolism and lipogenesis[35]. The large number
20 of OGT/OGA substrates and cellular pathways regulated by O-GlcNAcylation hampers a
21 detailed characterization of the role of these proteins in HCV infection. Since i) HCV
22 assembly takes place at ER-derived membranes, ii) OGT/OGA are not known to localize in
23 the ER lumen, and iii) O-GlcNAcylation of extracellular proteins containing EGF-like domains
24 is catalyzed by EGF domain-specific OGT (EOGT) in the ER lumen in an OGT-independent
25 manner[43]), OGT/OGA most likely modulate HCV infection by post-translationally modifying
26 one or several cellular factors required for HCV morphogenesis rather than by affecting viral
27 proteins, although HCV glycoproteins contain putative O-GlcNAcylation sites as determined
28 using OGlcNAcScan, OGTsite and YingOYang1.2 bioinformatics tools (data not shown).

Regarding HCV host factors that may be regulated by OGT/OGA, O-GlcNAcylation sites have been predicted in human CLDN1[44] and OCLN at serine sites that can also be phosphorylated and this has been suggested to potentially play a role for HCV entry[45]. However, in our experimental setting we did not observe a significant effect of OGT-silencing on the early steps of HCV infection, suggesting that O-GlcNAcylation of CLDN1 and/or OCLN likely does not play a major role in HCV infection. Other host factors important for the HCV life cycle are well-known O-GlcNAcylated proteins, as for example various nuclear pore complex proteins (Nups) including Nup98, Nup153 and Nup155 that are involved in HCV replication and assembly and/or may be associated with viral particles[46, 47, 48]. However, since depletion of Nups was reported to alter HCV replication and/or assembly but to have no impact on the specific infectivity of HCV particles[46] in contrast to the depletion of OGT as shown here, it is unlikely that a modulation of Nup O-GlcNAcylation accounts for the effects of OGT-silencing and/or OGT/OGA inhibitors on HCVcc infectivity observed in our study. This is in line with our observation that OGT knock-down had no effect on Dengue virus (DENV) replication and infectivity (unpublished observations KH, MZ and Evelyne Schaffer, IBMC, Strasbourg), although Nup98 had been suggested to potentially play a role for DENV infection[46]. These data suggest that OGT does not broadly modulate the infectivity of viruses of the *Flaviviridae* family.

However, OGT and/or O-GlcNAcylation have been reported to play a role in the infection with other viruses[49, 50, 51]. Interestingly, while OGT expression modulates the levels of human papillomavirus 16 (HPV16) oncoproteins E6 and E7[52], E6 in turn can up-regulate OGT to increase O-GlcNAcylation and the oncogene activities of HPV[53], suggesting that OGT/O-GlcNAcylation could play a role in virus-induced cancer. In cell culture, HCV infection appeared to be associated with a minor decrease in OGT expression in line with an antiviral role of O-GlcNAcylation. In contrast, an increased OGT expression was observed in HCC tissues of HCV-infected patients. Since OGT has been suggested to activate oncogenic signaling pathways in non-alcoholic steatohepatitis-related HCC[54] and O-GlcNAcylation has been associated with HCC recurrence linked to increased O-

GlcNAcylation after liver transplantation[38], these data suggest that in addition to their effect on the HCV life cycle, OGT/O-GlcNAcylation may also play a role in HCV-induced hepatocarcinogenesis.

Acknowledgments

We wish to thank Gerald W. Hart and Stéphan Hardivillé, the CardioPEG CoreC4 (NHLBI P01 HL107153) for providing AL24 and for useful technical discussions. We are grateful to David Vocadlo (Simon Fraser University, Burnaby, Canada) for the gift of Ac₄5S-GlcNAc. We also thank Ralf Bartenschlager (University of Heidelberg, Germany) for providing the plasmids for production of HCVcc and Frank Chisari (The Scripps Research Institute, La Jolla, CA) for the gift of Huh7.5.1 cells. We acknowledge Evelyne Schaeffer (CNRS UPR3572, IBMC, Strasbourg) for the DENV experiment, Charlotte Bach and Christine Thumann (Inserm, U1110, Strasbourg) for excellent technical work during the functional miRNA mimic screen, as well as Armando A. Roca-Suarez (Inserm, U1110, Strasbourg), Hussein El Saghire (Inserm, U1110, Strasbourg), Arnaud Kopp (IGBMC, Department of Functional Genomics and Cancer) and Erika Girardi (UPR 9002, IBMC, Strasbourg) for helpful discussions. We thank the INGESTEM infrastructure for access to the IGBMC high-throughput screening workstation.

References

- 1 Jopling CL, Yi M, Lancaster AM, *et al.* Modulation of hepatitis C virus RNA abundance by a liver-specific MicroRNA. *Science* 2005;**309**:1577-81.
- 2 Li Q, Lowey B, Sodroski C, *et al.* Cellular microRNA networks regulate host dependency of hepatitis C virus infection. *Nat Commun* 2017;**8**:1789.
- 3 Baumert TF, Juhling F, Ono A, *et al.* Hepatitis C-related hepatocellular carcinoma in the era of new generation antivirals. *BMC Med* 2017;**15**:52.

- 1
2
3 1 4 Pawlotsky JM. Hepatitis C Virus Resistance to Direct-Acting Antiviral Drugs in
4 2 Interferon-Free Regimens. *Gastroenterology* 2016;**151**:70-86.
5
6
7 3 5 Dietz J, Susser S, Vermehren J, *et al.* Patterns of Resistance-Associated
8 4 Substitutions in Patients With Chronic HCV Infection Following Treatment With Direct-Acting
9 5 Antivirals. *Gastroenterology* 2018;**154**:976-88 e4.
10
11
12 6 6 Zeisel MB, Baumert TF. Clinical development of hepatitis C virus host-targeting
13 7 agents. *Lancet* 2017;**389**:674-5.
14
15
16 8 7 Zeisel MB, Crouchet E, Baumert TF, *et al.* Host-Targeting Agents to Prevent and
17 9 Cure Hepatitis C Virus Infection. *Viruses* 2015;**7**:5659-85.
18
19
20 10 8 Lupberger J, Zeisel MB, Xiao F, *et al.* EGFR and EphA2 are host factors for hepatitis
21 11 C virus entry and possible targets for antiviral therapy. *Nature Medicine* 2011;**17**:589-95.
22
23
24 12 9 Fuchs BC, Hoshida Y, Fujii T, *et al.* Epidermal growth factor receptor inhibition
25 13 attenuates liver fibrosis and development of hepatocellular carcinoma. *Hepatology*
26 14 2014;**59**:1577-90.
27
28
29 15 10 Masaki T, Arend KC, Li Y, *et al.* miR-122 stimulates hepatitis C virus RNA synthesis
30 16 by altering the balance of viral RNAs engaged in replication versus translation. *Cell Host*
31 17 *Microbe* 2015;**17**:217-28.
32
33
34 18 11 Janssen HL, Reesink HW, Lawitz EJ, *et al.* Treatment of HCV infection by targeting
35 19 microRNA. *N Engl J Med* 2013;**368**:1685-94.
36
37
38 20 12 van der Ree MH, de Vree JM, Stelma F, *et al.* Safety, tolerability, and antiviral effect
39 21 of RG-101 in patients with chronic hepatitis C: a phase 1B, double-blind, randomised
40 22 controlled trial. *Lancet* 2017;**389**:709-17.
41
42
43 23 13 Bandiera S, Pfeffer S, Baumert TF, *et al.* miR-122--a key factor and therapeutic target
44 24 in liver disease. *J Hepatol* 2015;**62**:448-57.
45
46
47 25 14 Li H, Jiang JD, Peng ZG. MicroRNA-mediated interactions between host and hepatitis
48 26 C virus. *World J Gastroenterol* 2016;**22**:1487-96.
49
50
51 27 15 Li Q, Brass AL, Ng A, *et al.* A genome-wide genetic screen for host factors required
52 28 for hepatitis C virus propagation. *Proc Natl Acad Sci U S A* 2009;**106**:16410-5.

- 1
2
3 16 Poenisch M, Metz P, Blankenburg H, *et al.* Identification of HNRNPK as regulator of
4 hepatitis C virus particle production. PLoS Pathog 2015;**11**:e1004573.
5
6
7 17 Bandiera S, Pernot S, El Saghire H, *et al.* Hepatitis C Virus-Induced Upregulation of
8 MicroRNA miR-146a-5p in Hepatocytes Promotes Viral Infection and Deregulates Metabolic
9 Pathways Associated with Liver Disease Pathogenesis. J Virol 2016;**90**:6387-400.
10
11
12 18 Da Costa D, Turek M, Felmlee DJ, *et al.* Reconstitution of the entire hepatitis C virus
13 life cycle in non-hepatic cells. J Virol 2012;**86**:11919-25.
14
15
16 19 Gloster TM, Zandberg WF, Heinonen JE, *et al.* Hijacking a biosynthetic pathway
17 yields a glycosyltransferase inhibitor within cells. Nat Chem Biol 2011;**7**:174-81.
18
19
20 20 Yuzwa SA, Macauley MS, Heinonen JE, *et al.* A potent mechanism-inspired O-
21 GlcNAcase inhibitor that blocks phosphorylation of tau in vivo. Nat Chem Biol 2008;**4**:483-90.
22
23
24 21 Schmittgen TD, Livak KJ. Analyzing real-time PCR data by the comparative C(T)
25 method. Nat Protoc 2008;**3**:1101-8.
26
27
28 22 Jin Y, Chen Z, Liu X, *et al.* Evaluating the microRNA targeting sites by luciferase
29 reporter gene assay. Methods Mol Biol 2013;**936**:117-27.
30
31
32 23 Van Renne N, Roca Suarez AA, Duong FHT, *et al.* miR-135a-5p-mediated
33 downregulation of protein tyrosine phosphatase receptor delta is a candidate driver of HCV-
34 associated hepatocarcinogenesis. Gut 2018;**67**:953-62.
35
36
37 24 Mosteller F, Tukey J. Data Analysis and Regression. Reading, MA: Addison-Wesley,
38 1977.
39
40
41 25 Amaratunga D, Cabrera J. Analysis of Data from Viral DNA Microchips. Journal of the
42 American Statistical Association 2001;**96**:1161.
43
44
45 26 Smyth GK. Linear models and empirical Bayes methods for assessing differential
46 expression in microarray experiments. Statistical Applications in Genetics and Molecular
47 Biology 2004;**3**:Article 3.
48
49
50 27 Strimmer K. fdrtool: a versatile R package for estimating local and tail area-based
51 false discovery rates. Bioinformatics 2008;**24**:1461-2.
52
53
54
55
56
57
58
59
60

- 1
- 2
- 3 1 28 Cheng M, Si Y, Niu Y, *et al.* High-throughput profiling of alpha interferon- and
- 4 2 interleukin-28B-regulated microRNAs and identification of let-7s with anti-hepatitis C virus
- 5 3 activity by targeting IGF2BP1. J Virol 2013;**87**:9707-18.
- 6
- 7 4 29 Shirasaki T, Honda M, Shimakami T, *et al.* MicroRNA-27a regulates lipid metabolism
- 8 5 and inhibits hepatitis C virus replication in human hepatoma cells. J Virol 2013;**87**:5270-86.
- 9
- 10 6 30 Bandyopadhyay S, Friedman RC, Marquez RT, *et al.* Hepatitis C virus infection and
- 11 7 hepatic stellate cell activation downregulate miR-29: miR-29 overexpression reduces
- 12 8 hepatitis C viral abundance in culture. J Infect Dis 2011;**203**:1753-62.
- 13
- 14 9 31 Chen Y, Chen J, Wang H, *et al.* HCV-induced miR-21 contributes to evasion of host
- 15 10 immune system by targeting MyD88 and IRAK1. PLoS Pathog 2013;**9**:e1003248.
- 16
- 17 11 32 Ariumi Y, Kuroki M, Maki M, *et al.* The ESCRT system is required for hepatitis C virus
- 18 12 production. PLoS One 2011;**6**:e14517.
- 19
- 20 13 33 Paul D, Madan V, Bartenschlager R. Hepatitis C virus RNA replication and assembly:
- 21 14 living on the fat of the land. Cell Host Microbe 2014;**16**:569-79.
- 22
- 23 15 34 Meyers NL, Fontaine KA, Kumar GR, *et al.* Entangled in a membranous web: ER and
- 24 16 lipid droplet reorganization during hepatitis C virus infection. Curr Opin Cell Biol 2016;**41**:117-
- 25 17 24.
- 26
- 27 18 35 Yang X, Qian K. Protein O-GlcNAcylation: emerging mechanisms and functions. Nat
- 28 19 Rev Mol Cell Biol 2017;**18**:452-65.
- 29
- 30 20 36 Piver E, Boyer A, Gaillard J, *et al.* Ultrastructural organisation of HCV from the
- 31 21 bloodstream of infected patients revealed by electron microscopy after specific
- 32 22 immunocapture. Gut 2017;**66**:1487-95.
- 33
- 34 23 37 Lerat H, Honda M, Beard MR, *et al.* Steatosis and liver cancer in transgenic mice
- 35 24 expressing the structural and nonstructural proteins of hepatitis C virus. Gastroenterology
- 36 25 2002;**122**:352-65.
- 37
- 38 26 38 de Queiroz RM, Carvalho E, Dias WB. O-GlcNAcylation: The Sweet Side of the
- 39 27 Cancer. Front Oncol 2014;**4**:132.
- 40
- 41
- 42
- 43
- 44
- 45
- 46
- 47
- 48
- 49
- 50
- 51
- 52
- 53
- 54
- 55
- 56
- 57
- 58
- 59
- 60

- 1
2
3 1 39 Singaravelu R, O'Hara S, Jones DM, *et al.* MicroRNAs regulate the immunometabolic
4
5 2 response to viral infection in the liver. *Nat Chem Biol* 2015;**11**:988-93.
6
7 3 40 Lavie M, Hanouille X, Dubuisson J. Glycan Shielding and Modulation of Hepatitis C
8
9 4 Virus Neutralizing Antibodies. *Front Immunol* 2018;**9**:910.
10
11 5 41 Hart GW, Slawson C, Ramirez-Correa G, *et al.* Cross talk between O-GlcNAcylation
12
13 6 and phosphorylation: roles in signaling, transcription, and chronic disease. *Annu Rev*
14
15 7 *Biochem* 2011;**80**:825-58.
16
17 8 42 Hart GW, Greis KD, Dong LY, *et al.* O-linked N-acetylglucosamine: the "yin-yang" of
18
19 9 Ser/Thr phosphorylation? Nuclear and cytoplasmic glycosylation. *Adv Exp Med Biol*
20
21 10 1995;**376**:115-23.
22
23 11 43 Sakaidani Y, Nomura T, Matsuura A, *et al.* O-linked-N-acetylglucosamine on
24
25 12 extracellular protein domains mediates epithelial cell-matrix interactions. *Nat Commun*
26
27 13 2011;**2**:583.
28
29 14 44 Butt AM, Khan IB, Hussain M, *et al.* Role of post translational modifications and novel
30
31 15 crosstalk between phosphorylation and O-beta-GlcNAc modifications in human claudin-1, -3
32
33 16 and -4. *Mol Biol Rep* 2012;**39**:1359-69.
34
35 17 45 Butt AM, Feng D, Nasrullah I, *et al.* Computational identification of interplay between
36
37 18 phosphorylation and O-beta-glycosylation of human occludin as potential mechanism to
38
39 19 impair hepatitis C virus entry. *Infect Genet Evol* 2012;**12**:1235-45.
40
41 20 46 Neufeldt CJ, Joyce MA, Levin A, *et al.* Hepatitis C virus-induced cytoplasmic
42
43 21 organelles use the nuclear transport machinery to establish an environment conducive to
44
45 22 virus replication. *PLoS Pathog* 2013;**9**:e1003744.
46
47 23 47 Lussignol M, Kopp M, Molloy K, *et al.* Proteomics of HCV virions reveals an essential
48
49 24 role for the nucleoporin Nup98 in virus morphogenesis. *Proc Natl Acad Sci U S A*
50
51 25 2016;**113**:2484-9.
52
53 26 48 Zhu Y, Liu TW, Madden Z, *et al.* Post-translational O-GlcNAcylation is essential for
54
55 27 nuclear pore integrity and maintenance of the pore selectivity filter. *J Mol Cell Biol* 2016;**8**:2-
56
57 28 16.
58
59
60

1
2
3 1 49 Jochmann R, Thureau M, Jung S, *et al.* O-linked N-acetylglucosaminylation of Sp1
4
5 2 inhibits the human immunodeficiency virus type 1 promoter. *J Virol* 2009;**83**:3704-18.
6
7 3 50 Groussaud D, Khair M, Tollenaere AI, *et al.* Hijacking of the O-GlcNAcZYME complex
8
9 4 by the HTLV-1 Tax oncoprotein facilitates viral transcription. *PLoS Pathog*
10
11 5 2017;**13**:e1006518.
12
13 6 51 Angelova M, Ortiz-Meoz RF, Walker S, *et al.* Inhibition of O-Linked N-
14
15 7 Acetylglucosamine Transferase Reduces Replication of Herpes Simplex Virus and Human
16
17 8 Cytomegalovirus. *J Virol* 2015;**89**:8474-83.
18
19 9 52 Kim M, Kim YS, Kim H, *et al.* O-linked N-acetylglucosamine transferase promotes
20
21 10 cervical cancer tumorigenesis through human papillomaviruses E6 and E7 oncogenes.
22
23 11 *Oncotarget* 2016;**7**:44596-607.
24
25 12 53 Zeng Q, Zhao RX, Chen J, *et al.* O-linked GlcNAcylation elevated by HPV E6
26
27 13 mediates viral oncogenesis. *Proc Natl Acad Sci U S A* 2016;**113**:9333-8.
28
29 14 54 Xu W, Zhang X, Wu JL, *et al.* O-GlcNAc transferase promotes fatty liver-associated
30
31 15 liver cancer through inducing palmitic acid and activating endoplasmic reticulum stress. *J*
32
33 16 *Hepatol* 2017;**67**:310-20.
34
35 17 55 Boldanova T, Suslov A, Heim MH, *et al.* Transcriptional response to hepatitis C virus
36
37 18 infection and interferon-alpha treatment in the human liver. *EMBO Mol Med* 2017;**9**:816-34.
38
39
40
41
42
43
44
45
46
47
48
49
50
51
52
53
54
55
56
57
58
59
60

Figure legends

Figure 1. High-throughput screen identifies human miRNAs that regulate the HCV life

cycle. (A) Schematic outline of the miRNA mimic screen strategy. Huh7.5.1 cells were transfected with miRNA mimics or controls prior to infection with *Renilla* luciferase HCVcc (JcR2a) two days later (part 1). Cell supernatants of part 1 were used to inoculate naïve Huh7.5.1 cells (part 2). Cells from part 1 and part 2 were lysed at the end of each infection step (2 and 3 days post infection, respectively) to determine luciferase activity. (B) Modulation of HCV entry and replication (part 1) and/or assembly and infectivity (part 2) upon transfection of control non-targeting siRNA (siCtrl, negative control), siCD81 (inhibiting viral entry) or siApoE (inhibiting viral assembly). By inhibiting HCV entry, siCD81 impacts part 1 as well as part 2. In contrast, by specifically impairing late steps of HCV replication cycle, siApoE inhibits HCV infection only in part 2. The box plots show the sample lower quartile (25th percentile; bottom of the box), the median (50th percentile; horizontal line in box) and the upper quartile (75th percentile; top of the box) of relative light units (RLU) in each lysate. The whiskers indicate s.d. Data are from three independent experiments. (C) Effects of miRNA overexpression on each part of the HCV life cycle. Data were tested using a moderated t-test (empirical Bayes shrinkage, R-package limma[26]) for the null-hypothesis of no change of a given miRNA compared to the negative control. The resulting p-values for independent testing of each miRNA were corrected for the multiple testing situation and expressed as local false discovery rate (lfdr, R-package fdrtool[27]). miRNAs having a significant effect on either part 1 or 2 of the screen are below the thresholds indicated by dashed lines ($lfdr < 0.00027$ or 0.1226 , respectively). miRNAs that were previously reported to impact on HCV infection as well as miR-140-3p, miR-501-3p, miR-619-3p and miR-4778-5p are highlighted in blue ($Log_2(FC) < 0$) or red ($Log_2(FC) > 0$). Data are from three independent experiments. (D) Effect of miR-140-3p, miR-501-3p, miR-619-3p and miR-4778-5p on the HCV life cycle. Huh7.5.1 cells were transfected with siCtrl (Ctrl), miR-140-3p, miR-501-3p, miR-619-3p or miR-4778-5p and infection experiments were carried out as described in A. HCV infection was determined as luciferase activity. Results represent mean

1
2
3 1 percentage \pm s.d. from three independent experiments in triplicate. The dashed line indicates
4
5 2 values from control-transfected cells set at 100%. Statistics: *, p -value ≤ 0.05 , Mann-Whitney
6
7 3 test.
8
9 4

11 **Figure 2. OGT is a novel host cell factor involved in the late steps of the HCV life cycle.**

12
13
14 6 Huh7.5.1 cells were transfected with a set of siRNAs against 28 predicted targets of miR-
15
16 7 501-3p and/or miR-619-3p, and infected with HCVcc JcR2A according to the two-step
17
18 8 protocol depicted in Fig. 1A. siCD81, antagomiR-122 and siApoE were used as loss-of-
19
20 9 function controls to perturb HCV entry, translation/replication and assembly, respectively.
21
22 10 miR-501-3p and miR-619-3p, which were ineffective in part 1 of the screen but enhanced
23
24 11 HCV infection in part 2, were transfected in parallel. HCV infection was quantified as fold
25
26 12 change of luciferase activity with respect to negative control (siCtrl). Results for different
27
28 13 replicates are shown as individual points. For each gene, median fold change of luciferase
29
30 14 activity \pm s.d. is shown as black horizontal lines. The dashed line indicates a fold change of
31
32 15 1. Data are from three independent experiments in triplicate. Results for miR-501-3p, miR-
33
34 16 619-3p and siOGT that increase HCV infection in part 2 are depicted in red. Results for
35
36 17 siRNA targeting *PPP3CA*, *CEBPA*, *MID1*, *WDFY3*, *DCX*, *SLC35D1*, *CSDE1*, *GAN*, *USP37*,
37
38 18 *MAPK9*, *DCC*, *RNF144A*, or *PPP2R2C* that significantly modulated HCV infection in part 1
39
40 19 and/or part 2 but did not phenocopy the effect of miR-501-3p and miR-619-3p are depicted in
41
42 20 blue.
43
44
45 21

47 **Figure 3. miR-501-3p mediates post-transcriptional regulation of OGT by decreasing**

48
49 23 **its expression at the protein level.** Huh7.5.1 cells were transfected with siCtrl (Ctrl), a pool
50
51 24 of siRNA against *OGT*, miR-501-3p or miR-619-3p. After 96h, RNA and proteins were
52
53 25 purified, and OGT expression analyzed by RT-qPCR and Western blot. (A) Percentage of
54
55 26 *OGT* mRNA expression in miRNA-transfected cells as compared to negative control. Results
56
57 27 are presented as mean \pm s.d. and are from three independent experiments in triplicate. The
58
59 28 dashed line indicates values from control-transfected cells set at 100%. Statistics: *, p -value

1 ≤ 0.05 , t-test (B) OGT protein expression. Left: percentage of OGT protein expression in
2 siRNA- or miRNA-transfected cells as assessed by quantification of Western blots. OGT
3 levels were normalized to actin levels using ImageLab™ 5.2.1 software (BioRad). Results
4 are presented as mean \pm s.d. and are from three independent experiments. The dashed line
5 indicates values from control-transfected cells set at 100%. Statistics: *, p -value ≤ 0.05 , t-
6 test. Right: representative Western blot analysis. (C) Analysis of miRNA targeting of *OGT*
7 expression by dual luciferase reporter assay. Left: HeLa cells were co-transfected with a
8 miR-501-3p mimic and a dual luciferase reporter plasmid containing either wild type miR-
9 501-3p (RLuc wt *OGT* 3'UTR) or mutated miR-501-3p binding site (RLuc mt *OGT* 3'UTR) to
10 modulate RLuc expression. Co-transfection of the miR-501-3p mimic and empty RLuc vector
11 was used as control. Data are expressed as mean percentage of *Renilla* luciferase activity \pm
12 s.d. normalized to *firefly* luciferase, and relative to co-transfection of the vectors with non-
13 targeting miRNA (miR-Ctrl). Results are from three independent experiments in triplicate.
14 The dashed line indicates values from control-transfected cells set at 100%. Statistics: *, p -
15 value ≤ 0.05 , t-test. Right: Schematic representation of the used constructs.

16
17 **Figure 4. Silencing of *OGT* affects HCV morphogenesis and infectivity.** (A) Analysis of
18 HCV infectivity. Huh7.5.1 cells were transfected with siCtrl, a pool of siRNA against *OGT* or
19 ApoE as a loss-of-function control to perturb HCV assembly, prior to infection with HCVcc
20 (Jc1) two days later (entry and replication). Mock-transfected cells were used as control
21 (Ctrl). After another 48h, intra- and extracellular HCVcc particles were used to infect naïve
22 Huh7.5.1 cells (assembly and infectivity). Virus supernatants of Huh7.5.1 cells were assayed
23 by (left) endpoint dilution assay (TCID₅₀). Intra- and extracellular HCV RNA was purified and
24 analyzed by RT-qPCR to calculate (right) the specific infectivity (TCID₅₀/RNA). Data are
25 expressed as mean percentage as compared to control \pm s.d. Results are from four
26 independent experiments in triplicate. The dashed line indicates values from control-
27 transfected cells set at 100%. Statistics: *, p -value ≤ 0.05 , Mann-Whitney test. (B) Genotype-
28 independent effect of *OGT* on HCV infection. Huh7.5.1 cells were transfected with siCtrl or

1 siOGT prior to infection with HCVcc JcR2a (genotype 2a), H77R2a (genotype 1a) or
 2 Con1R2a (genotype 1b). Experiments were carried out and analyzed as described in A. Data
 3 are expressed as mean percentage of Renilla luciferase activity as compared to control \pm s.d.
 4 Results are from three independent experiments in quadruplicate. The dashed line indicates
 5 values from control-transfected cells set at 100%. Statistics: *, p -value < 0.05, Mann-Whitney
 6 test. (C) Activity of OGT/OGA inhibitors on O-GlcNAcylation. The activity of Ac₄5S-GlcNAc
 7 (OGT inhibitor) or Thiamet G (OGA inhibitor) on O-GlcNAcylation of proteins in Huh7.5.1
 8 cells was demonstrated by Western blot as described in Supplementary Methods. (D) Effect
 9 of O-GlcNAcylation on HCV infectivity. Huh7.5.1 cells were electroporated with HCVcc
 10 (JcR2a), prior to treatment with increasing concentrations of Ac₄5S-GlcNAc (OGT inhibitor,
 11 left) or Thiamet G (OGA inhibitor, right) 4h later. After 96h, supernatants were transferred
 12 onto naïve Huh7.5.1 cells and electroporated cells were lysed to determine luciferase
 13 activity. Luciferase activity in infected Huh7.5.1 cells was assessed 72h later. Data are
 14 expressed as mean percentage as compared to control \pm s.d. Results are from three
 15 independent experiments in quadruplicate. The dashed line indicates values from vehicle-
 16 treated cells set at 100%. Statistics: *, p -value < 0.05, Mann-Whitney test.

Figure 5. Silencing of OGT modulates HCVcc biophysical properties. (A) Separation of
 HCVcc by iodixanol density gradient ultracentrifugation. HCVcc were produced in non-
 targeting siRNA control- or siOGT-transfected Huh7.5.1 cells. After overlaying HCVcc
 (JcR2A) on a 4%-40% iodixanol step gradient and ultracentrifugation for 16h, fractions of
 HCV particles were used to infect naïve Huh7.5.1 cells in order to determine TCID₅₀. HCV
 RNA of each fraction was purified and analyzed by RT-qPCR. Data are expressed as mean \pm
 s.d. from three independent experiments. (B) Specific infectivity (TCID₅₀/RNA) was
 calculated and the density was determined by weighting each fraction. Specific infectivity of
 each fraction is expressed as fold change as compared to the total infectivity of the control.
 Data are expressed as mean \pm s.d. from three independent experiments. (C-D) ApoE and
 ApoB concentrations in the individual fractions were determined by ELISA. The dashed lines

indicate limits of quantification of the assays. Data are expressed as mean \pm s.d. from three independent experiments.

Figure 6. Silencing of *OGT* increases the size of HCVcc. (A) Representative pictures of HCV particles generated in Huh7.5.1 cells transfected with non-targeting siRNA (siCtrl) or siOGT. (B-F) Comparative analysis of particle size distribution for immunocapture (IC) from HCV particles produced in Huh7.5.1 cells transfected with siCtrl or siOGT prior to infection with HCVcc (JcR2a) following sucrose-cushion purification (B) or iodixanol gradient fractionation (C-F) of HCVcc. HCVcc were transferred via anti-E2 antibody AR3A on electron microscopy (EM) grids through IC. Particle size distribution was assessed from a series of randomly acquired electron micrographs with Image-J software (NIH). Results from one of three (A-B) or two (C-F) independent experiments are shown. Black lines: size distribution of immunocaptured HCVcc produced in siCtrl-transfected cells. Grey lines: size distribution of immunocaptured HCVcc produced in siOGT-transfected cells.

Figure 7. *OGT* expression increases in HCC. (A-B) Huh7.5.1 cells were infected with HCV (JcR2a). After 72h, RNA and proteins were purified, and *OGT* expression analyzed by RT-qPCR and Western blot. (A) Percentage of *OGT* mRNA expression relative to uninfected Huh7.5.1 cells (Ctrl). Results are presented as mean \pm s.d. from three independent experiments in duplicate. The dashed line indicates values from uninfected Huh7.5.1 cells set at 100%. Statistics: *, p -value < 0.05, Mann-Whitney test. (B) *OGT* protein expression. Left: percentage of *OGT* protein expression relative to uninfected Huh7.5.1 cells (Ctrl) following quantification of Western blots as described in Supplementary Methods. Results are presented as mean \pm s.d. from three independent experiments. The dashed line indicates values from uninfected Huh7.5.1 cells set at 100%. Statistics: *, p -value < 0.05, Mann-Whitney test. Right: representative Western blot analysis of *OGT* and actin. (C) *OGT* expression and viral load in liver tissue from 22 HCV-infected patients and 6 patients not infected with HCV described in[55]. Spearman correlation: $\rho = 0.06004019$, p -value = 0.77.

1
2
3 1 (D-E) OGT expression in liver tissue from 22 HCV-infected patients and 6 patients not
4
5 2 infected with HCV according to fibrosis (D) or activity (E) scores described in[55]. Wilcoxon
6
7 3 test: F1 vs F0 p-value = 0,38; F2 vs F0 p-value = 0,18; F3 vs F0 p-value = 0,43; F4 vs F0 p-
8
9 4 value = 0,17; A1 vs A0 p-value = 0,28; A2 vs A0 p-value = 0,23; A3 vs A0 p-value = 0,09. (F)
10
11 5 OGT expression in tumor (HCC) and non-tumor (Ctrl) liver tissue from 39 HCV-infected
12
13 6 patients, 83 HBV-infected, 80 patients with alcoholic liver disease (ALD) and 13 patients with
14
15 7 non-alcoholic liver disease (NAFLD) as described in Supplementary Methods. *, p-value <
16
17 8 0.05, Wilcoxon test.
18
19
20 9
21
22
23
24
25
26
27
28
29
30
31
32
33
34
35
36
37
38
39
40
41
42
43
44
45
46
47
48
49
50
51
52
53
54
55
56
57
58
59
60

Table 1. Computational analysis of miR-501-3p and miR-619-3p targets and pathway enrichment.

miRNA ID	Target gene symbol	Pathway or network
miR-501-3p	<i>MEF2A; PPP3CA; PPP3CC</i>	<i>Calcium signaling</i>
	<i>HMGCS1</i>	<i>Cholesterol biosynthesis</i>
	<i>AFF4; CHMP1B; CUX1; DCLK1;</i>	Inflammatory response, dermatological
	<i>LMX1A; PTBP2; RBMS1; RC3H1;</i>	diseases and conditions, inflammatory
	<i>SCN2A; SEC63; ZFH4</i>	disease
	<i>CDK6; CSDE1; GLI2; HOXD10;</i>	Cellular development, nervous system
	<i>LSM5; MEF2A; MYCN; OGT;</i>	development and function; organ
	<i>PPP2R2C; PPP2R5E; SEMA3C;</i>	morphology
	<i>TFDP2</i>	
	<i>CIT; COL10A1; FNBP1L; GAN;</i>	Cell death and survival; cellular
miR-619-3p	<i>HERC1; KPNA4; NONO; SHPRH;</i>	compromise; free radical scavenging
	<i>STRN; TARDBP; UBE2H; USP37</i>	
	<i>ATXN1; CBLL1; CEBPA; DCC;</i>	Cell morphology, cellular assembly and
	<i>PEX5L; RCC2; RNF144A; ZC3H12C</i>	organization; cellular function and
		maintenance
	<i>RUNX1T1; SMAD3</i>	<i>Adipocyte biogenesis</i>
	<i>FOXG1; GPBP1; MID1; MKL2; MSI1;</i>	Cell cycle; organismal injury and
	<i>PCBP2; WDFY3</i>	abnormalities; cancer
	<i>ACVR2B; DCX; ESRRG; MAPK9;</i>	Carbohydrate metabolism, energy
	<i>OGT; PCBP1; PDE3B; SMAD3;</i>	production; small molecule biochemistry
miR-619-3p	<i>SMARCC1; TGFB3; PAPOLA</i>	
	<i>RUNX1T1; SHANK2; SLC35D1</i>	Gene expression, lipid metabolism, small molecule biochemistry

Supplementary Information

A functional microRNA screen uncovers O-linked N-acetylglucosamine transferase as a host factor modulating hepatitis C virus morphogenesis

Katharina Herzog^{1,2*}, Simonetta Bandiera^{1,2*}, Sophie Pernot^{1,2}, Catherine Fauvelle^{1,2}, Frank Jühling^{1,2}, Amélie Weiss^{2,3,4,5}, Anne Bull⁶, Sarah C. Durand^{1,2}, Béatrice Chane-Woon-Ming^{2,7}, Sébastien Pfeffer^{2,7}, Marion Mercey⁸, Hervé Lerat⁸, Jean-Christophe Meunier⁶, Wolfgang Raffelsberger^{2,3,4,5}, Laurent Brino^{2,3,4,5}, Thomas F. Baumert^{1,2,9,#}, Mirjam B. Zeisel^{1,2,10,#}

¹Inserm, U1110, Institut de Recherche sur les Maladies Virales et Hépatiques, Strasbourg, France; ²Université de Strasbourg, Strasbourg, France; ³Institut de Génétique et de Biologie Moléculaire et Cellulaire, Illkirch, France ; ⁴CNRS, UMR7104, Illkirch, France ; ⁵Inserm, U1258, Illkirch, France ; ⁶Inserm U1259, Faculté de Médecine, Université François Rabelais and CHRU de Tours, Tours, France ; ⁷Architecture et Réactivité de l'ARN – UPR 9002, Institut de Biologie Moléculaire et Cellulaire du CNRS, Strasbourg, France; ⁸Institute for Advanced Biosciences, Centre de Recherche UGA - Inserm U1209 - CNRS UMR 5309, Grenoble, France, ⁹Institut Hospitalo-Universitaire, Pôle Hépato-digestif, Hôpitaux Universitaires de Strasbourg, Strasbourg, France; ¹⁰Inserm, U1052, CNRS UMR 5286, Centre Léon Bérard (CLB), Cancer Research Center of Lyon (CRCL), Université de Lyon (UCBL), Lyon, France

*Authors contributed equally to this work

Supplementary Material and methods

Cells and cell culture conditions. The source and culture conditions of Huh7.5.1 cells have been described[1]. HeLa cells were purchased from ATCC and cultured in Dulbecco's modified Eagle medium (Gibco® DMEM GlutaMAX™, ThermoFisher Scientific) containing 1% sodium pyruvate as described for Huh7.5.1 cells[1].

Viruses and infectivity assays. Cell culture-derived recombinant cell culture-derived hepatitis C virus (HCVcc) Jc1 (genotype 2a/2a chimera), H77R2a (genotype 1a/2a chimera engineered for *Renilla* luciferase expression), Con1R2a (genotype 1b/2b chimera engineered for *Renilla* luciferase expression), and JcR2a (genotype 2a/2a chimera engineered for *Renilla* luciferase expression) were generated in Huh7.5.1 cells as described[1, 2, 3, 4]. HCVcc infectivity was determined by calculating the 50% tissue culture infectious dose (TCID₅₀) using anti-NS5A antibody as described[5, 6] or by assessing luciferase activity. HCVcc were used at 10⁵-10⁶ TCID₅₀/mL throughout the study. HCV RNA was purified using a QIAmp viral RNA minikit (Qiagen) and analyzed by one-step RT-qPCR using a Sensi Fast NO ROX kit (Bioline) according to the manufacturer's instructions. Standard curves were performed using 10-fold dilution series of HCV RNA.

Purification of HCVcc particles using sucrose cushion or iodixanol density gradient.

HCVcc (JcR2a) were concentrated 10-fold using a Vivaspin column (GE Healthcare). For sucrose cushion purification, HCVcc were purified by overlaying 3.5 mL of culture media on 1.5 mL of 20% sucrose, and by ultracentrifuging samples for 4h at 40,000 rpm on a SW-55 rotor (Beckman Coulter). Purified HCVcc were resuspended in 30 µL of PBS for analysis via immunocapture and electron microscopy. Density distributions of infectious HCVcc were determined by overlaying 0.5 mL culture media on a 5 mL, 4%-40% iodixanol step gradient, and ultracentrifuging samples for 16h at 40,000 rpm on a SW-55 rotor (Beckman Coulter): 625 µL fractions were carefully harvested from the top of each tube, and density was determined by weighing. Infectivity of each fraction was quantified by TCID₅₀ using anti-NS5A antibody as described[5, 6], while HCV RNA of fractions was purified and analyzed as described above. ApoB and ApoE concentrations of fractions were determined by enzyme-linked immunosorbent assay (Human Apolipoprotein B or E ELISA^{PRO} kit, Mabtech) undiluted or in a 1:50 dilution, respectively, according to the manufacturer's instructions (Mabtech).

1
2
3
4
5
6
7
8
9
10
11
12
13
14
15
16
17
18
19
20
21
22
23
24
25
26
27
28
29
30
31
32
33
34
35
36
37
38
39
40
41
42
43
44
45
46
47
48
49
50
51
52
53
54
55
56
57
58
59
60

miRNA mimics and siRNAs. Non-targeting control miRNA, miR-501-3p mimic, miR-619-3p mimic, antagomiR-122, antagomiR-501-3p, non-targeting control antagomiR, non-targeting control siRNA, siRNAs targeting *OGT*, *CD81* or *apolipoprotein E (ApoE)* and a library of 28 custom ON-TARGETplus smart pool siRNAs were purchased from Dharmacon (GE Healthcare).

miRNA expression analysis. Total RNA (100 ng) was purified from control or HCV-infected Huh7.5.1 cells using Tri reagent® (Thermo Scientific) and Direct-zol™ RNA purification kit (Zymo Research). Total RNA was first polyadenylated and reverse transcribed using a miScript II RT system (Qiagen) according to the manufacturer's instructions. The obtained cDNA was subjected to RT-qPCR using miScript SYBR Green kit (Qiagen). Primers were the mature miRNA sequence for the forward primer (Thermo Scientific) and the universal miScript primer (Qiagen) for the reverse primer. Data were analyzed by the $\Delta\Delta C_t$ method using small nucleolar RNA, C/D box 61 (SNORD61) as an endogenous reference and the non-infected samples as a calibrator[7].

Antibodies. Rabbit anti-OGT antibodies DM-17 and AL24 were purchased from Sigma or kindly provided by Dr. G. W. Hart and Dr. S. Hardivillé (Johns Hopkins University School of Medicine, Baltimore, MD)[8], respectively. Mouse anti- β -actin antibody was purchased from Abcam and mouse, rabbit or sheep HRP-conjugated secondary antibodies (A9044, A0545 and A3415, respectively) were purchased from Sigma. Sheep anti-NS5A serum for determination of TCID50 was a kind gift from M. Harris[9]. Human anti-E2 (AR3A) antibody[10] for electron microscopy analysis was kindly provided by Mansun Law (SCRIPPS, California, USA).

Western blotting. OGT and actin protein expression in human cells was assessed by Western blot as described[8] with some modifications. Briefly, cells were lysed in lysis buffer no. 6 (R&D Systems) according to the manufacturer's instructions. Equal amounts of protein

(40 µg) were size-separated through a Mini PROTEAN® TGX Stain-Free™ gel electrophoresis (Bio-Rad) and transferred to PVDF membranes (Bio-Rad). Immunoblots were performed using rabbit anti-OGT (1:2000) and mouse anti-β-actin (1:1000) antibodies[8, 11]. Antigen-antibody complexes were detected by incubating the membrane with the appropriate HRP-conjugated secondary antibodies (1:5000; 1:10,000) and imaged by enhanced chemiluminescence with a ChemiDoc MP imager (Bio-Rad). Quantification of protein expression was performed using ImageLab™ 5.2.1 software (BioRad). For analysis of OGT and GAPDH expression in liver tissue from HCV transgenic (FL-N/35) or wild-type mice[12], crude protein extracts were prepared by homogenization of frozen mouse livers (50–100 µg) in tissue lysis buffer from the Ambion PARIS RNA (Thermo Scientific) and protein isolation kit, supplemented with protease inhibitors (cOmplete™ EDTA-free protease inhibitor mixture, Sigma-Aldrich) and phosphatase inhibitors (PhosSTOP™, Sigma-Aldrich), using a tissue homogenizer (MP Fast Prep24, MP Biomedicals, Santa Ana, CA) and MP Lysing Matrix A tubes. Proteins were quantified using the BCA assay (Thermo Fisher Scientific). Western blotting was performed as described above.

Immunocapture and electron microscopy analysis of viral particles. Sucrose-cushion purified or iodixanol gradient fractionated HCVcc (JcR2a) produced in cells transfected with a non-targeting siRNA control or a pool of siRNA against OGT were transferred via anti-E2 antibody AR3A on electron microscopy (EM) grids through immunocapture (IC) as described[13]. Particles were stained with uranyl acetate dihydrate and observed in a JEOL 1230 electron microscope. Series of electron micrographs were acquired at random from IC EM grids. The images were then analyzed with Image-J software, to determine the particle size distribution.

Gene expression analysis in patient-derived liver tissue. For OGT expression analysis in patient's samples, raw data were retrieved from the Gene Expression Omnibus (GSE84346) and re-analyzed by quality-trimming (cutadapt) and mapping (HISAT2) to human genome

1
2
3
4
5
6
7
8
9
10
11
12
13
14
15
16
17
18
19
20
21
22
23
24
25
26
27
28
29
30
31
32
33
34
35
36
37
38
39
40
41
42
43
44
45
46
47
48
49
50
51
52
53
54
55
56
57
58
59
60

assembly hg19. Reads mapping to Gencode v.19 genes were counted using htseq-count and normalized applying DESeq2. Activity and fibrosis scores as well as viral load were taken from the supplemental data published in[14]. To analyze OGT expression in liver tissue of chronic hepatitis B or C patients, FPKM values and clinical data were retrieved from The Cancer Genome Atlas (TCGA, <https://www.cancer.gov/about-nci/organization/ccg/research/structural-genomics/tcga>). This data set includes samples from 39 HCV-infected patients, 83 hepatitis B virus (HBV)-infected, 80 patients with alcoholic liver disease (ALD) and 13 patients with non-alcoholic fatty liver disease (NAFLD).

Supplementary References

1 Zhong J, Gastaminza P, Cheng G, *et al.* Robust hepatitis C virus infection in vitro. Proc Natl Acad Sci U S A 2005;**102**:9294-9.

2 Reiss S, Rebhan I, Backes P, *et al.* Recruitment and activation of a lipid kinase by hepatitis C virus NS5A is essential for integrity of the membranous replication compartment. Cell Host Microbe 2011;**9**:32-45.

3 Da Costa D, Turek M, Felmlee DJ, *et al.* Reconstitution of the entire hepatitis C virus life cycle in non-hepatic cells. J Virol 2012;**86**:11919-25.

4 Fauvelle C, Felmlee DJ, Crouchet E, *et al.* Apolipoprotein E Mediates Evasion From Hepatitis C Virus Neutralizing Antibodies. Gastroenterology 2016;**150**:206-17 e4.

5 Lindenbach BD, Evans MJ, Syder AJ, *et al.* Complete replication of hepatitis C virus in cell culture. Science 2005;**309**:623-6.

6 Bandiera S, Pernot S, El Saghire H, *et al.* Hepatitis C Virus-Induced Upregulation of MicroRNA miR-146a-5p in Hepatocytes Promotes Viral Infection and Deregulates Metabolic Pathways Associated with Liver Disease Pathogenesis. J Virol 2016;**90**:6387-400.

7 Schmittgen TD, Livak KJ. Analyzing real-time PCR data by the comparative C(T) method. Nat Protoc 2008;**3**:1101-8.

8 Iyer SP, Akimoto Y, Hart GW. Identification and cloning of a novel family of coiled-coil domain proteins that interact with O-GlcNAc transferase. J Biol Chem 2003;**278**:5399-409.

Macdonald A, Crowder K, Street A, *et al.* The hepatitis C virus non-structural NS5A protein inhibits activating protein-1 function by perturbing ras-ERK pathway signaling. *J Biol Chem* 2003;**278**:17775-84.

Giang E, Dorner M, Prentoe JC, *et al.* Human broadly neutralizing antibodies to the envelope glycoprotein complex of hepatitis C virus. *Proc Natl Acad Sci U S A* 2012;**109**:6205-10.

Verrier ER, Colpitts CC, Bach C, *et al.* A targeted functional RNA interference screen uncovers glypican 5 as an entry factor for hepatitis B and D viruses. *Hepatology* 2016;**63**:35-48.

Lerat H, Honda M, Beard MR, *et al.* Steatosis and liver cancer in transgenic mice expressing the structural and nonstructural proteins of hepatitis C virus. *Gastroenterology* 2002;**122**:352-65.

Piver E, Boyer A, Gaillard J, *et al.* Ultrastructural organisation of HCV from the bloodstream of infected patients revealed by electron microscopy after specific immunocapture. *Gut* 2017;**66**:1487-95.

Boldanova T, Suslov A, Heim MH, *et al.* Transcriptional response to hepatitis C virus infection and interferon-alpha treatment in the human liver. *EMBO Mol Med* 2017;**9**:816-34.

Supplementary figure legends

Figure S1. (A) Effect of miR-501-3p inhibition on HCV infectivity. Huh7.5.1 cells were transfected with control antagomiR (Ctrl), antagomiR-122 as loss-of-function control to perturb HCV replication and antagomiR-501-3p, prior to infection with HCVcc (JcR2a) according to the two-step protocol depicted in Fig. 1A. After 48h, supernatants were transferred onto naive Huh7.5.1 cells. After 72h, Renilla Luciferase activity of infected Huh7.5.1 cells was determined. Data are expressed as mean percentage as compared to Ctrl \pm s.d. Results are from four independent experiments in quadruplicate. The dashed line indicates values from vehicle-treated cells set at 100%. Statistics: *, p -value < 0.05, Mann-Whitney test. (B) miR-501-3p expression upon HCV infection. Huh7.5.1 cells were infected with HCVcc (JcR2a).

1
2
3 1 After 72h, RNA was purified and miR-501-3p expression analyzed by RT-qPCR. Percentage
4 2 of miR-501-3p expression relative to uninfected Huh7.5.1 cells (Ctrl). Results are presented
5 3 as mean \pm s.d. from three independent experiments in duplicate. The dashed line indicates
6 4 values from uninfected Huh7.5.1 cells set at 100%. Statistics: *, p -value < 0.05, Mann-Whitney
7 5 test.

13
14 6
15
16 7 **Supplementary Table 1. A genome-wide miRNA mimic screen identifies cellular**
17 8 **miRNAs modulating HCV infection.** Log2(FC), lfdr and effect on HCV infection in part 1 and
18 9 part 2 of the screen are shown for the individual miRNAs of the miRNA mimic library. In red:
19
20
21
22 10 proviral effect, in blue: antiviral effect. FC: fold change, lfdr: local false discovery rate